RESEARCH & DEVELOPMENT

Design of Temporary Slopes and Excavations in Residual Soils

Roy H. Borden, PhD, PE

Mohammed A. Gabr, PhD, PE

Jungmok Lee, PhD

Chien-Ting Tang

Cheng Wang, PhD

Department of Civil, Construction, and Environmental Engineering

North Carolina State University

NCDOT Project 2013-07

FHWA/NC/2013-07

August 2016

Design of Temporary Slopes and Excavations in Residual Soils

By

Roy H. Borden, PhD, PE

Mohammed A. Gabr, PhD, PE

Jungmok Lee, PhD

Chien-Ting Tang

Cheng Wang, PhD

Department of Civil, Construction, and Environmental Engineering

North Carolina State University

In Cooperation with the North Carolina Department of Transportation

1. Report No. FHWA/NC/2013-07	2. Government Accession No. …	3. Recipient's Catalog No.
4. Title and Subtitle Design of Temporary Slopes and Excavations in NC Residual Soils		5. Report Date August 2016
		6. Performing Organization Code
7. Author(s) Roy H. Borden, Ph.D, P.E. Mohammed A. Gabr, Ph.D, P.E. Jungmok Lee, Ph.D Chien-Ting Tang Cheng Wang, Ph.D		8. Performing Organization Report No.
9. Performing Organization Name and Address: Department of Civil, Construction, and Environmental Engineering North Carolina State University Campus Box 7908 Raleigh, NC 27695		10. Work Unit No. (TRAIS) …
		11. Contract or Grant No. …
12. Sponsoring Agency Name and Address: North Carolina Department of Transportation Research and Development Unit 104 Fayetteville Street Raleigh, North Carolina 27601		13. Type of Report and Period Covered Final Report January,2013-August, 2016
		14. Sponsoring Agency Code 2013-07
Supplementary Notes: …		

16. Abstract

In general, current design methods and procedures for temporary slopes and temporary excavation support systems do not consider the suction-induced characteristics of unsaturated residual soils, and therefore may result in overly conservative designs and unnecessary construction costs. The main objective of this research project was investigating the possibility of a more cost-effective design of temporary slopes and retaining structures in residual soils based on the incorporation of matric suction in the analyses approach. The components of this research project included: field and laboratory testing program, evaluation and development of predictive models, and analysis of cut slopes and sheet pile walls in excavation and considering water infiltration effect on suction. A full-scale field experimental program was conducted in Greensboro, NC, and included the excavation of three slopes (1:1, 0.5:1 and 0.25:1) and the construction of a cantilever sheet pile wall. Installed sensors included tensiometers for matric suction and moisture content measurements, inclinometer casings, strain gauges and pressure cells. Collected field data included suction measurements, and deformation data and the changes occurring in such data due to three excavation levels (4.6m, 6.1m and 6.7m) as well as due to water infiltration. Laboratory tests were performed on retrieved undisturbed specimens taken from the test site. Laboratory testing included measuring soil water characteristic curves, unsaturated shear strength and the physical properties of the site soils. Models for predicting matric suction as a function of volumetric water content, and shear strength as a function of matric suction were developed based on the experimental results. Utilizing the database of field and laboratory test data, as well as the developed predictive models, slope stability analyses and PLAXIS numerical models of the tested sheet pile wall in the unsaturated site conditions were performed and verified with field measurements. Both stage-excavation and infiltration effect were analyzed. Based on the results of the numerical analyses, a simplified approach for determining the required depth of embedment of a cantilever wall incorporating the effect of matric suction is proposed. The proposed approach is termed Suction Stability Number (SSN) and accounts for the stabilizing influence of matric suction in a similar manner to cohesion in the conventional stability number.

17. Key Words Infiltration, Road, Slope, Soil, Strength, Suction, Unsaturated, Wall	18. Distribution Statement		
19. Security Classif. (of this report) Unclassified	20. Security Classif. (of this page) Unclassified	21. No. of Pages 91	22. Price

Form DOT F 1700.7 (8-72) **Reproduction of completed page authorized**

Disclaimer

The contents of this report reflect the views of the authors and not necessarily the views of the University. The authors are responsible for the facts and the accuracy of the data presented herein. The contents do not necessarily reflect the official views or policies of either the North Carolina Department of Transportation or the Federal Highway Administration at the time of publication. This report does not constitute a standard, specification or regulation.

Acknowledgments

The authors would like to thank the members of the NCDOT Geotechnical, Materials, and Construction divisions who worked on this project. The time, expertise and guidance of NCDOT engineers were invaluable to this project. Special thanks are due to the members of the steering committee:

Kyung J. Kim, Ph.D., P.E. (Chair)
Mark R. Freeman, P.E.
J. Dean Hardister, P.E
Chris Kreider, P.E.
Chun Kun Su
Michael D. Valiquette, P.E.
John L. Pilipchuk, P.E., L.G.
Ernest Morrison, P.E.

Additionally, special thanks are due to:

Dr. K. J. Kim for coordinating overall project for the NCDOT;

Mr. Michael Valiquette, Christopher A. Kreider, and Neil Roberson for helping us with the installation of field instruments;

Gary P. Crowder for obtaining field LiDAR scans and assisting with their interpretation;

Chun Kun Su and Suriyati Supaat of the NCDOT Geotechnical lab for their significant help in soil characterization and the valuable experimental data on saturated triaxial compression test specimens which they provided for this research;

Numerous other NCDOT personnel for their generous help with the field work; and finally, former postdoc, Dr. Carlos Cary and lab technicians Jake Rhoads and Jerry Atkinson, for suggestions and assistance in the laboratory testing set-up for the unsaturated soil testing.

Executive Summary

The main objective of this research project was investigating the utilization of matric suction for a more economical design of temporary slopes and retaining structures in unsaturated North Carolina residual soils. In general, current design methods and procedures for temporary slopes and temporary excavation support systems do not consider the suction-induced characteristics of unsaturated residual soils, and therefore often result in overly conservative designs and unnecessary construction costs.

The components of this research project were: the performance of field and laboratory tests, the evaluation and development of prediction models, the mathematical modeling of slopes and sheet pile walls during excavation and surface-water infiltration situations. A field experimental program was conducted in Greensboro, NC, and included the performance monitoring of three cut slopes (1:1, 0.5:1 and 0.25:1) and a cantilever sheet pile wall. Successive excavation stages of the slopes as well as the 1-month infiltration period on the top of the slopes were induced and the performance monitored for 30 days after construction is completed. Sensors for matric suction and moisture content measurement, as well as inclinometer casings, strain gauges and pressure cells were installed and the changes in measured parameters due to three excavation depths (4.6m, 6.1m and 6.7m) and infiltration were recorded.

A series of laboratory tests were performed on undisturbed specimens from Shelby tubes taken from the test site; these specimens were used to develop soil water characteristic curves, unsaturated shear strength and physical properties for the site materials encountered. Models for predicting matric suction as a function of volumetric water content and shear strength as a function of matric suction were developed based on the experimental results.

Utilizing the extensive database of the field measurements and the comprehensive program of laboratory testing, along with the developed prediction models, numerical analyses were performed for establishment of the effect of matric suction on the temporary slopes and walls. These included stability analyses of the three cut-slopes and finite element modeling of the sheet pile wall in the natural, unsaturated condition. The models were verified with data from the field measurements. The successive excavation stages as well as the 1-month infiltration period were analyzed. Base on the FEM results, a simplified method for cantilever wall design incorporating the effect of matric suction was developed.

This document presents a summary of the main findings of the research program in an abbreviated manner. The details and the data are included in Appendices A through I. The main chapters of the report include approaches for the more economical design of temporary slopes and excavation support walls in unsaturated residual soils. The work product includes validated models for estimation the Soil Water Characteristic Curves (SWCC). The SWCC data are then used to estimate the unsaturated shear strength of residual soils, with proposed approaches that are applicable to the soils tested in this study. The main findings of the field instrumentation and monitoring components are coupled with the approach for estimating the shear strength to provide guidance on the stability of temporary steep slopes in residual soils with water infiltration. The work extends the monitored field data to develop an approach for estimating the lateral earth pressure diagram for cantilever sheep pile walls in unsaturated residual soils.

Table of Contents

List of Tables

List of Figures

CHAPTER 1. Introduction

1.1. Background

In the Piedmont region of North Carolina, excavated slopes and temporary retaining structures are often constructed in unsaturated soils. However, the education and practice of many engineers have focused on saturated soil mechanics, which is based on the concept of positive pore water pressure and the corresponding effective stress (Terzaghi and Peck in 1967). However, in unsaturated soils, the matric suction force must be taken into account when considering soil behavior that includes shear strength, volume change, and seepage.

The unsaturated soil matrix consists of water, air, and solid soil particles. The pressure difference between the air and water drive capillary tension forces and affect the soil's behavior, especially for soils that contain finer particles. For example, silty and clayey soils conform to unsaturated soil behavior because their water contents paired with fines content generate capillary force, which is related to matric suction. The contribution of suction to the behavior of unsaturated soil depends on the degree of saturation. Piedmont residual soil contains fines content (silty clay), and therefore unsaturated soil mechanics should be used to explain the behavior and perform the appropriate design and analysis of temporary slopes and excavation support systems in such profiles.

1.2. Purpose and scope

This research report includes the presentation of experimental data from both laboratory testing and field construction and monitoring program. In addition, the evaluation of prediction models for matric suction and unsaturated shear strength is presented along with methods for incorporating the effect of matric suction into slope stability analysis and sheet pile wall design.

Full-scale field testing and extensive laboratory and *in situ* tests were conducted for this study to investigate the effects of matric suction on the behavior of unsaturated Piedmont residual soils. Furthermore, the study examines the inclusion of matric suction in the design of temporary slope and retaining wall systems. An additional objective is to provide a better understanding of the behavior of unsaturated residual soils that are subjected to surface-water infiltration, and how such quantity may be used for a better design of temporary slope and excavation support systems.

The specific objectives of this research were to:

1. Characterize unsaturated Piedmont residual soil profiles at a selected test site where three slopes and a wall were constructed and monitored. Retrieve samples for physical and engineering characterization of the sites soils and integrate all the test and monitored data into a comprehensive database.
2. Develop prediction models to estimate the matric suction as a function of volumetric water content for the tested residual soils.
3. Develop prediction models to estimate the increase in shear strength as a function of matric suction for the undisturbed residual soils tested.
4. Perform deformation analyses with consideration of the unsaturated condition for temporary retaining wall systems and develop lateral earth pressure diagram including the effect of matric suction.
5. Investigate the appropriate incline (angle) of unsaturated temporary slopes and the duration period of construction based on the results of stability and infiltration analyses.
6. Evaluate shear strength and deformation behavior of the constructed geostructures at the site including the influence of changing soil suction with rainfall infiltration.

1.3. Organization of the report

The work performed for this research project was completed between January, 2013 and June, 2016. The report is organized into 9 chapters, as follows:

Chapter 1: Introduction

Chapter 2: Site description and laboratory testing program

Chapter 3: Prediction of matric suction as a function of volumetric water content

Chapter 4: Prediction of shear strength as a function of matric suction

Chapter 5: Application of unsaturated soil properties to slope stability analysis.

Chapter 6: Modeling deformation of the sheet pile wall during excavation and infiltration.

Chapter 7: A simplified design method for cantilever wall design in unsaturated soil.

Chapter 8: Findings and conclusions

Chapter 9: References

A comprehensive record of all measured data from laboratory and field tests, and background information on modeling are presented in Appendices A thru G. Content in each appendix is listed below:

Appendix A: Literature Review

Appendix B: Test site and field test program

Appendix C: Field monitoring instruments

Appendix D: Laboratory testing program

Appendix E: Suction measurement and prediction of SWCC

Appendix F: Measurement and prediction of unsaturated shear strength

Appendix G: Application of matric suction to slope stability

Appendix H: Modeling of cantilever sheet pile wall in unsaturated residual soil

Appendix I: Test data from NCDOT's lab

CHAPTER 2. Site Description and Laboratory Testing Program

This chapter presents a general overview of the field test and the laboratory testing program. A comprehensive description of each type of sensor installed at the site and the data measured during each of the three stages of excavation and subsequent period of surface-water infiltration are presented in Appendix B. The details of tested soil in each Shelby tube and introduction of each experimental device used in this research project are presented in Appendix C.

2.1. Site description and field test program

Location of test site

In order to accomplish the stated objectives of developing a database of residual soil shear strength and suction parameters, an experimental program was undertaken on samples retrieved from a construction site in Greensboro, North Carolina. The test site location is shown in Figure 2-1. The Project was given a No. 39406.1.1, and the construction site is located at Alamance Road, Greensboro, Guilford County, North Carolina.

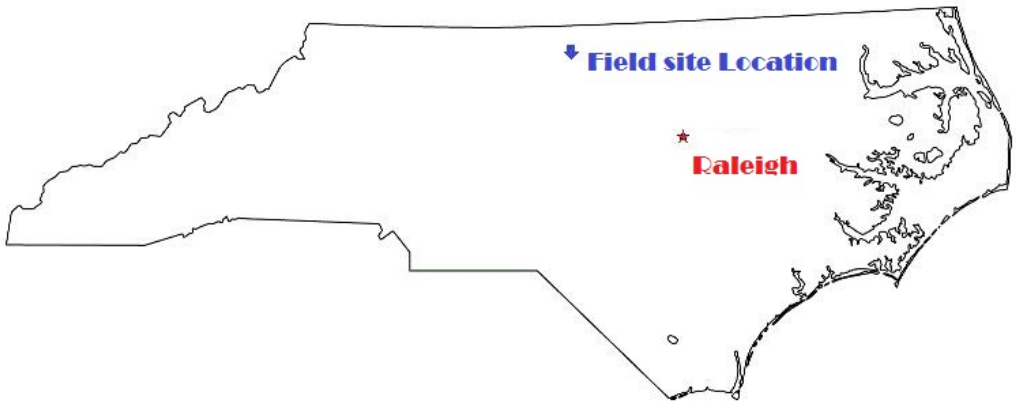

Figure 2-1 Location of test site in this research

The field testing program included the cutting of three slopes of varying steepness (0.25:1, 0.5:1, and 1:1) on one side, and the installation of one cantilever sheet pile wall on the other side of the proposed roadway cut, as shown schematically in **Figure 2-2**. The soil between the intended slopes and the sheet pile wall was excavated in three stages to a final depth of 22 feet. **Figure 2-2** shows a plan view of the entire test site, in which the locations of the three slopes with their respective inclinations as well as the location of the sheet pile wall are marked. A photograph of the test site after excavation is shown in Figure **2-3**.

Soil profiles with SPT-N values are shown in Figures B-7 through B-13 in Appendix B, and CPT measurements are in Figures B-8 to B-11, for each location shown in **Figure 2-2**. Field monitoring devices, including FTC-200 (matric suction sensor) and moisture content sensors, inclinometer casings, pressure cells and strain gauges were installed. Figure **2-4** shows the location and depth of the instruments in the sheet pile area. A detailed description of each instrument and the locations in each slope is listed in Appendix B.3.

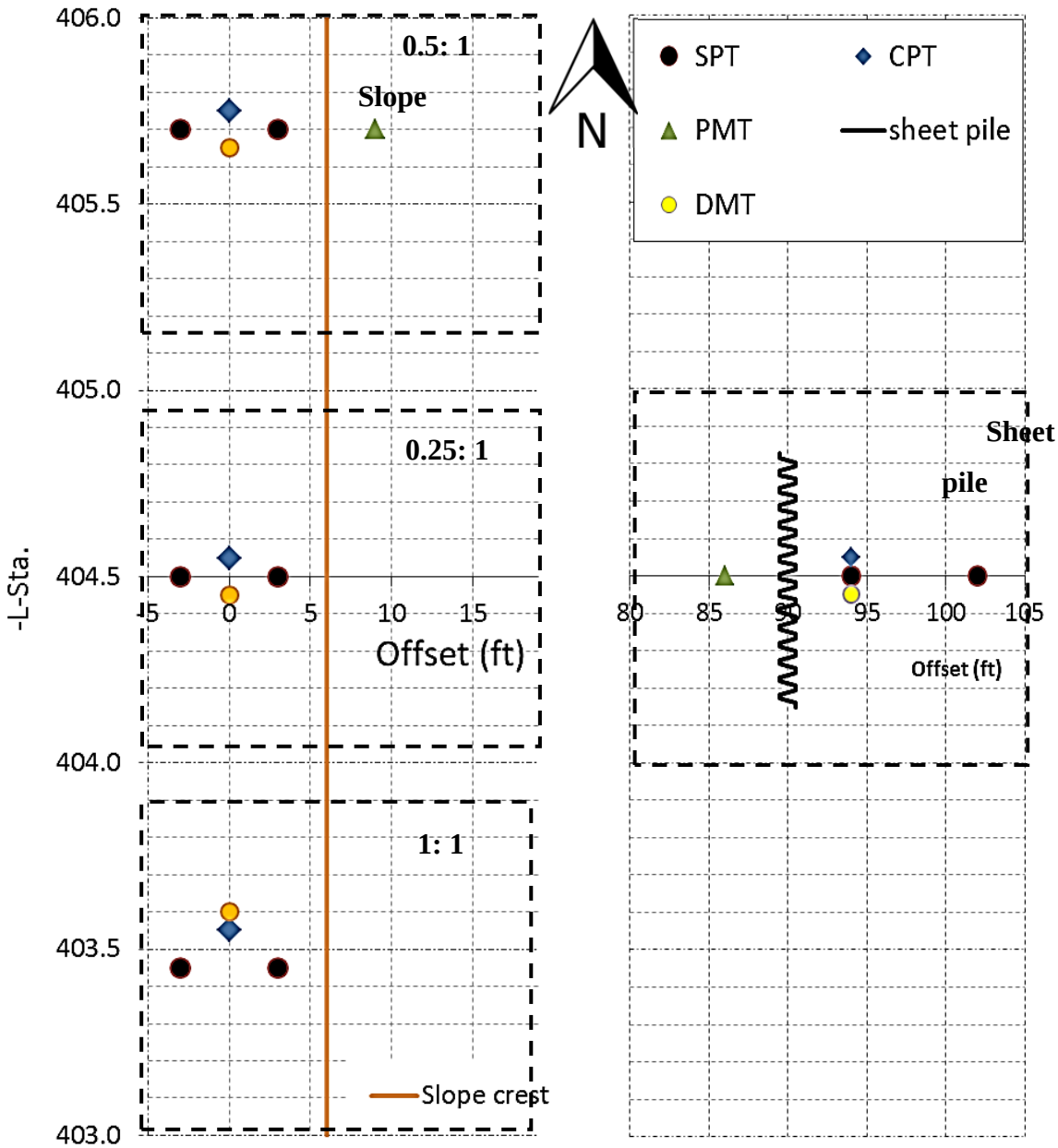

Figure 2-2 Plan view of the test site

Figure 2-3 View of site after 22-ft excavation

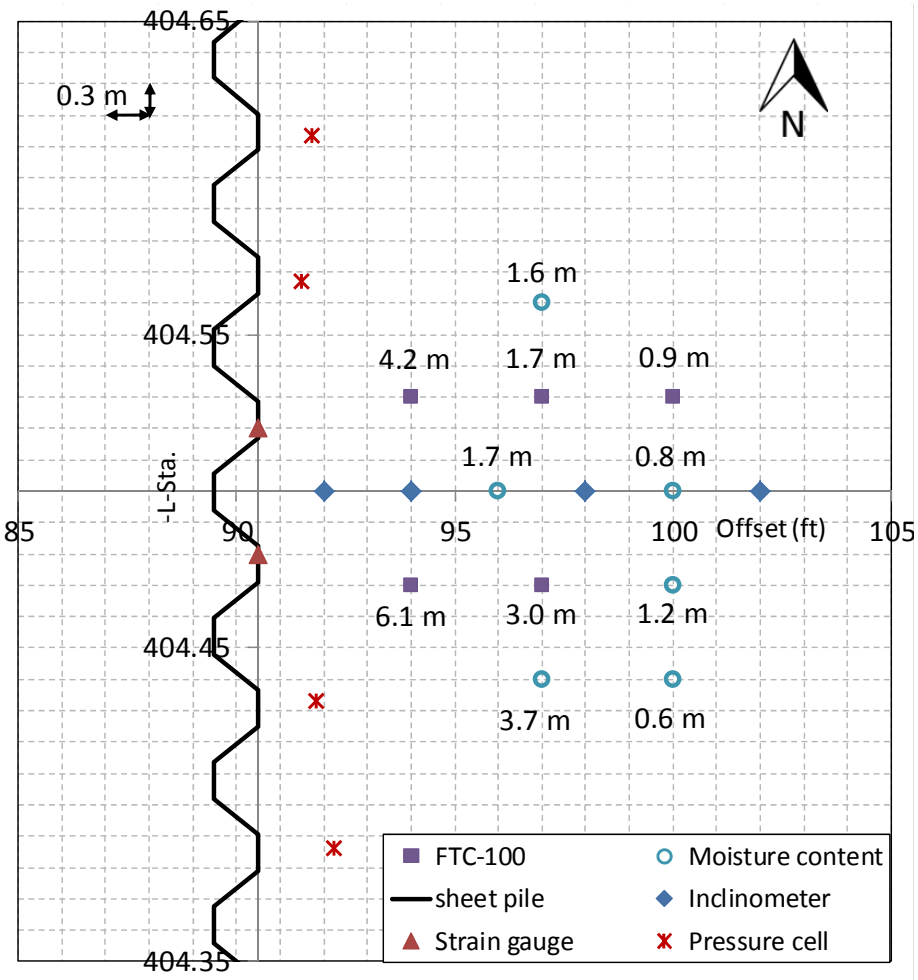

Figure 2-4 Locations and depths of sensors in sheet pile area

The measured changes in sensor readings due to the excavation process and subsequent surface-water infiltration will be discussed and used in modeling the behavior of both the sheet pile wall and slopes.

2.2. Laboratory testing program

A total of ninety-four Shelby tubes were retrieved from the test site, from 10 borings, and at depth that ranged from 0.6 to 15.5 m (2 to 52 ft). Twenty Shelby tubes were sent to the NCDOT laboratory for consolidated undrained triaxial tests, and 66 Shelby tubes were sent to CFL lab at NC State University for testing. The laboratory testing program included matric suction measurements (filter paper, pressure plate and potentiometer tests) and unsaturated triaxial tests. The testing program is summarized in Table **2-1**, and the locations of Shelby tubes are shown in Figure **2-5**.

Table 2-1 Test program

	Tube number	Test types	# of test	Note
NCDOT Geotechnical Lab	ST-1 to ST-25, ST-27, ST-29, ST-31, ST-33 and ST-35	Consolidation test	1 per tube	
		CIU triaxial test	1~3 per tube	
		Permeability test	1	ST-27 (A-4 soil)
NCState CFL Soil Lab	ST-28, ST-30, ST-32, ST-34 and ST-36 to ST-94	Matric suction measurement	Every tube	Measured by tensiometer
		Pressure plate test	10	
		Unsaturated triaxial test	46	20 single stage; 26 multistage

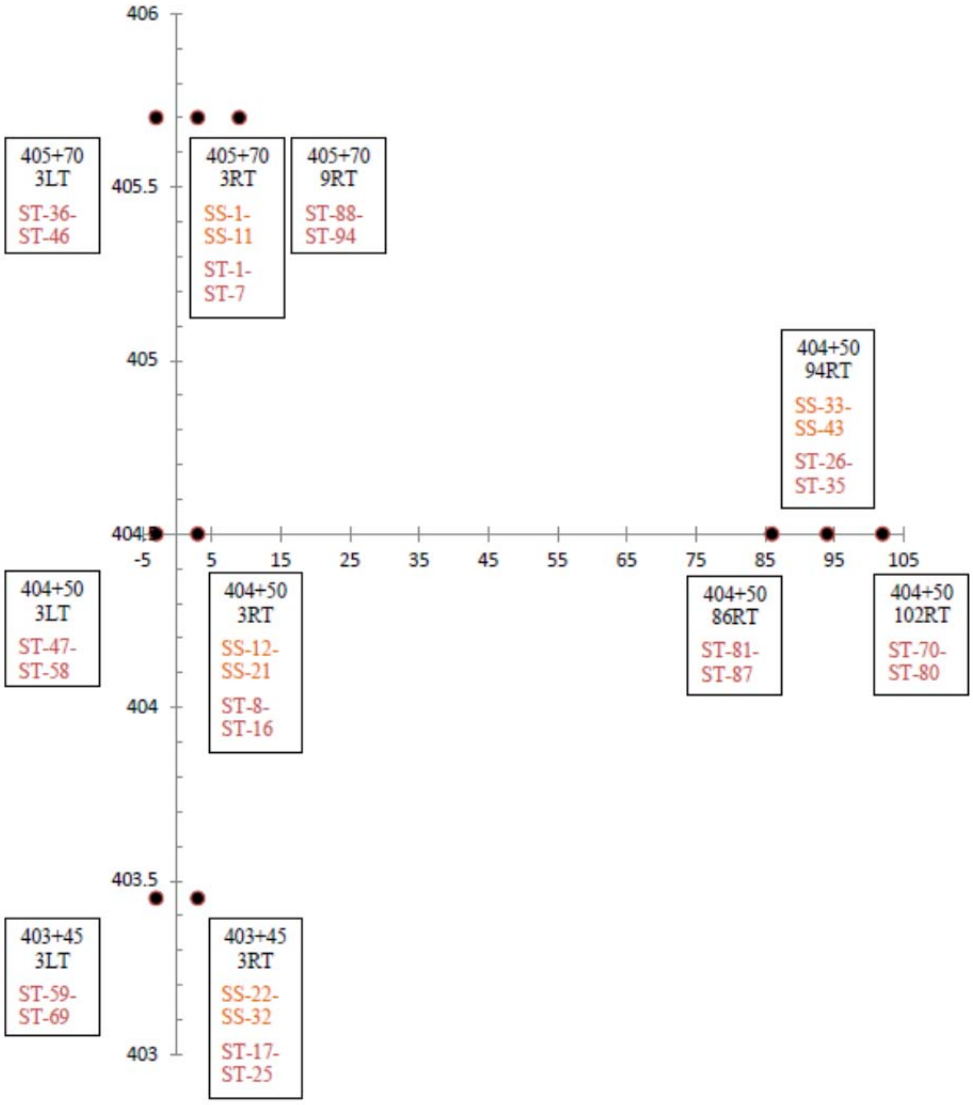

Figure 2-5 Locations of Shelby tubes

The site soils are mainly red silty clay and tan sandy silt. These colors resulted from the various degrees of chemical weathering. The red color is due to iron oxides content. The soil at shallower depths experienced a higher degree of weathering, which results in a darker red color and higher percentage of finer particles. The tan color is closer to the color of original rock (gneiss, schist and granite). The tan colored soil exists at deeper depths, is less weathered and has lower fines content.

According to ASSHTO classification, four major groups of soil were found at this site, A-7-5, A-4, A-5 and A-2-6. The properties of the site soils are listed in Table **2-2** along with the corresponding USCS classifications (MH, ML and SC). For a detailed record, soil properties for each Shelby tube are listed in Tables C-3 to C-9, in Appendix C.

Table 2-2 Properties of major group of soil in this research

Symbol	Soil Type (USCS)	Soil Type (AASHTO)	Depth (ft)	ρ_d (g/cm^3)	Gs	LL (%)	PI (%)	< #200 (%)	Clay (%)	Silt (%)	Sand (%)	φ' (deg)	c' (psi)
G1	MH	A-7-5	5-12	1.11	2.76	61	22	88	15	73	12	27	1.9
G2	ML	A-4	24-50	1.61	2.70	40	6	60	4	56	45	30	2.8
G3	ML	A-5	13-27	1.65	2.73	45	10	84	6	78	16	28	2.5
G4	SC	A-2-6	2-7	1.75	2.68	34	11	32	10	22	68	36	0

Test devices used in this research at the NCSU CFL Geotechnical Lab included:

1. Tensiometers: for measuring the matric suction in each Shelby tube, to obtain the existing matric suction.
2. Pressure plate: for measuring soil water characteristic curves (SWCC)
3. Unsaturated triaxial test: for measuring unsaturated shear strength

Measured data and developed models for predicting matric suction are presented in Chapter 3 and measured data and developed models for predicting unsaturated shear strength are presented in Chapter 4.

CHAPTER 3. Measured and Modeled Soil Water Characteristic Curves

3.1. Evaluation of existing models

Utilizing the experimental data generated from pressure plate tests, and the procedure presented in Appendix C, the soil water characteristic curves (SWCC) were curve-fitted using the Fredlund and Xing (1994) model shown in Equation 3-1.

$$\theta = \left(1 - \frac{\ln\left(1+\frac{\phi}{\phi_r}\right)}{\ln\left(1+\frac{1000000}{\phi_r}\right)}\right)\theta_s\left(\frac{1}{\left(\ln\left[e+\left(\frac{\phi}{a_p}\right)^{n_p}\right]\right)^{m_p}}\right)] \quad (3\text{-}1)$$

where ϕ = matric suction; ϕ_r = the residual matric suction and a_p, n_p, m_p are the fitting parameters.

The SWCC data for the A-7-5 soil samples are shown in **Figure 3-1**. The SWCCs of the other soil types and the parameters *a*, *n*, and *m* for the Fredlund-Xing model are presented in Appendix D.

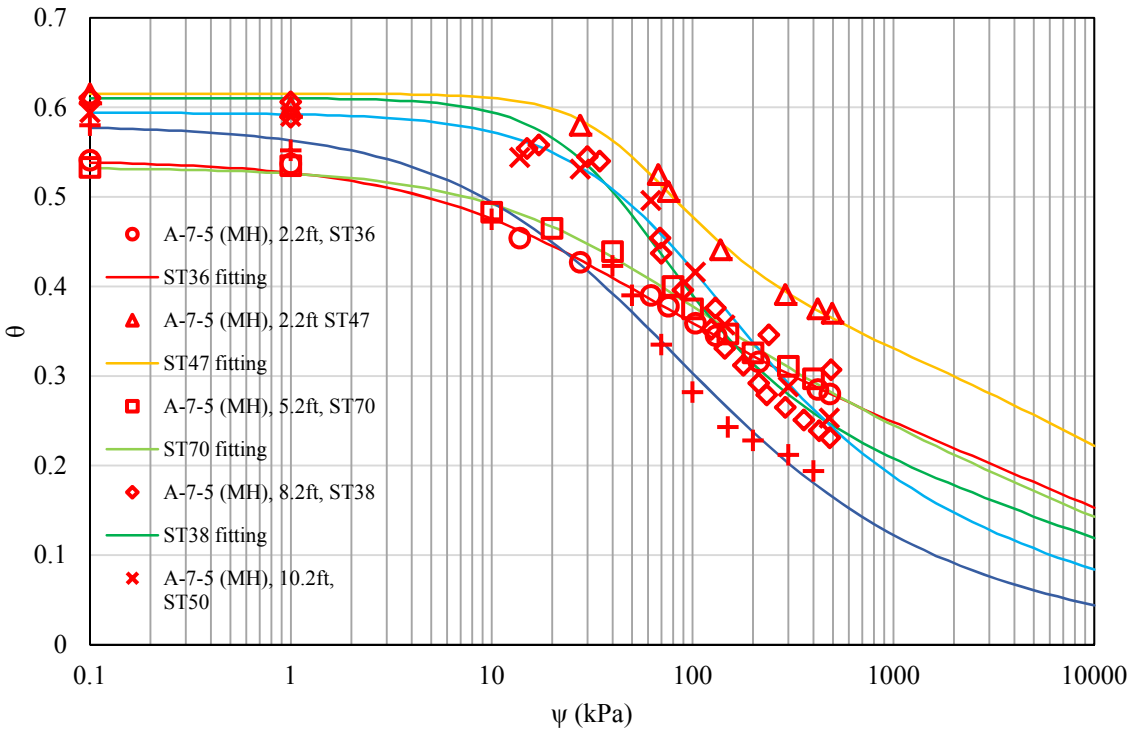

Figure 3-1 Soil water characteristic curves of A-7-5 (MH) soil samples

Two existing suction prediction models, Zapata et al. (2000) and Fredlund et al. (1997), were used to predict the suction of the tested residual soils. In the model proposed by Zapata, a weighted plasticity index (PI), i.e., wPI, is used as the main variable to correlate the SWCC parameters. wPI is expressed as the percentage passing the #200 sieve (as a decimal) multiplied by the PI, as a percentage. The equations for the Fredlund and Xing 1994 SWCC parameters as a function of wPI are shown as Equations 3-2 to 3-5:

$$\mathrm{a} = 0.00364(wPI)^{3.35} + 4(wPI) + 11 \qquad (3-2)$$

$$\frac{n}{m} = -2.313(wPI)^{0.14} + 5 \qquad (3-3)$$

$$\mathrm{m} = 0.0514(wPI)^{0.465} + 0.5 \qquad (3-4)$$

$$\frac{\psi_r}{a} = 32.44e^{0.0186(wPI)} \qquad (3-5)$$

Fredlund et al. (1997) model was used to estimate the SWCCs using grain size distribution data and volume-mass properties. The grain size distribution of the soil is divided into small ranges of relatively uniform particles. The data points of applied matric suction and measured volumetric water content of each soil specimen are summed to generate the final SWCC. The predicted SWCCs were generated by inputting the grain size distribution data and volume-mass properties into SoilVision software, from Soilvision Systems Ltd.

The suction values determined from the twelve pressure plate tests were compared to those predicted from the Zapata model and SoilVision database, as shown in **Figure 3-2** and **Figure 3-3**, respectively. The results from both the Zapata model and SoilVision software show a significant amount of deviation from the measured data, which have coefficients of determination, R^2, of 0.51 and 0.48, respectively. Because these existing models did not provide very high confidence levels in the suction predictions, an empirical model based on grain size distribution and a soil volume-mass relationship was explored. That is, a new model specifically designed for the North Carolina residual soil tested is proposed herein.

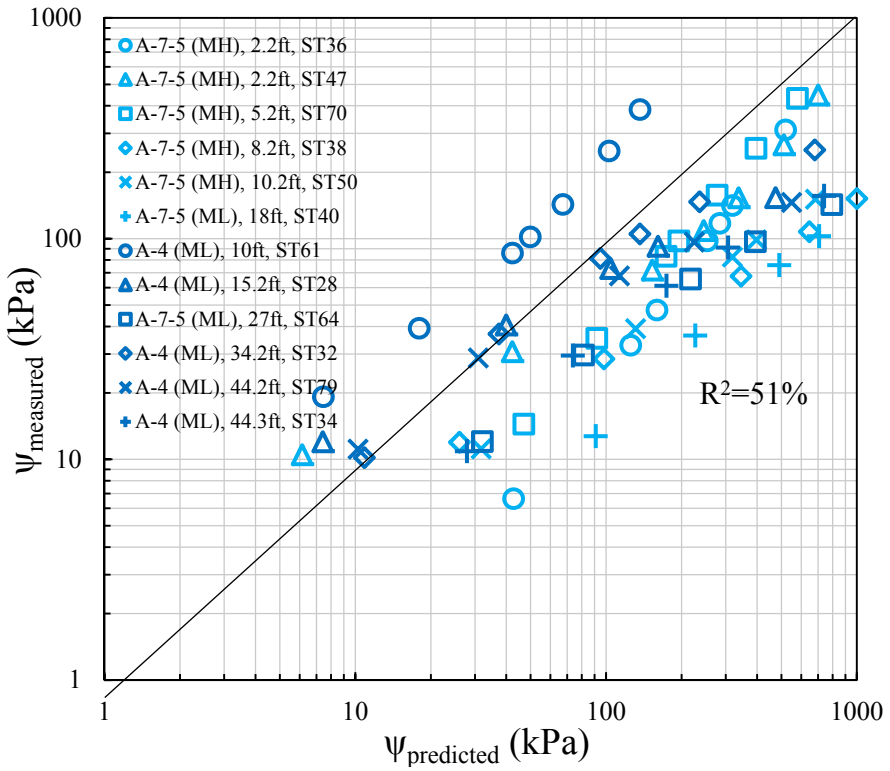

Figure 3-2 Measured vs predicted suction by Zapata model

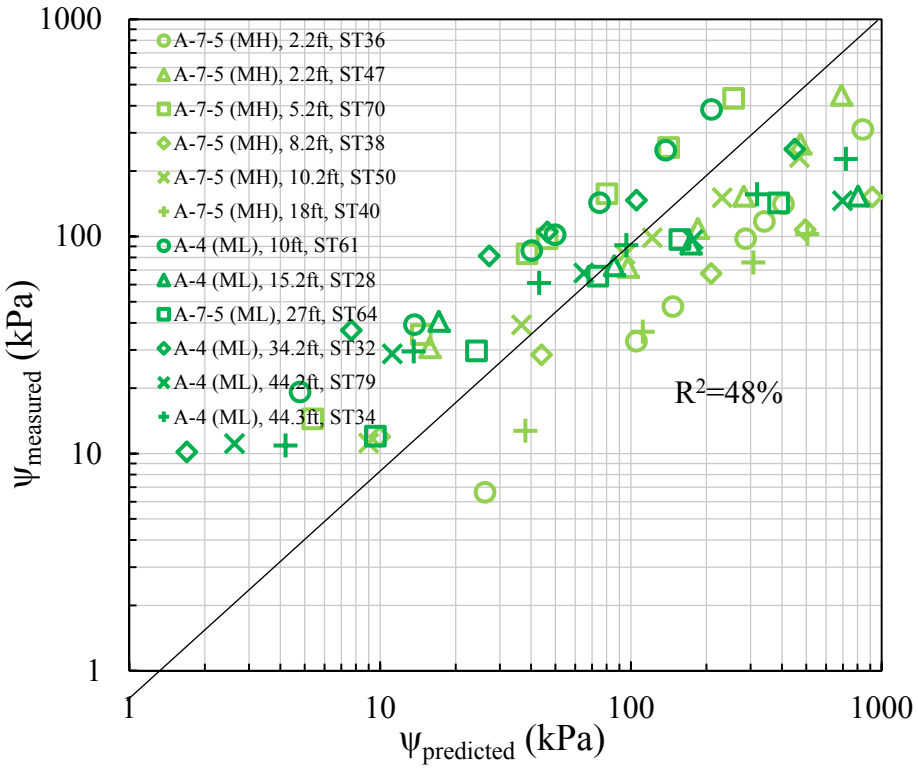

Figure 3-3 Measured vs predicted suction by SoilVision

3.2. Proposed prediction model

For the model development, SWCCs from twelve samples were used and included six high plasticity and six low plasticity silty soils. The corresponding soil properties, such as grain size distribution, were also assessed. The first step was to include as many properties as possible in the statistical analysis because no physical theory was available to support which properties should be included or excluded. Also, some of the possible parameters might have an effect on the curvature of the SWCCs. Three categories of soil properties were included for the new model development: grain size distribution, Atterberg limits, and volume-mass relationships.

The prediction models for each Fredlund-Xing *a*, *n*, and *m* parameters were developed and are shown in Equation 3-6 to 3-8:

$$a = 17.2 + \frac{1.89}{D_{60}} - \frac{0.363}{D_{30}} - \frac{0.063}{D_{10}} + 2.5 * \frac{D_{60}}{D_{10}} \quad (3\text{-}6)$$

$$n = -0.105 - 0.018 * P200 + 9.55 * D_{60} + \frac{0.012}{D_{30}} - 0.057 * \frac{D_{60}}{D_{10}} + 1.203 * \rho_d \quad (3\text{-}7)$$

$$m = 11.24 + 0.0074 * P200 - 0.075 * 5\mu m - 2.665 * G_s - 1.452 * \rho_d \quad (3\text{-}8)$$

Due to the limitation of the data used for generating the model, the bounds for the parameter are designated and the correlation coefficients used to quantify the fitness of the model as shown in **Table 3-1**.

Table 3-1 Correlation Coefficients to Quantify Fitness of Proposed Model

	R^2 (%)	Adjusted- R^2 (%)	Predicted-R^2 (%)	Bound
a	86.5	78.8	50	(14, 74)
n	93.7	88.4	67.4	(0.7, 2.1)
m	97.6	96.2	93.9	(0.3, 1.8)

The predicted suction values determined by the proposed model were compared to the measured suction values, as shown in **Figure 3-4**. The figure indicates that most of the data

points for predicted suction versus measured suction fall on the 1:1 ratio line and that the R-square value is 93%, which indicates a better fit than both the Zapata model (R^2 is 51%) and SoilVision (R^2 is 48%).

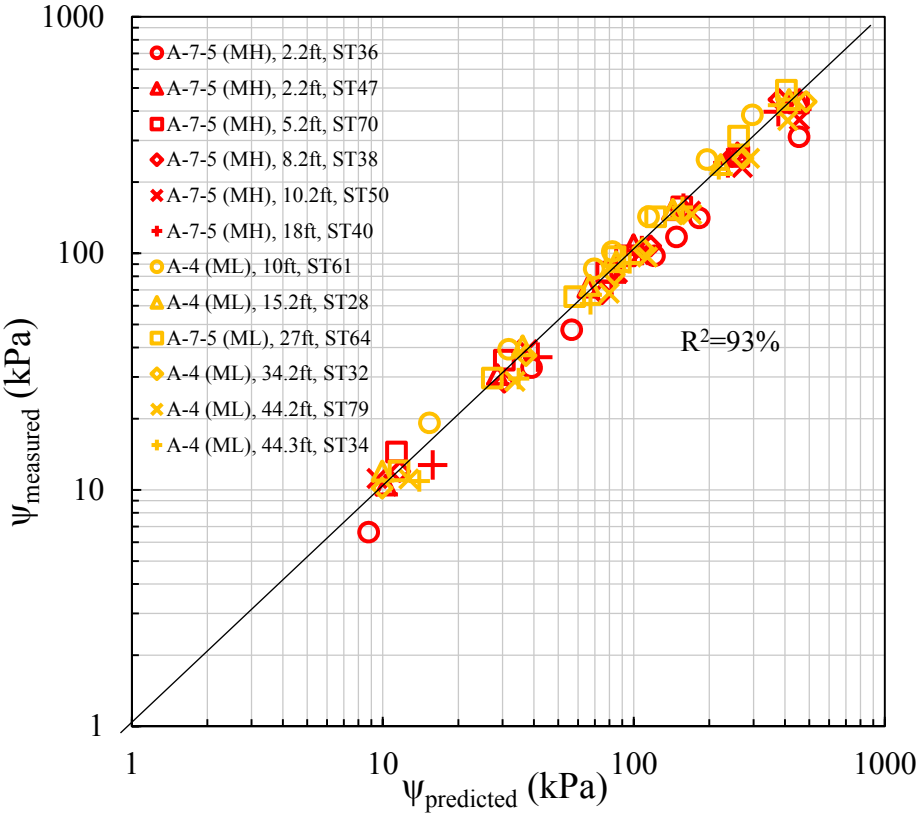

Figure 3-4 Measured vs predicted suction using suction prediction model

Suggested correction for design purpose

In order to consider the variability of the data from an engineering design point of view, a suggested correction factor, based on 95% confidence limits of the data, should be applied to the predicted suction values.

The comparison of the suction values obtained by the prediction model and the actual measurements, as shown in **Figure 3-4**, is transposed to **Figure 3-5**. Knowing the predicted suction values from the Equation 3-1 with parameters, a, n and m utilizing Equation 3-6 to Equation 3-8, the best-fit function of the actual suction can be expressed as

$$\psi_{measured} = 3.572 - 0.972\psi_{predicted} \quad (3\text{-}9)$$

In order to account for the variability (scatter) in the measured data, a lower bound model, such as one that includes a 95% confidence limit, could be used as shown in Equation 3-10:

$$\psi_{measured} = 3.57 + 0.97\psi_{predicted} - 59.4\left[0.012 + \frac{\left(\psi_{predicted} - 146.5\right)^2}{10^6}\right]^{0.5} \quad (3\text{-}10)$$

However, instead of using Equation 3-11, a simple correction factor of 0.94 that is based on the lower prediction at the mean of the data is shown in **Figure 3-5** to provide a very reasonable approximation of the more complex function. Thus, the following model is derived:

$$\psi_{measured} = 0.94\psi_{predicted} \quad (3\text{-}11)$$

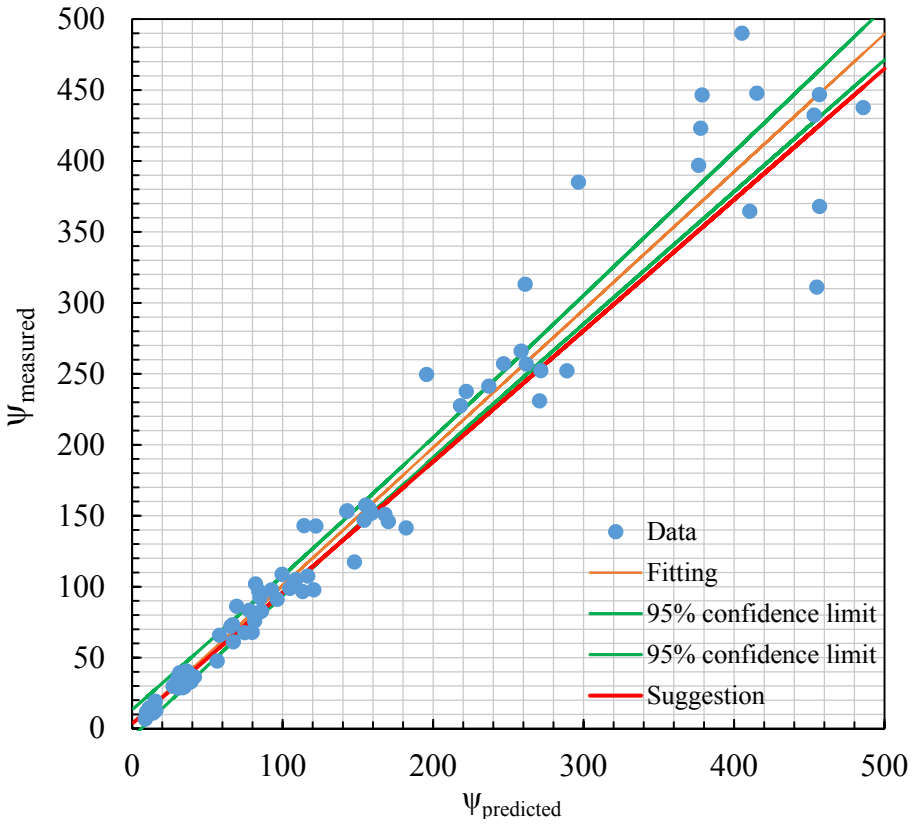

Figure 3-5 Suggested correction for the predicted suction

Field SWCC curve shift

A field curve concept based on actual tensiometer suction measurements is also proposed. The basis for the field curve concept is the fact that the actual suction conditions in the field are different from the suction on the drying curve due to the existence of hysteresis. To define the wetting curve from the drying curve data, Fredlund et al. (2011) recommended shifting the drying curve as shown in **Table 3-2**.

Table 3-2 Suggested Shifts of Inflection Point between Drying and Wetting Curves for Various Soils (Fredlund et al. 2011)

Soil Type	Range of Typical Shifts (% of a log cycle)	Average Shift (% of a log cycle)
Sand	15-35	25
Silt and loam	35-60	50
Clay	-	Up to 100

In order to consider the actual suction conditions in the soil, a procedure to determine the field curve of the soil is proposed. First, the drying curve of the sample is determined using the pressure plate test or another prediction model. The Fredlund-Xing curve-fitting parameters then are determined.

Second, the suction and water content of the natural soil are determined using a tensiometer on the retrieved soil specimens. Then, the one-point data from the tensiometer measurements is plotted with the drying curve. Third, in order to shift the drying curve to pass through the tensiometer measured suction at the known moisture content, a series of drying curves must be generated by reducing the *a* value in the Fredlund-Xing equation. The reduction of the *a* value can be stepwise at a rate of 5 percent. After the third step, two shifted curves that are closest to the point of the tensiometer reading can be determined. Then, in between the two chosen curves, a set of ten decomposed curves is generated. The best fit to the one-point tensiometer measurement is quantified using the least-square method. Thus, in practical usage, the SWCCs obtained from the suction prediction model are shifted to pass through the tensiometer measured suction, at its measured volumetric water content. This process was used to develop the SWCCs incorporated into the numerical analyses to be described in subsequent chapters.

CHAPTER 4. Measured and Modeled Unsaturated Shear Strength

In order to evaluate the unsaturated shear strength of the residual soils from the Greensboro test site, a total of 19 unsaturated triaxial tests, including 8 single stage tests and 11 multistage tests, were performed on the four groups of soils of three types (MH, ML and SC). The stress-strain curves and values of deviatoric stress at failure for each test are in Appendix E.

The results presented in this section are from four major groups of soils from the site. Each group has several specimens with very similar soil properties. However, test results of specimens with properties different from the four groups are also presented in Appendix E.

4.1. Evaluation of existing models

As anticipated from the literature, the measured data indicate that both increases in net confining pressure and matric suction result in an increase of shear strength. The total cohesion is defined for each individual test from the intercept of the Mohr-Coulomb failure envelope based on the effective friction angle obtained from saturated tests for each soil group. Therefore, the increase in total cohesion intercept represents the contribution of matric suction to shear strength, apart from the effect of net confining pressure. Figure **4-1** (a, b, c and d) presents the total cohesion values as a function of matric suction for each of the four soil groups.

In conjunction with the measured data, the predicted total cohesions from three existing models, computed at zero net confining pressure, are plotted. The first method is based on the Fredlund et al. (1996) approach, utilizing an exponent kappa (κ) on the degree of saturation term, with the values of 'κ' based on recommendations by Vanapalli and Fredlund (2000). Methods 2 and 3 were proposed by Vanapalli et al. (1996) and Houston et al. (2008), respectively. The equation and parameters of each method are listed in Table **4-1**.

The first two methods were both applied utilizing the matric suction from the appropriate SWCCs and the effective friction angle to predict the magnitude of total cohesion. Method 3, by Houston et al. (2008), was applied on the basis of the grain size distribution parameters D_{30}, D_{60} and percentage of sand, instead of using the SWCC.

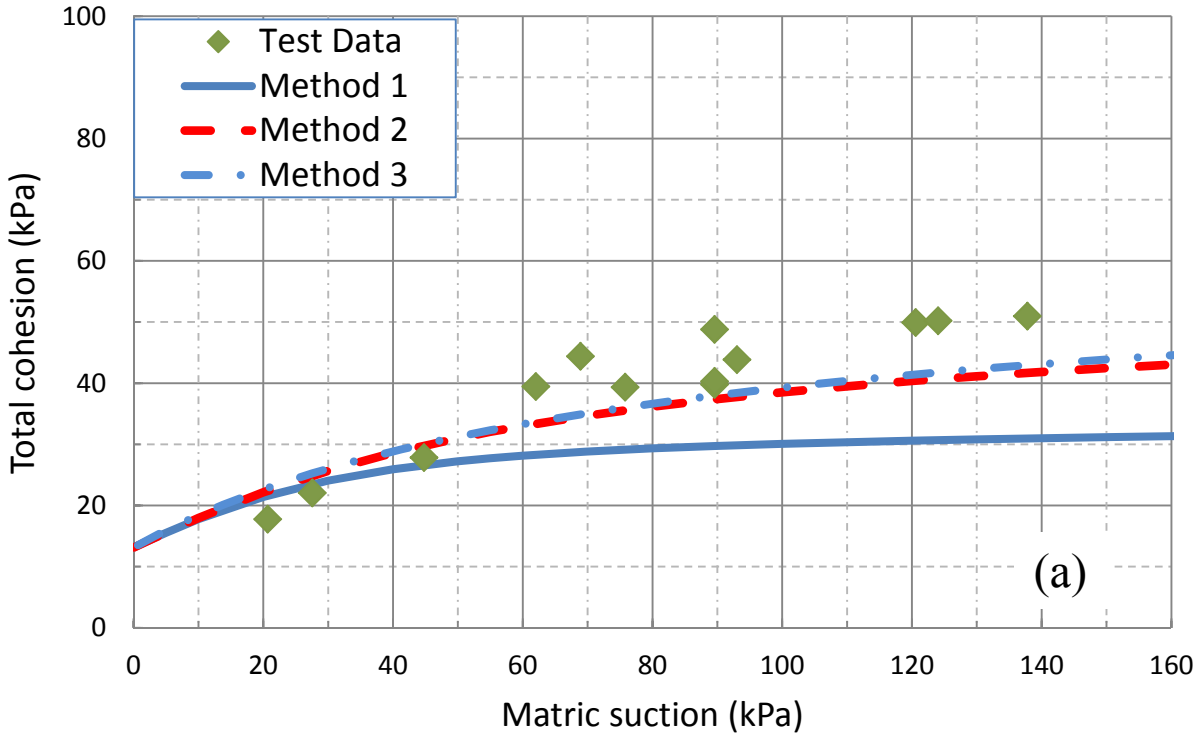
Test Data
Method 1
Method 2
Method 3
Total cohesion (kPa)
Matric suction (kPa)
(a)
0
20
40
60
80
100
120
140
160

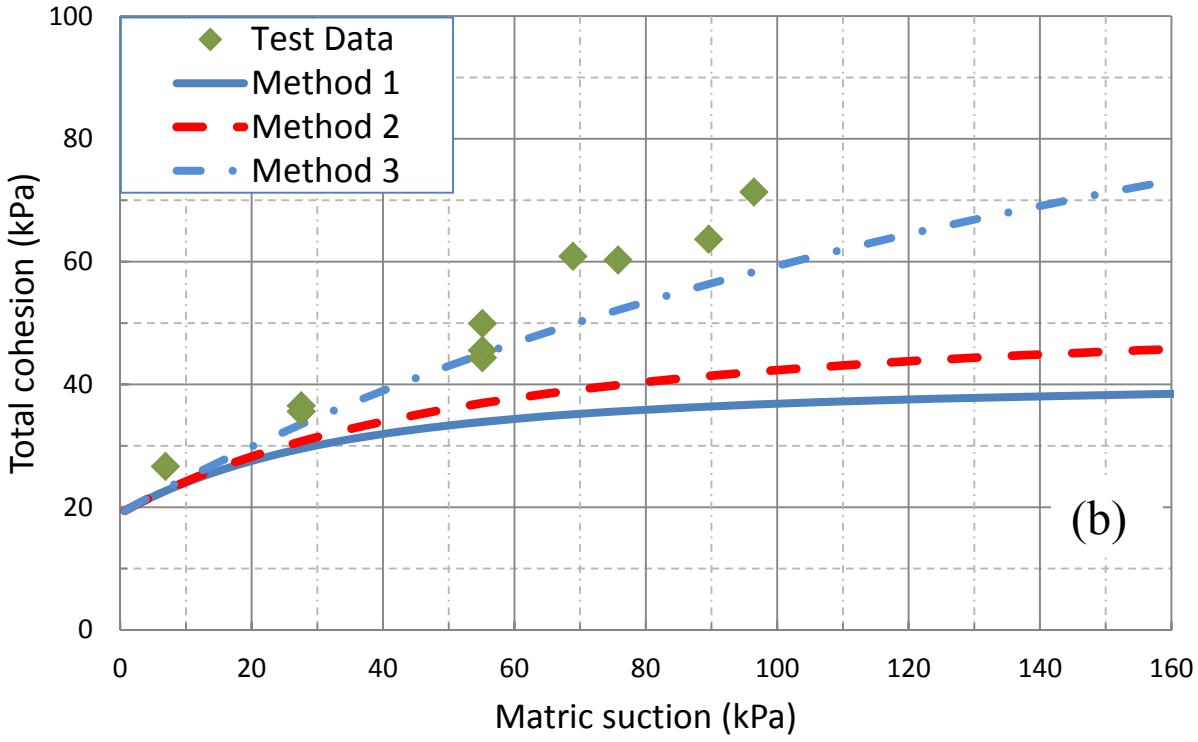
Test Data
Method 1
Method 2
Method 3
Total cohesion (kPa)
Matric suction (kPa)
(b)
0
20
40
60
80
100
120
140
160

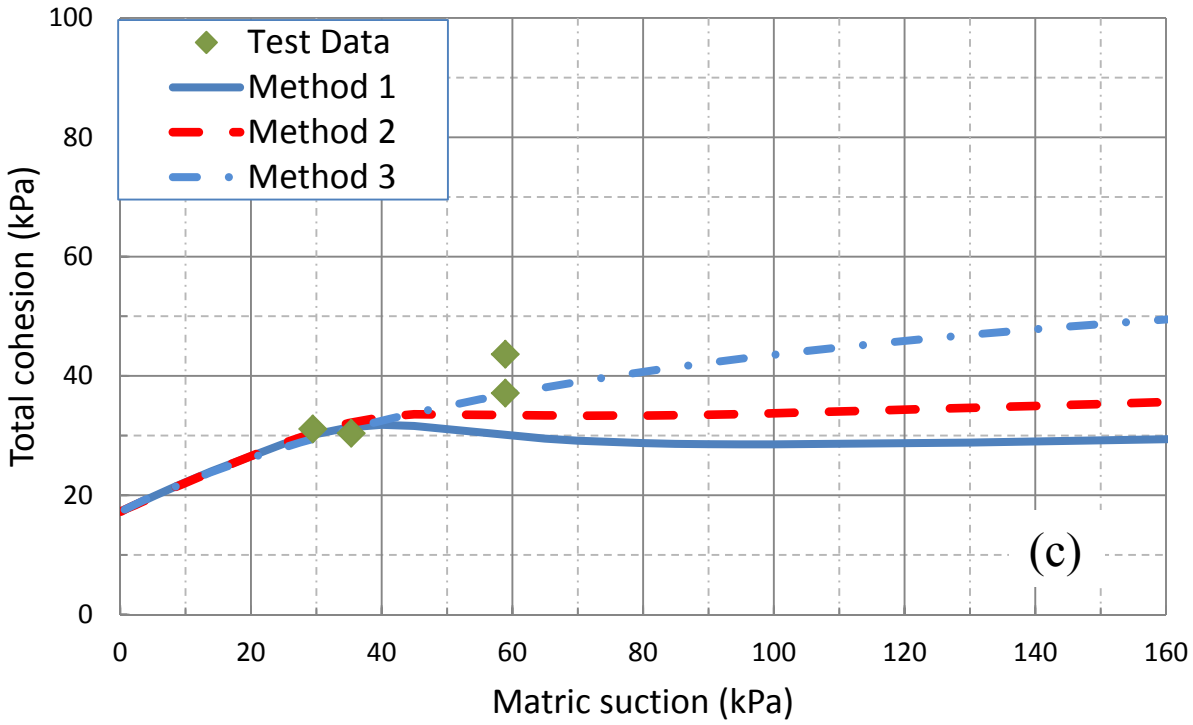

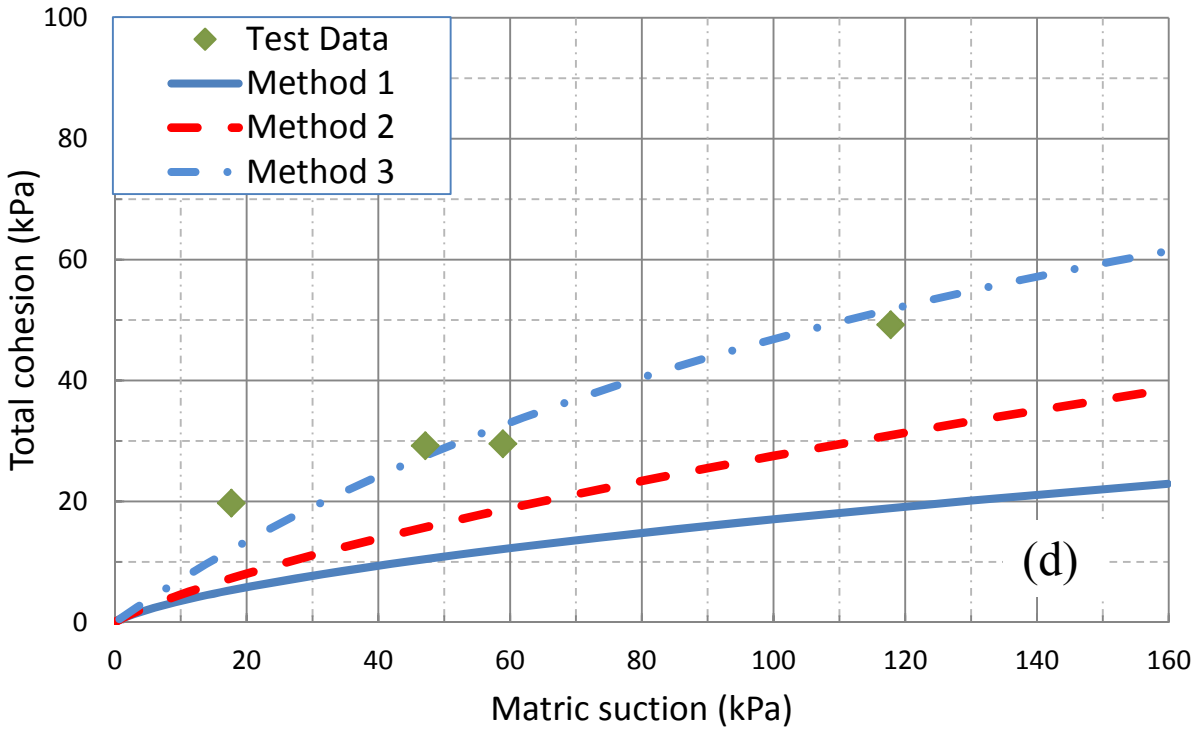

Figure 4-1 Total cohesion intercept vs. matric suction for: (a) G1; (b) G2; (c) G3; (d) G4

Table 4-1 Equations of each method

Number	Author	Predicting formula	Parameters
Method 1	Fredlund, et al. (1996)	$\tau = c' + (\sigma - u_a)tan\varphi' + (u_a - u_w)[(\Theta^{\kappa})tan\varphi']$ $k = -0.0016Ip^2 + 0.0975Ip + 1$	Θ = *Normalized* θ Ip = Plasticity Index
Method 2	Vanapalli, et al. (1996)	$\tau = [c' + (\sigma - u_a)tan\varphi'] + (u_a - u_w)[(tan\varphi')(\frac{\theta - \theta_r}{\theta_s - \theta_r})]$	θ = Volumetric water content θ_s = Saturated θ θ_r = Residual θ
Method 3	Houston, et al. (2008)	$\tau = c' + (\sigma - u_a)tan\varphi' + (u_a - u_w)tan\varphi_b$ $a + b\Psi^* = \frac{\Psi^*}{\varphi' - \varphi^b}$ $\quad b = 1/\varphi'$ $a = 2.23 - 71.8 \cdot D_{30} - 5.33 \cdot D_{60} + 0.168 \cdot (\%sand)$	Grain size distribution: Diameter of 30 %, 60 % and percentage of sand

Of the three applied prediction models, Method 3 yields computed values closest to the measured data points, in comparison to those from Methods 1 and 2. **Figure 4-2** shows the comparison between measured and predicted data by Method 3. The use of Method 3 provides predictions within +/- 15% of the measured data, with an R^2 value of 0.77.

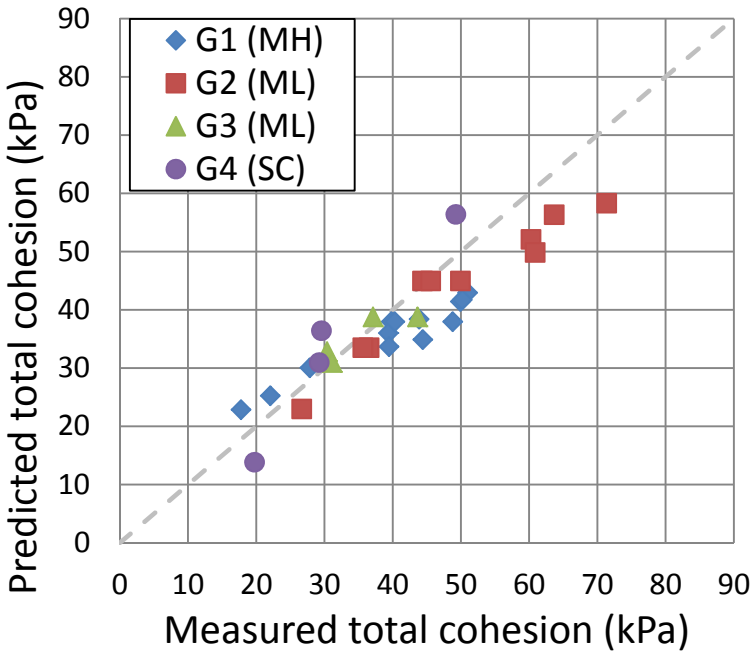

Figure 4-2 Measured versus predicted total cohesion from Houston et al. (2008)

The residual soil samples tested in this research are classified as MH, ML and SC. Test data from the literature were included to extend the range of soils involved in the discussion of the prediction models. These literature data cover five soil types, and their properties and parameters are shown in **Table 4-2**. The evaluation of shear strength prediction herein uses the term "apparent cohesion due to suction" to represent the increase of shear strength due to increase of matric suction.

Table 4-2 Properties of the Soils in Model Calculation

Reference	Soil name	Soil Classification		φ'	c'	θ_r	Fines	LL	PI	$\kappa^{(1)}$	$\kappa^{(2)}$
		USCS	ASSHTO	(°)	(kPa)		(%)	(%)	(%)		
G1 in this research	Residual soil in NC	MH	A-7-5	27	13	0.16	88	58	22	2.37	1.08
G2 in this research	Residual soil in NC	ML	A-4	30	19	0.05	60	34	6	1.53	0.25
G3 in this research	Residual soil in NC	ML	A-4	28	17	0.08	84	45	10	1.82	0.80
G4 in this research	Residual soil in NC	SC	A-2-6	36	0	0.09	32	34	11	1.88	0.77
Miao, et al., 2002	Nanyang soil	MH	A-7-5	21	42	0.09	93	58	32	2.48	1.41
Lee, et al., 2004	Weathered granite	SM	A-2-4	42	19	n/a	12	NP		1.00	1.40
Rahardgo, et al., 2004	Jurong sedimentary	CL	A-6	32	0.0	0.06	66	36	15	2.09	0.61
Kayadelen, et al., 2007	Residual clay	MH	A-7-5	22	25	0.05	95	77	32	2.48	1.85
Burrage et al., 2012	Residual soil	ML	A-4	32	16	n/a	71	38	3	1.28	0.42
Schnellmann, et al., 2013	Coasrse sand	SM-SW	A-2-4	34	0	0.08	11	NP		1.00	1.34

$\kappa^{(1)}$ = the value calculated from Equation 3

$\kappa^{(2)}$ = the value by best-fit analysis on measured data

The comparisons between values predicted by the Fredlund et al. (1996) and Vanapilli et al. (1996) models and measured values, both from the current research and that reported in the literature, are shown in **Figure 4-3** a and **Figure 4-3** b, respectively. The ability of the two models to estimate the measured apparent cohesion due to suction at increasing levels of matric suction is indicated by the proximity of points to the 1:1 line. Not all the data from the literature were plotted in **Figure 4-3** (b), because the value of the residual water content was not reported in each reference. The Houston et al. (2008) model is not shown here because limitations were found for the SM and SM-SW soils from literature. The SM soil has D_{30} of 0.2 mm, D_{60} of 0.8 mm and 58 percent of sand; the SM-SW soil has D_{30} of 0.2 mm, D_{60} of 0.5 mm and 75 percent of sand. The calculation for the "a" parameter in Equation 5 leads to values of -6.7 for the SM soil and -2.2 for the SM-SW soil. In these two cases, because of the negative values of "a", the equation no longer yields a hyperbolic shape for predicting the increase of total cohesion. In addition, detailed grain size data were not available for other soils in published data in Table 4-2.

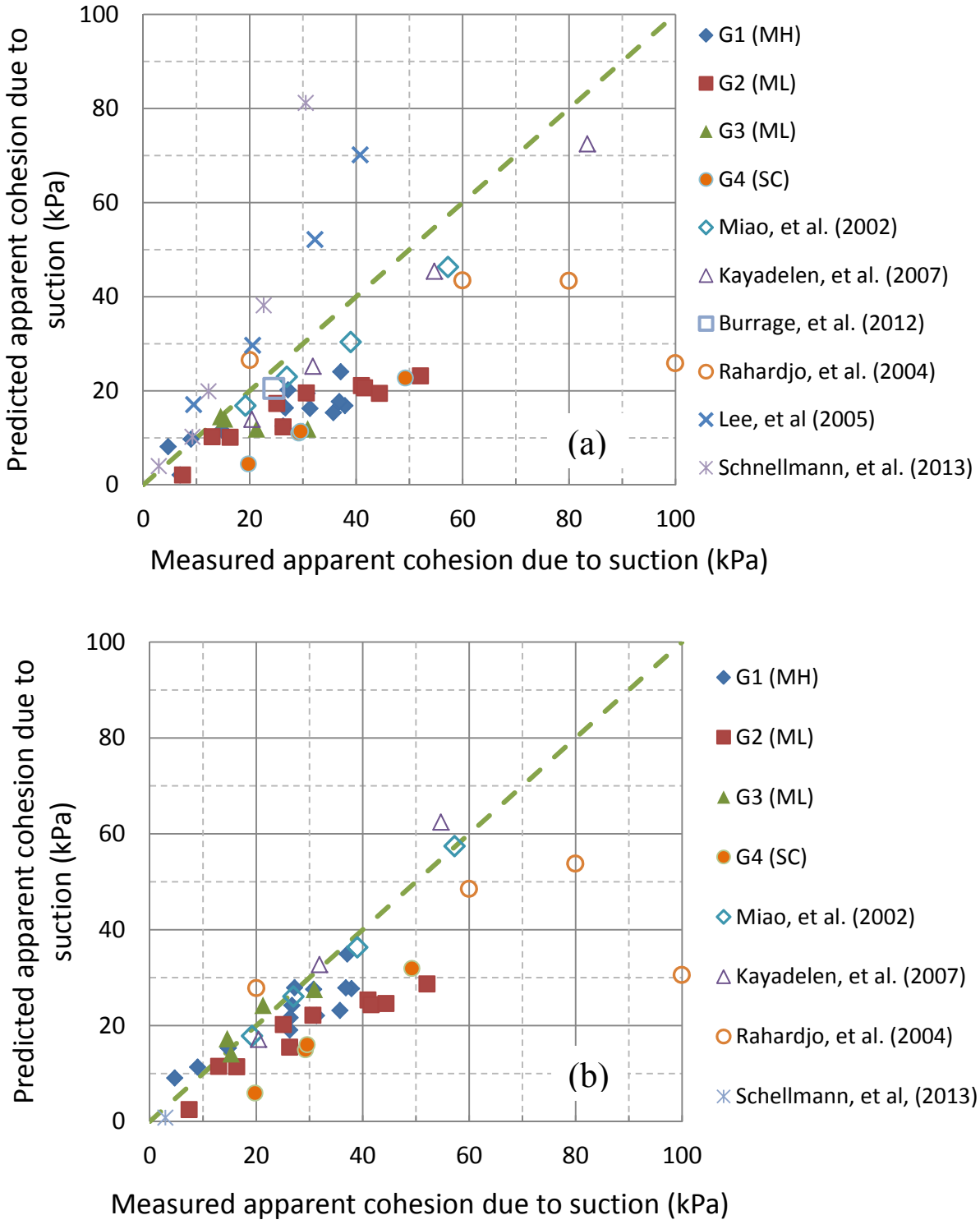

Figure 4-3 Measured versus predicted apparent cohesion due to suction by applying: (a) Fredlund et al. (1996) and (b) Vanapalli et al. (1996) models

In **Figure 4-3** (a), where the Fredlund et al. (1996) model with the κ value provided by Vanapalli and Fredlund (2000) is applied**,** the majority of data fall under the 1:1 slope line; except for the SM and SM-SW soils, for which the apparent cohesion due to matric suction is overestimated. Best-fit lines can also be found by separating the soils into groups on the basis of the PI value. Curve fitting a linear regression line with zero intercept for the two soils with PI of 32% yields a 0.83 slope, which indicates that the model underestimates the apparent cohesion due to suction of this MH soil group by 17%.

Excluding data for the two sandy soils, the model yields results that under-predict the measured values by more than 40%. Accordingly, it seems that the Fredlund et al. (1996) model provides a better prediction when the test soil has a relatively high PI value of 32%, but does not well estimate the increase of apparent cohesion with increasing matric suction for lower PI soils.

Data in **Figure 4-3** (b) show that the Vanapalli et al. (1996) model underestimates nearly the entire data set with a regression slope of 0.8. Not all of the measured data from the literature is shown in this plot due to the lack of having SWCCs presented with the strength data. If only the soils classified as MH are used for the regression analysis, the slope is 1, which indicates on the average an accurate prediction by the model in this type of soil. For the G2 and CL soils from literature, the Vanapalli et al. (1996) model underestimates the increase of apparent cohesion due to matric suction.

4.2. Development of an empirical model

Based on the application of the existing models to the above data, the Fredlund et al. (1996) model predictions showed significant variation from the measured values; the Vanapalli et al. (1996) model requires a good estimation of residual water content; and the Houston et al. (2008) has limitation of input parameters. Therefore, an empirical model to provide more accurate predictions and to be utilized with parameters from conventional soil tests was explored.

Statistical analyses to find the κ values that produced the best-fit with the measured data from this research produced an average R^2 value of 0.9. It can be concluded that the increase of total cohesion can be modeled by determining the fitting parameter, κ, from test data. Therefore, in an effort to improve the quality of total cohesion estimation using the first and third terms of

Equation 4-1, an improved equation for estimating the κ value from measured soil parameters was explored.

The best-fit κ value from each data set was seen to produce a good fit in predicting shear strength via Equation 4-1. Therefore, after obtaining the value of κ for each soil, a regression analysis was performed exploring multiple soil properties as variables in order to obtain a predictive equation for κ. A number of different combinations of parameters were tested, with Equation 4-2 providing the best fit.

$$\tau = c' + (\sigma - u_a)tan\varphi' + (u_a - u_w)[(\Theta^{\kappa})tan\varphi'] \qquad (4-1)$$

$$\kappa = 0.39 \cdot \left(\%\frac{fines}{100}\%\right)^2 + 0.018 \cdot (PI) + 1.33 \cdot \left(\frac{1-PI}{1-LL}\right) \qquad (4-2)$$

This equation utilizes the percentage of fines, PI and a ratio between PI and LL (with all values expressed as whole numbers and values for LL and PI taken as zero for non-plastic soils). The comparison between κ values obtained from best-fit analysis of the test data and the values predicted by Equation 4-2 is shown in Figure **4-4**, as well as values predicted by Method 1. The values of the "best-fit κ" from each data set are shown in **Table 4-2**. The diamond symbols shown in Figure **4-4**, indicate that the use of Method 1 leads to the over prediction of the κ parameter, for the ten sets of data presented herein. However, the solid circles indicate that Equation 4-2 is able to explain the existing variability in the data.

The computed values of κ were then used in Equation 4-1 to predict the suction-induced cohesion. The measured values and values computed on the basis of Equation 4-1, with κ values obtained from Equation 4-2, are compared in Figure **4-5**.

The best-fit line to the entire data set shown in **Figure 4-5** yields a slope of 0.94, which indicates that the computed values slightly underestimate the measured data, with an R^2 value of 0.9. Accordingly, it can be seen that use of the proposed regression equation for predicting κ provides the ability to estimate cohesion values that are consistent with those measured in the 10 data sets presented herein.

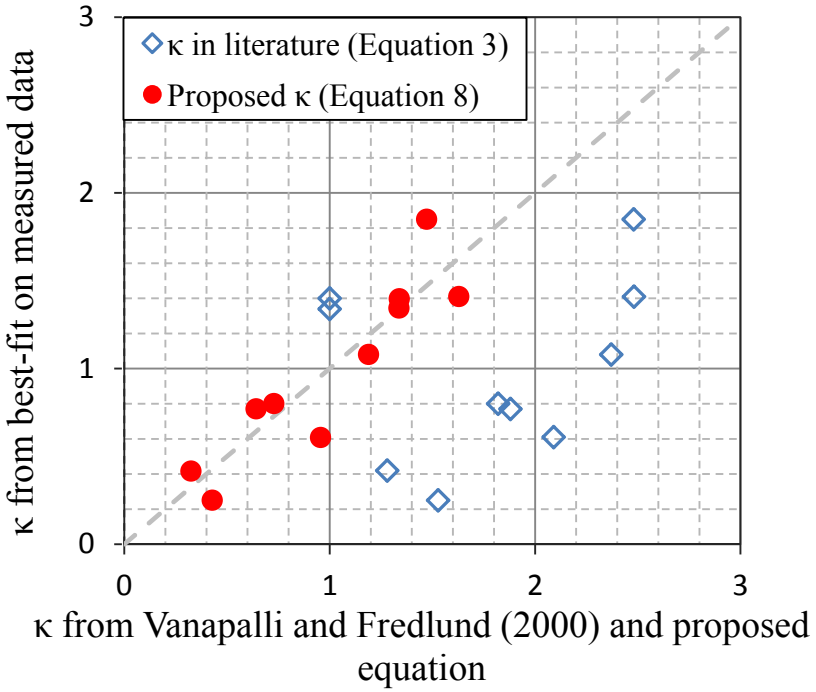

Figure 4-4 κ from best-fit analysis on measured data vs. κ from prediction equations

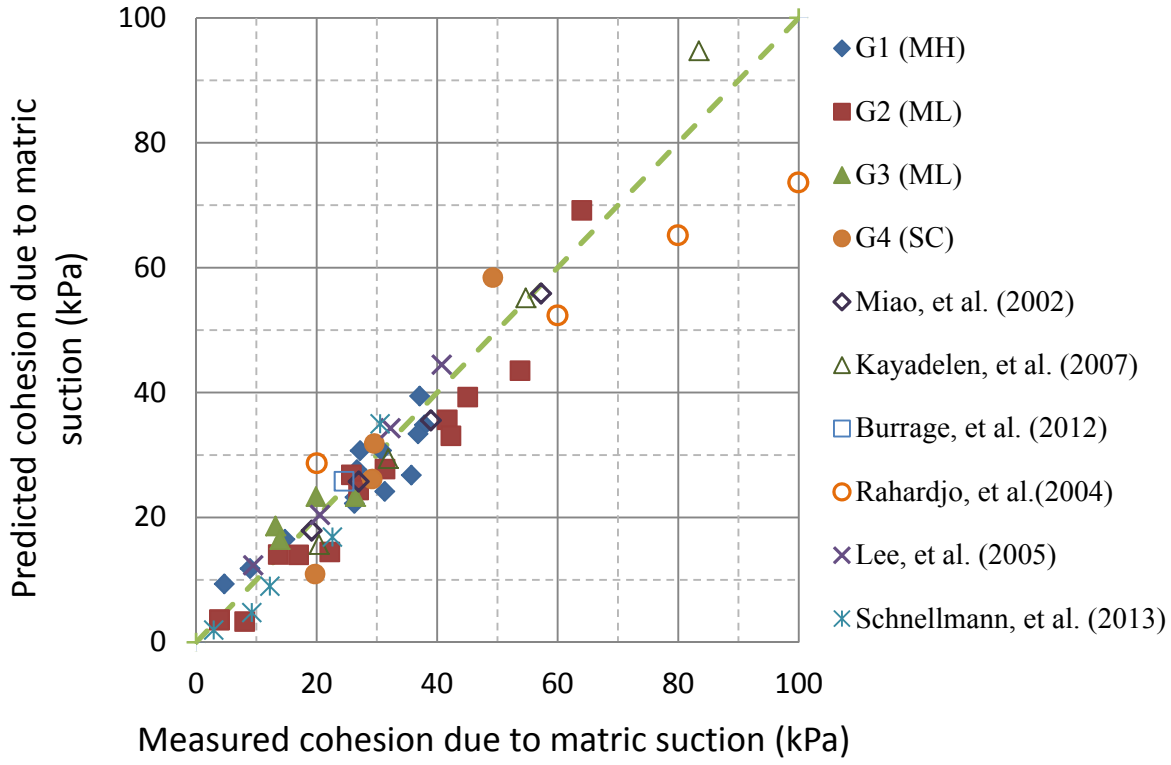

Figure 4-5 Measured versus computed apparent cohesion by the proposed method

4.3. Application of the empirical approach to effective stress concept

The incorporation of matric suction into the effective stress equation is another method for accounting for the effect of matric suction on shear strength. An estimation equation, developed based on the utilization of effective degree of saturation by Lu and Liko (2006), is shown in Equation 4-3. The effective stress concept using Equation 4-3 is presented and compared to the empirical approach, Equation 4-4, presented in the prior section.

$$\sigma'^{*} = \sigma_{Total} - u_a + \left(\frac{S - S_r}{1 - S_r}\right)(u_a - u_w) \qquad (4-3)$$

$$\sigma'^{*} = \sigma_{Total} - u_a + S^{\kappa}(u_a - u_w) \qquad (4-4)$$

*note: σ' in this equation represents effective stress with matric suction incorporated.

Equations 4-3 and 4-4 were used to calculate the mean effective stress, and then p'-q diagrams is plotted for the failure stress points (for the four soil types) as shown in Figure **4-6**. The p' in Figure **4-6** represents both saturated and unsaturated effective stress: in the saturated case, p' was total stress minus pore water pressure, shown as diamond symbols; in the unsaturated case, Equation 4-3 and 4-4 both were applied, shown as square and circle symbols, respectively.

The K_f line in each plot was obtained from saturated triaxial test results. The similar slope based on both the saturated and unsaturated test results indicates the feasibility of the concept of unsaturated effective stress. The pore water pressures generated in CIU tests result in different p' values at failure. The unsaturated triaxial tests are performed as constant matric suction tests, so the p' values have a constant suction stress while shearing.

The two approaches for calculating unsaturated effective stress (Equation 4-3 and 4-4) provide a similar prediction, with each having an advantage. The use of Equation 4-4 does not rely on the measurement or estimation of the residual degree of saturation, and the equation can be utilized by knowing soil properties obtained from basic index tests. For Equation 4-3, a closed-form relationship is developed based on Equation 4-3 and Van Genuchten equation for SWCC model, so the effective stress as a function of matric suction can be obtained by knowing fitting parameters, α and n.

$$\sigma' = (\sigma - u_a) + S_e(u_a - u_w) = (\sigma - u_a) + \left[\frac{1}{(1+(a\psi)^n}\right]^{1-1/n}(u_a - u_w) \quad (4\text{-}5)$$

The use of the effective stress concept has the advantage of providing the ability to be directly inputted as an option in the PLAXIS computing code.

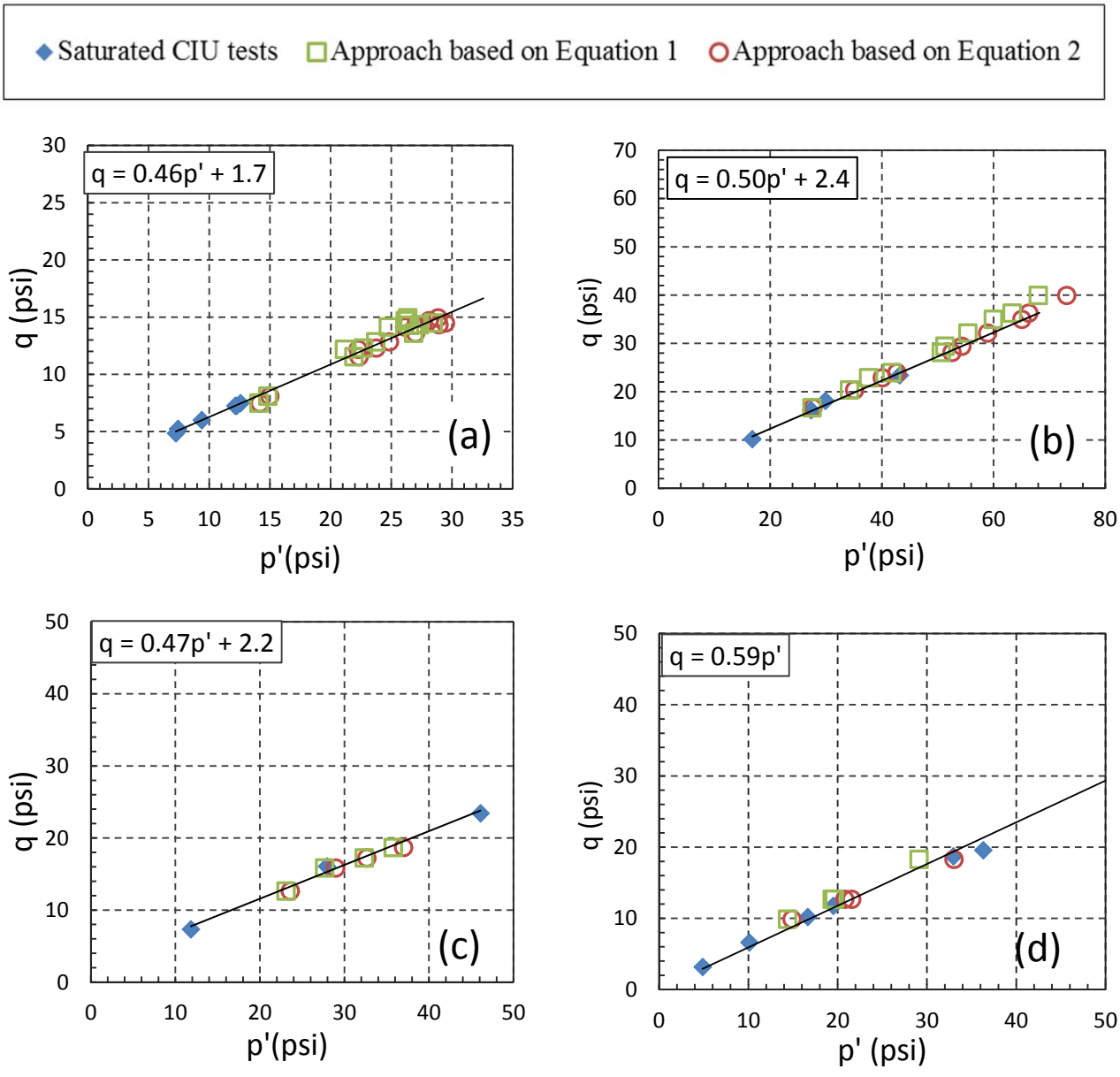

Figure 4-6 MIT p'-q plots of the four soils (a. A-7-5 soil; b. A-4 soil; c. A-5 soil; d. A-2-6 soil)

CHAPTER 5. Unsaturated Slope Stability

5.1. Factor of safety of test slopes with initial suction profile

Slope stability analyses were conducted using SEEP/W and SLOPW/W platforms (GEO-SLOPE International, Ltd.). The initial matric suction distribution within the modeled soil profiles and any subsequent variation induced by infiltration were simulated by SEEP/W. Then, using the generated pore water pressure contours and calculated unsaturated shear strength values, SLOPE/W was used to estimate the FS of the slope according to the Bishop's Method of Slices.

Table 5-1 summarizes the FS for each of the different initial matric suction profile assumptions. As shown, when using the effective shear strength (effective friction angle of 27° and effective cohesion of 10 kPa) but without the inclusion of matric suction, the FS of the 0.25:1 slope is 0.80, which implies failure would have taken place. However, this steep slope remained stable over the three-month project duration when matric suction was included.

Table 5-1 Factors of Safety for Different Initial Matric Suction Profile Conditions

Initial matric suction profile	FS		
	0.25:1 slope	0.5:1 slope	1:1 slope
Measured	1.55	1.75	1.91
Hydrostatic equilibrium from water table	2.01	2.26	2.87
No matric suction	0.80	1.02	0.86

The FS for the 1:1 slope without matric suction is 0.86, which is lower than the FS of the 0.5:1 slope without matric suction, because the upper part of the 1:1 slope consisted of A-2-6 material that has a friction angle of 36 degrees but zero effective cohesion. In this case, the calculated failure surface was close to the slope face; however, in the field, no shallow failure was observed.

When the initial matric suction profile was generated linearly based on the pore water pressure at the bottom of the deepest soil layer, as shown in Table 5-1, the FS was computed to be over 2.0 for all slopes. However, this is due to the significantly over-estimated matric suction values. It is interesting that the tensiometer-measured suction increase (at the zero day, or equilibrium condition) from depths of approximately 9 m to 1.5 m is essentially parallel to the hydrostatic line, but clearly relatively little increase in suction occurred between 15 m and 9 m.

These analysis results and the data generated from this site demonstrate the need for more depth-specific estimations of suction value, either measured or predicted from empirical models, in order to obtain an accurate assessment of stability. Evaporation and surface-water infiltration will certainly affect the near-surface suction values, as evidenced in the initial suction profile.

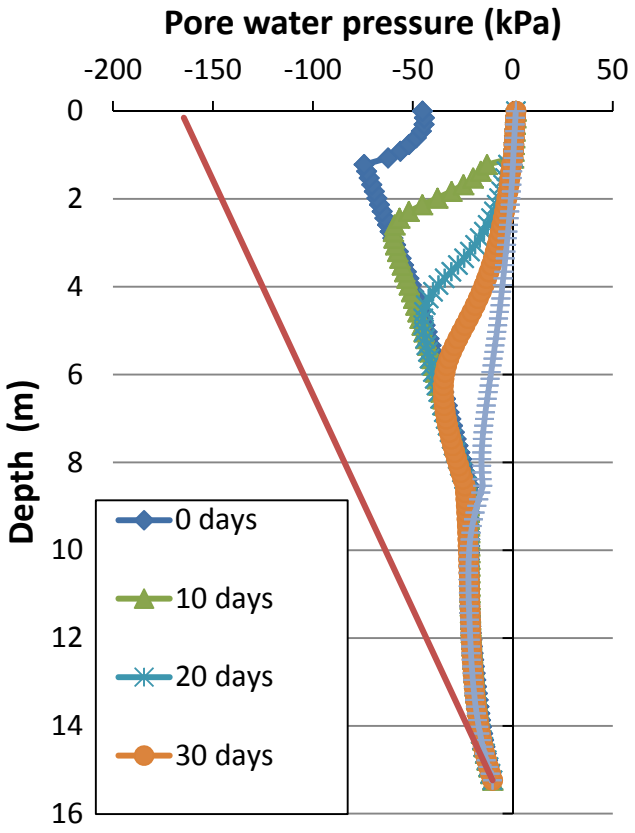

Figure 5-1 Pore water pressure change over time along section A-A' in Figure 5-2 (a)

Results of the numerical analyses, which incorporate field-measured matric suction values, show FS values in excess of 1.5 for even the steepest slope of 0.25:1. As the steep slope was observed to be stable throughout the field monitoring duration of three months, the calculated results seem reasonable, despite the fact that even these results are likely to be considered conservative, as the model-calculated shear strengths values are less than those measured from laboratory tests, as shown in Figure **4-1** (a).

A simple analysis of the measured and predicted strength values over the range of suction values from 25 kPa to 80 kPa that is appropriate for the test slopes suggests that the shear strength values are conservative and underestimated by 1 to 30 percent at 25 kPa and 20 to 85 percent at 80 kPa; thus, an approximate underestimation of the shear strength by 30 percent to 50 percent might be expected.

5.2. Surface-water infiltration

The cut slopes were observed over a period of two months after excavation to a depth of 6.7 m. During the second month, 152 mm of water was added to ponds constructed at the top of the slopes and used to induce the effects of surface-water infiltration. Infiltration analyses were performed using the Van Gunuchten model, with the SWCC parameters shown in Table **5-2**, in SEEP/W to estimate permeability as a function of matric suction. The SEEP/W-generated pore water pressure contours were then used as inputs to SLOPE/W in order to conduct the stability analysis. As infiltration, and therefore wetting, occurred, the degree of saturation increased, resulting in an increase in the soil weight, which also must be considered. The procedure described above for the 0.25:1 slope also was applied for the 0.5:1 and 1:1 slopes.

Table 5-2 Van Genuchten SWCC Parameters for Slopes area

SLOPE angle	Depth (m)	Soil type	θ_s	θ_r	a (1/kPa)	n	m
0.25 : 1	0-1.2	A-7-5 (1)	0.615	0.17	0.098	1.359	0.263
	1.2-8.5	A-7-5 (2)	0.594	0.17	0.022	1.725	0.42
	8.5-15.2	A-4 (1)	0.509	0.038	0.050	1.589	0.37
0.5 : 1	0-1.8	A-7-5 (3)	0.541	0.17	0.165	1.29	0.224
	1.8-4.3	A-7-5(4)	0.611	0.17	0.051	1.706	0.413
	4.3-8.5	A-7-5 (3)	0.541	0.17	0.165	1.29	0.224
	8.5-15.2	A-4 (2)	0.456	0.038	0.057	1.678	0.404
1 : 1	0-3	A-2-6	0.384	0.11	0.752	1.186	0.157
	3-9.1	A-7-5 (5)	0.442	0.17	0.030	1.622	0.383
	9.1-15.2	A-4 (2)	0.456	0.038	0.057	1.678	0.404

Infiltration analyses were conducted using SEEP/W, as previously described, for each of the three temporary cut-slope inclinations (0.25:1, 0.5:1, and 1:1 slopes). In these analyses, the 150 mm water level on top of the slope crest was assumed as constant over time. Figure 5-2 (a) and (b) present the predicted pore water pressure levels after one month and two months of

infiltration, respectively. Figure 5-1 shows the changes in pore water pressure values from the initial matric suction profile at the cross section A-A' after 10, 20, 30 and 50 days of continuous infiltration. The data used to generate the pore pressure contours were then carried over to the stability analysis (from SEEP/W to SLOPE/W) to investigate infiltration-induced changes in the FS over time.

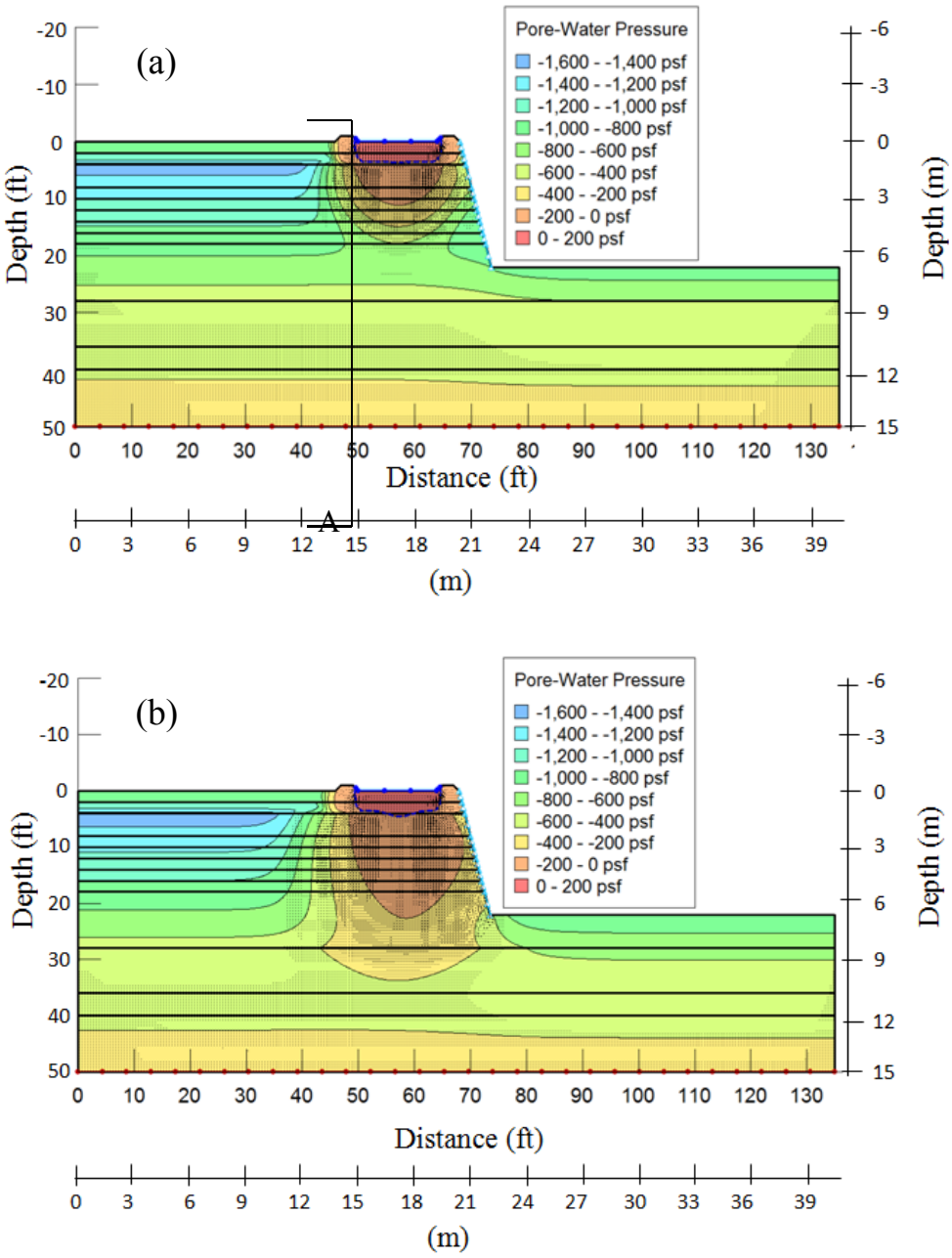

Figure 5-2 Pore water pressure profiles at (a) 30 days and (b) 57 days after adding water to ponds for 0.25:1 slope (100 kPa = 2000 psf)

Figure **5-3** presents the results of the stability analyses. These were performed to represent different times over a three-month period for the 0.25:1, 0.5:1 and 1:1 slopes, although the field infiltration period lasted only one month. After 30 days, the FS for the 0.25:1 slope was found to be close to 1.25. After 57 days of continuous infiltration (a worst-case scenario), the FS reduced to 1.0 for the 0.25:1 slope. Based on the results of similar analyses, an allowable construction period for a temporary slope could be estimated. However, the analysis results reported in this paper would produce a very conservative construction period, because they represent a condition in which a constant 150 mm water level was maintained at the top of the slopes. More site specific analyses could be performed with periods of infiltration followed by periods of evaporation to produce an appropriate design.

As shown by the inclinometer data, the lateral displacement profiles (Figure F-3 in Appendix F) obtained after the 30-day infiltration period show very little additional movement. The magnitude of these seepage-induced changes suggests that one month of infiltration could not induce significant shear deformations within the slopes.

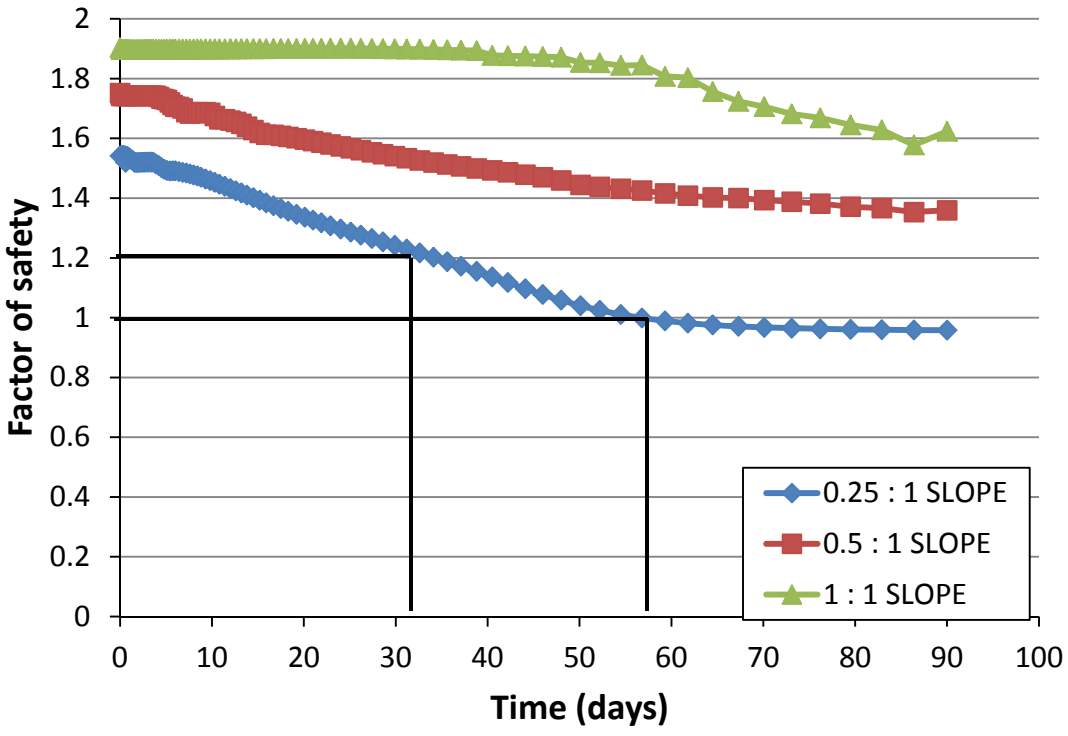

Figure 5-3 Effects of infiltration on slope stability for 0.25:1 and 0.5:1 slopes

From analyses and evaluations presented in this chapter, the following observations can be concluded:

1. Compared to assuming no matric suction, the inclusion of a matric suction profile that decreased from approximately 80 kPa near the ground surface to 25 kPa at the base of a 6.7 m cut in an A-7-5 soil profile caused the calculated FS of 0.25:1 and 0.5:1 slopes to increase from 0.8 to 1.55 and 1.02 to 1.75, respectively.
2. The effect of continuous surface-water infiltration was shown to decrease both the matric suction and the resulting FS, with the 0.25:1 slope FS decreasing from 1.55 to 1.25 after 30 days and to 1.0 after 57 days, while the 0.5:1 slope FS decreased from 1.75 to 1.55 and 1.42 after 30 and 57 days of infiltration, respectively.
3. Predicted shear strength using the Vanapalli et al. model (2000), which incorporates the SWCC via Van Genuchten's model, was shown to under predict the laboratory measured unsaturated shear strength by an average of 30 to 50 percent over the range of matric suction from 25 kPa to 80 kPa applicable to the suction values found in the in situ slopes. The FS would increase by 30 to 50 percent by taking into account the under estimation of the model-predicted strength.
4. Measured inclinometer data 1 m behind the crest of each slope showed lateral displacements less than 0.5 inches, even after one month of surface-water infiltration. After one month, the FS was calculated to be1.25, and could have been 30 to 50% greater, which appears reasonable given the small displacements.
5. The initial matric suction profile generated linearly from the water table produced computed values of FS that were over 2 for all slopes, due to the significantly over-estimated matric suction values. In order to appropriately conduct slope stability analysis, more depth-specific estimation of the suction profile is needed.

CHAPTER 6. Measured Behavior and Modeling of Cantilever Sheet Pile Wall

6.1. Modeling of cantilever sheet pile wall at initial matric suction condition

This section presents the details of the wall data as a case study documenting the performance of a cantilever sheet pile wall installed to a depth of 10.7m below ground surface. After installation, the soil in front of the retaining wall was excavated to a depth of 6.7 m. Numerical analyses of the soil-sheet pile wall system were performed in PLAXIS and incorporated the suction profile based on measured suction data. Assigned parameters were obtained from an extensive site investigation that included laboratory tests, in situ tests, and instrumentation monitoring of the behavior of the sheet pile and soil behind the sheet pile wall. The results of the numerical analyses were validated based on measured data and, subsequently, the lateral earth pressure on the sheet pile wall was estimated.

Background studies are recorded in Appendix G, including Bishop's effective stress concept, hardening soil model, estimation of K_o, unsaturated shear strength, magnitude of stress dependency, m, E_{50}^{ref} for each layer, optimization process used, interface properties and the logic behind the rainfall infiltration analysis.

Model of subsurface profile

Based on the results obtained from the subsurface exploration and laboratory testing program, an idealized profile was developed with 15 discrete layers to a depth of 15 m. **Figure 6-1** shows the geometry of the sheet pile wall used in the analyses; the associated soil properties are recorded in **Table 6-1**. Based on sensitivity trials, the extent to the lateral boundaries from the sheet pile wall was chosen as three times the depth of excavation (6.7m), and the distance to the vertical boundary as two times the depth of excavation (6.7 m). The layers were defined according to the variations in soil properties and the measured initial matric suction values. Each layer was assigned its own SWCC, which was selected based on the soil properties, including dry density, percentage of fines and the PI. The water table was not observed in the upper 15 m of the profile.

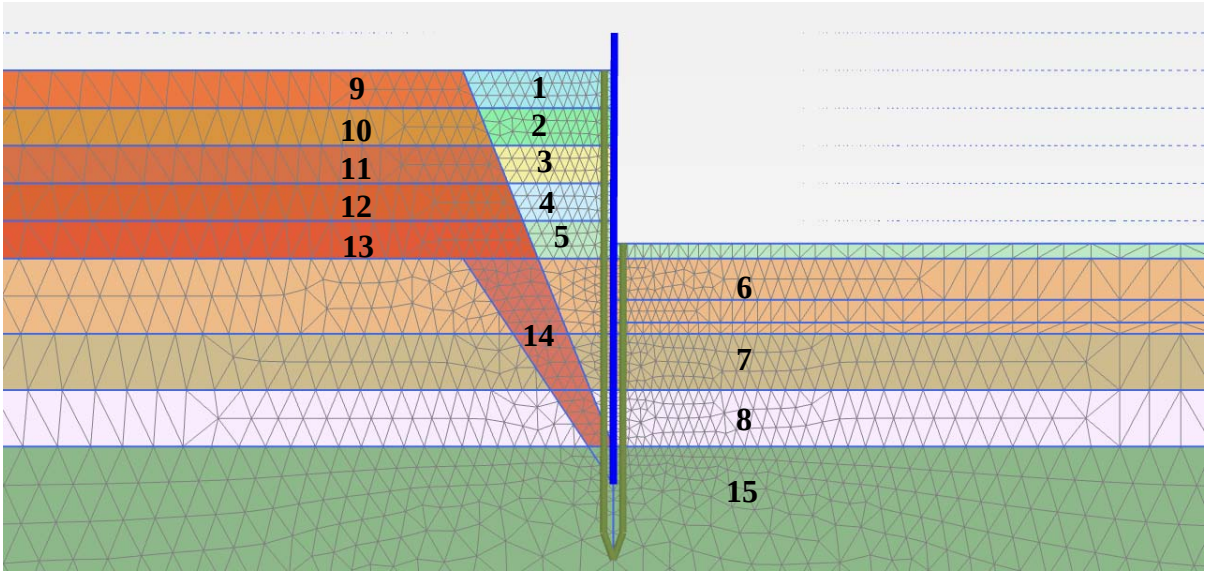

Figure 6-1 Geometry of numerical analysis

Table 6-1 Material Properties for Sheet pile wall area

Layer	Soil type	Layer thickness	γ_{sat}	γ_{dry}	Fines	PI	E_{50}^{ref}	c'	φ'
		(m)	(kN/m^3)	(kN/m^3)	%		(MPa)	(kPa)	(deg.)
1	A-4	1	17	11	61	7	13	0	30
2	A-4	1	17	11	61	7	10	0	30
3	A -4	1	18	13	61	8	15	0	30
4	A-4	1	18	13	61	7	13	0	30
5	A-4	1	18	13	64	6	10	0	30
6	A-4	2	18	13	64	7	14	0	30
7	A-4	1.5	19	14	64	7	7	0	30
8	A-4	1.5	19	14	57	8	19	19	30
9	A-7-5	1	18	13	72	19	8	10	27
10	A-7-5	1	18	13	72	19	7	10	27
11	A-7-5	1	20	16	75	19	10	10	27
12	A-7-5	1	20	16	77	14	10	10	27
13	A-7-5	1	19	14	60	11	7	10	27
14	A-7-5	5	18	13	64	33	9	10	27
15	A-4	10	20	16	57	6	6	19	30

Initial matric suction

Based on an optimization process using measured data, after the 4.6 m excavation stage, an unloading/reloading modulus ratio of 6.0 was determined and applied to the subsequent excavation steps (to depths of 6.1 m and 6.7 m) without considering any changes in the suction profile. The lateral displacements predicted by the numerical analysis matched well the soil displacements measured by the inclinometers behind the sheet pile wall until an excavation depth of 6.1 m was reached. However, as shown in **Figure 6-2**, upon excavation to 6.7 m, the predicted lateral displacements of the soil, especially at 0.6 m and 1.5 m behind the sheet pile wall, are significantly different than that measured.

The predicted and measured lateral deflections of the sheet pile also did not match each other, as shown in **Figure 6-3**. The deflections of the sheet pile wall determined from the numerical analysis were significantly less than that measured, especially after excavation to 6.7 m. Using the initial matric suction profile (no change in matric suction), the shear strength of the soil due to matric suction was large enough to inhibit the development of significant shear deformations in the retained soil mass, according to the numerical analysis results. After the 6.7 m excavation, however, relatively large cracks appeared behind the sheet pile wall in the field where the A-4 soil areas were located. These cracks were evidence of large shear deformations and an indication that the numerical analysis was unable to capture the large shear deformation of the soil behind the sheet pile wall, because the shear strength of the soil as modeled was higher than that actually existing, at that time.

As shown in Figure **6-4**, the maximum bending moments in the sheet pile wall (determined from strain gauges mounted to the back of sheeting sections) after the 4.6 m and 6.1 m excavation depths are seen to be somewhat larger than those predicted by the numerical analysis, with the locations of the maximum bending moments moving downward as the excavation depth increases. After excavation to the 6.7 m excavation, the bending moments were more significantly underestimated in the results of the numerical analysis compared to those determined from the measured data. It appeared very likely that surface-water infiltration over the project duration was influencing the existing suction profile, reducing the soil strength and responsible for increasing lateral deflections and bending moments in the sheeting and that these factors must be included in the analyses.

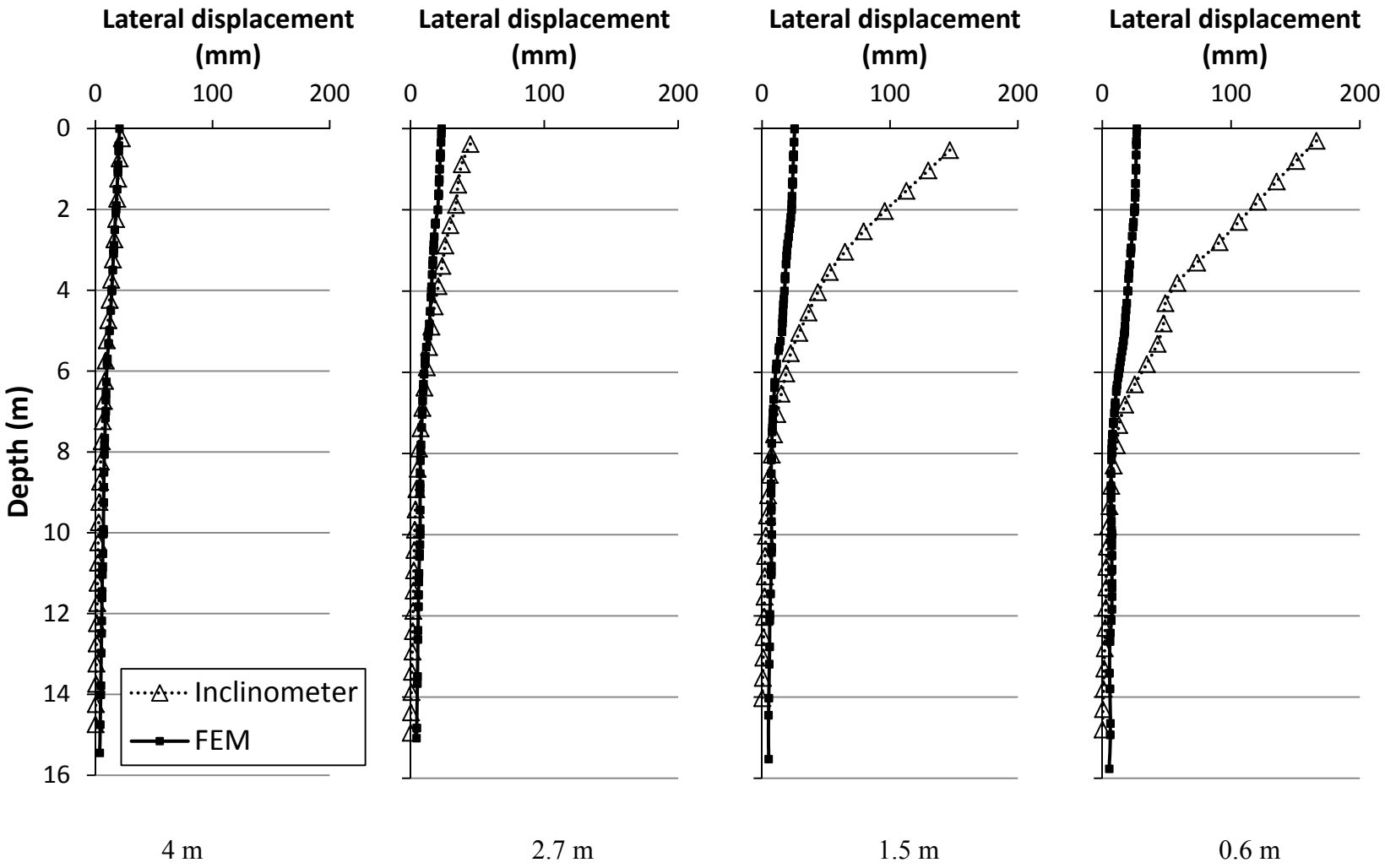

Figure 6-2 Comparisons between measured inclinometer data and numerical analysis results after 6.7 m excavation without suction profile change

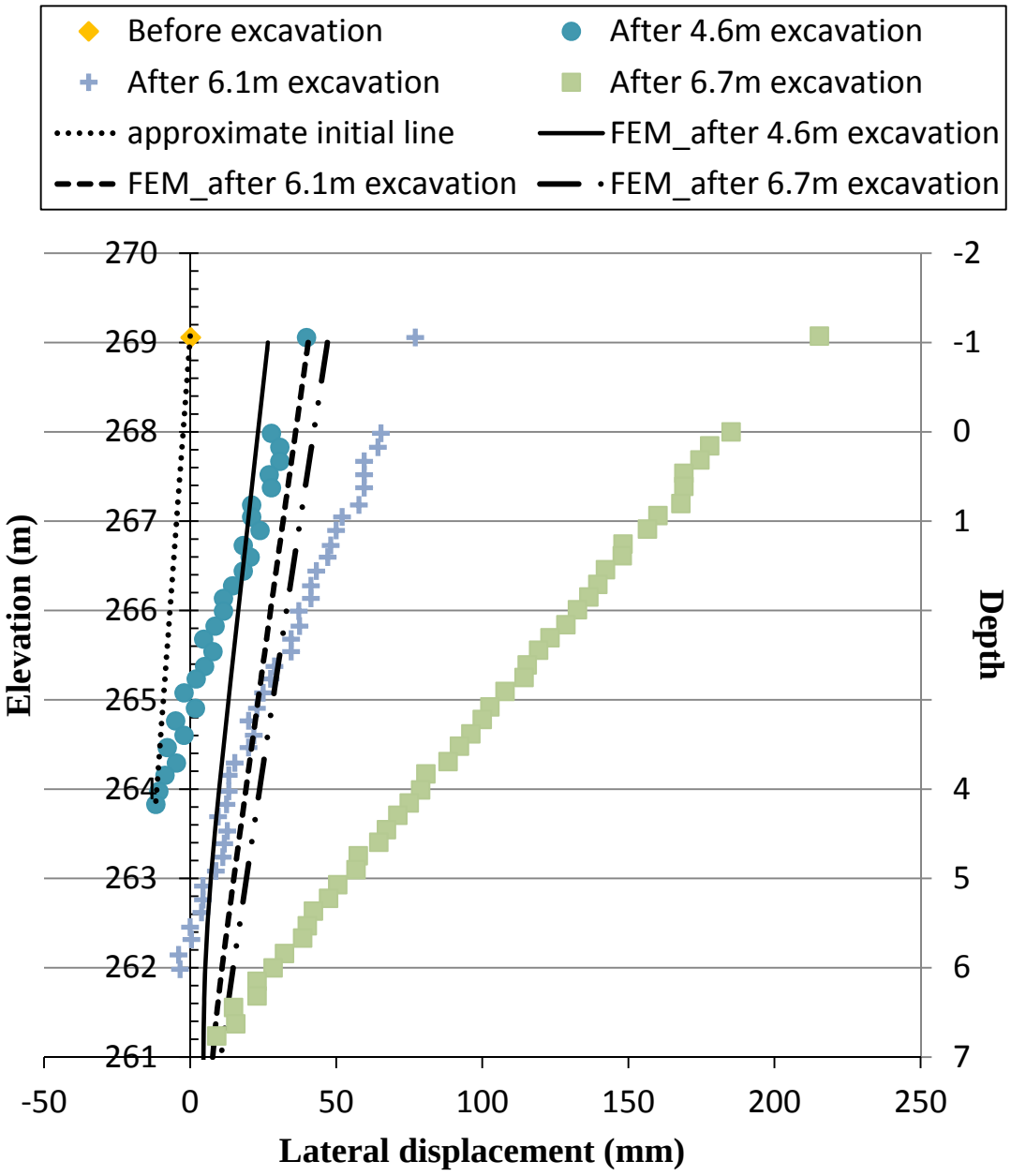

Figure 6-3 Comparison between measured deflections of sheet pile wall and numerical analysis results with initial suction profile

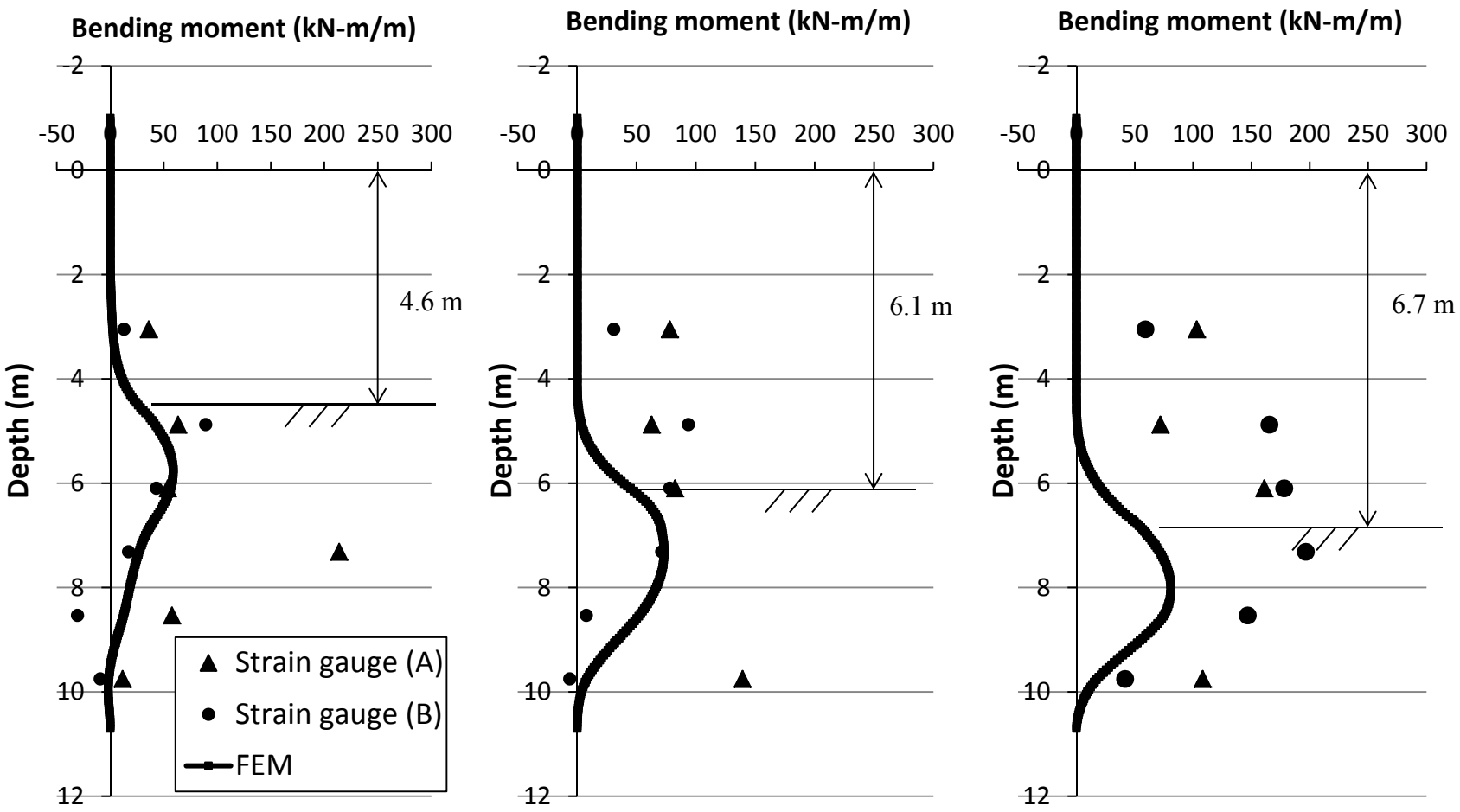

4.6 m excavation 6.1 m excavation 6.7 m excavation

Figure 6-4 Comparisons between measured bending moments and numerical analysis results with initial suction profile

6.2. Modeling of sheet pile wall with the effect of rainfall infiltration

Rainfall infiltration results

Suction profiles were developed using the results of numerical analysis and measured data. The suction profiles for the A-7-5 soil area were developed using runoff coefficients of 0, 0.2 and 0.3, as shown in **Figure 6-5,** with a value of 0.2 found to produce results that matched well with the measured suction profiles at the end of the field work (February 20, 2014). The suction profile for A-7-5 (BH3) could then be estimated over time, as shown **Figure 6-5** (b), with time increments of one month for each stage of excavation.

For the A-4 soil (BH2), where surface cracks were observed, the installed FTC sensor data were used to infer suction profile change over time (**Figure 6-6** (a)). Reduction factors were calculated from the changes in suction value obtained from the FTC sensors (**Figure 6-6** (b)) on June 27, 2014 and were applied to the seepage analysis to develop a new suction profile with infiltration. The calculated reduction factors were only applied to the initial suction profile, and the incremental changes in the suction profile over time were computed (**Figure 6-6** (c)). Especially after the third stage of excavation, the matric suction dramatically decreased over depths from 0 m to 5 m. The monitored field reduction in the matric suction profiles in the A-4 soils was caused by stormwater infiltration through soil cracks and a gap between the soil and sheet pile wall. The FTC sensors captured the reduced suction values, which were close to 0 from depths of 0 m to 5 m after the third stage of excavation. The loss of matric suction led to a decrease in shear strength and modulus values in the A-4 soil and subsequently allowed the development of larger shear deformations.

Suction profile changes over time in front of the sheet pile wall were also taken into account, as analyses showed that the suction in front of the sheet pile affected the deformation of the sheet pile wall. As shown in **Figure 6-7**, over time the suction value changes due to rainfall were estimated using the seepage analyses based on net precipitation, using the same runoff coefficient of 0.2. However, when compared with the measured data, the measured suction values are relatively lower than the predicted values at the end stage of the excavation. This outcome can be explained by the local water retention in front of the sheet pile wall and the fact that suction measurements were taken at the ground surface, which is a sensitive location for suction measurements with the occurrence of ponded water.

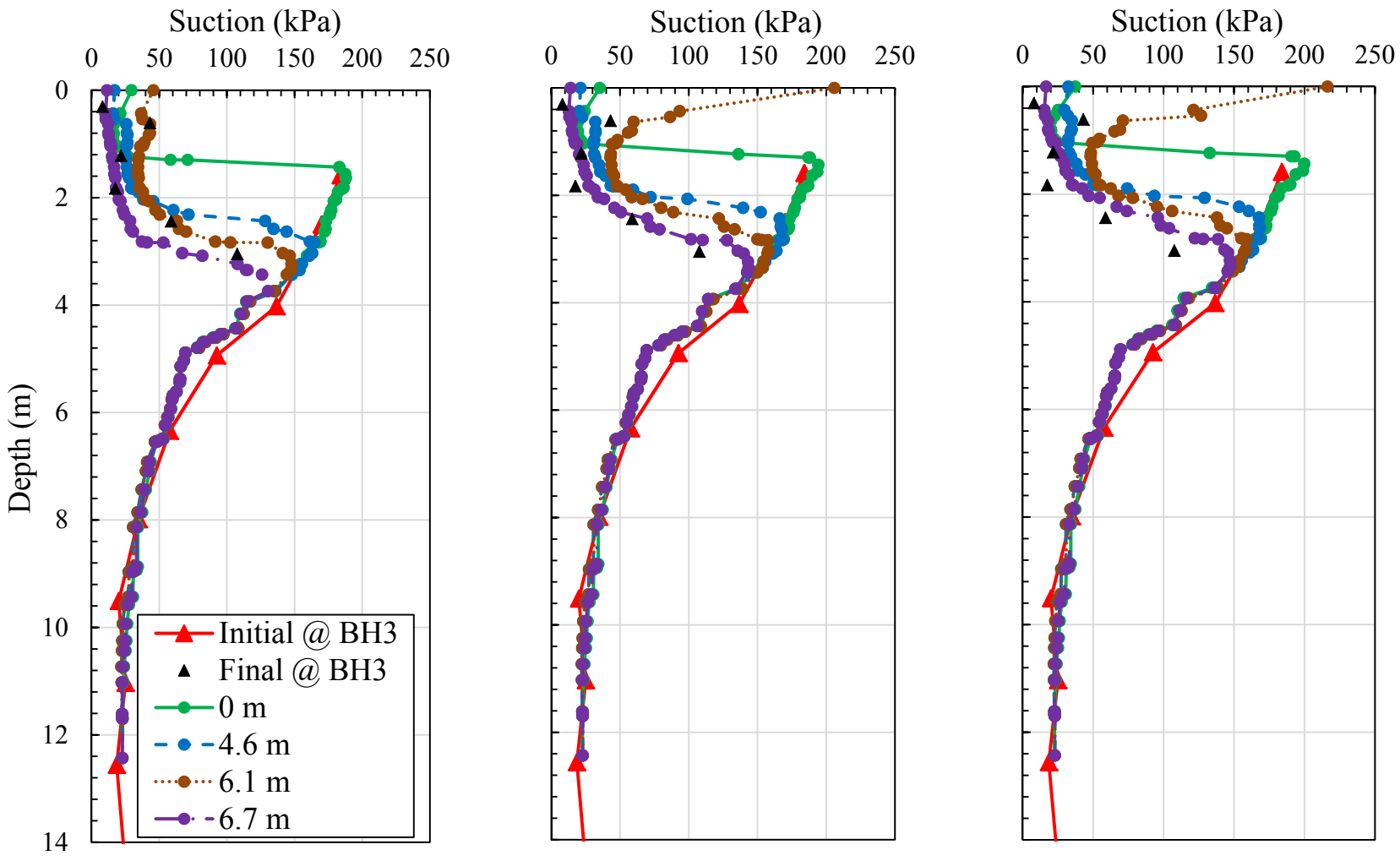

(a) a= 0 (b) a=0.2 (c) a=0.3

Figure 6-5 Matric suction profiles using different runoff coefficients as used for calibration of the net precipitation equation for the A-7-5 soils (BH3)

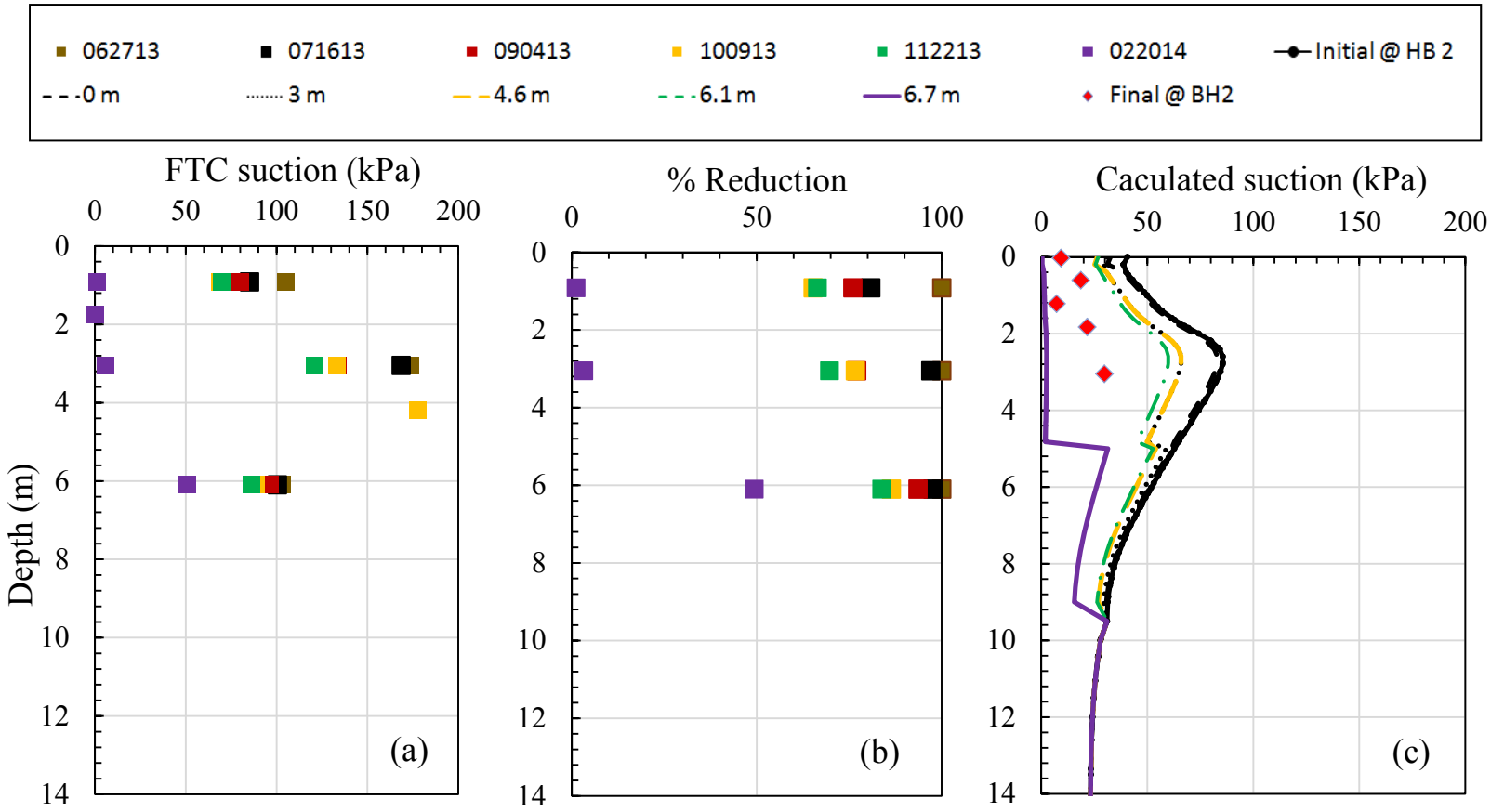

Figure 6-6 Developed suction profiles for A-4 soil (BH2)

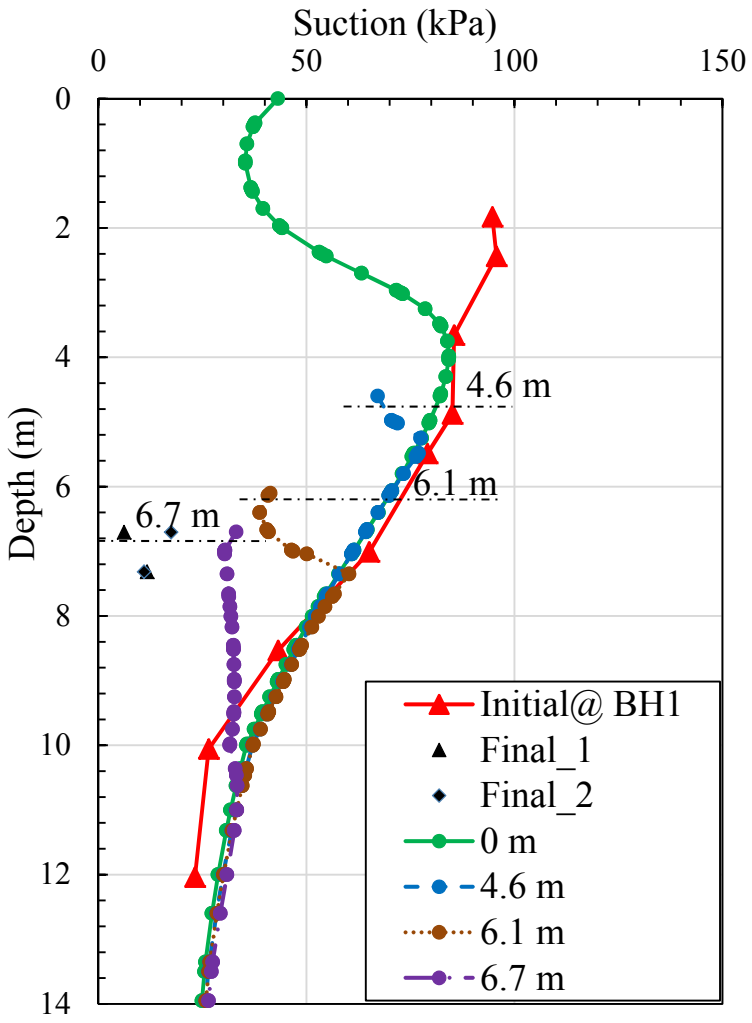

Figure 6-7 Suction profiles in front of sheet pile wall (BH1) during excavation stages

Variation of suction profile over time

The suction profiles that were developed from the infiltration analyses were manually assigned to the numerical deformation analyses. With these revised suction profiles, the results of the numerical analysis after the 6.7 m excavation were seen to match well the measured data.

Figure 6-8 shows the lateral displacement of the soil behind the sheet pile wall after the 6.7 m excavation. The lateral displacements at 0.6 m and 1.5 m behind the sheet pile wall from the numerical modeling match well with the measured inclinometer data. The reduction

in the suction values within the A-4 soil caused significantly larger shear deformations in the retained soil mass during excavation from 6.1 to 6.7 m.

As shown in **Figure 6-9,** the predicted lateral deflection profile of the sheet pile wall also matches well with measured data from LiDAR scans after excavation to the 6.7 m depth. Finally, **Figure 6-10** shows the predicted sheet pile wall bending moment diagram determined from these updated numerical analyses in comparison with the values back-calculated from the strain gauge data. Comparing Figures 6-10 and 6-4, it is shown that the reduction in matric suction which did occur in the field, and was incorporated into the current analyses, enabled the numerical results to more closely approximate the field-measured bending moments. Overall, it can be seen that the results of numerical analyses, which account for appropriate changes in matric suction profile changes over time, can produce lateral deflection and bending moment profiles that match the measured data reasonably well.

6.3. Estimating net pressure diagram for sheet pile wall from PLAXIS analyses

As shown **in Figure 6-8, Figure 6-9 and Figure 6-10**, the measured lateral displacements of the soil behind the sheet pile wall, the deflections of the sheet pile wall and the bending moments in the sheeting determined from the PLAXIS analyses are in reasonably good agreement with the field measured values. This suggests that the numerical model is well calibrated with the measured data. At this stage, the next objective was to use these numerical analyses to estimate a net soil-pressure diagram acting on the sheet pile wall and to validate or suggest a procedure that could be used for design purposes.

Net pressure diagrams for the sheet pile wall were generated based on the total soil pressure acting on both the retained and the excavated soil sides. As shown in **Figure** 6-11, the analyses suggested that no pressure was exerted on the upper parts of the sheet pile during excavation from the ground surface to depths of 4.6 m and 6.1 m, respectively. This behavior can be attributed to the magnitude of the matric suction force within the soil that reduced the lateral pressure on the sheet pile wall.

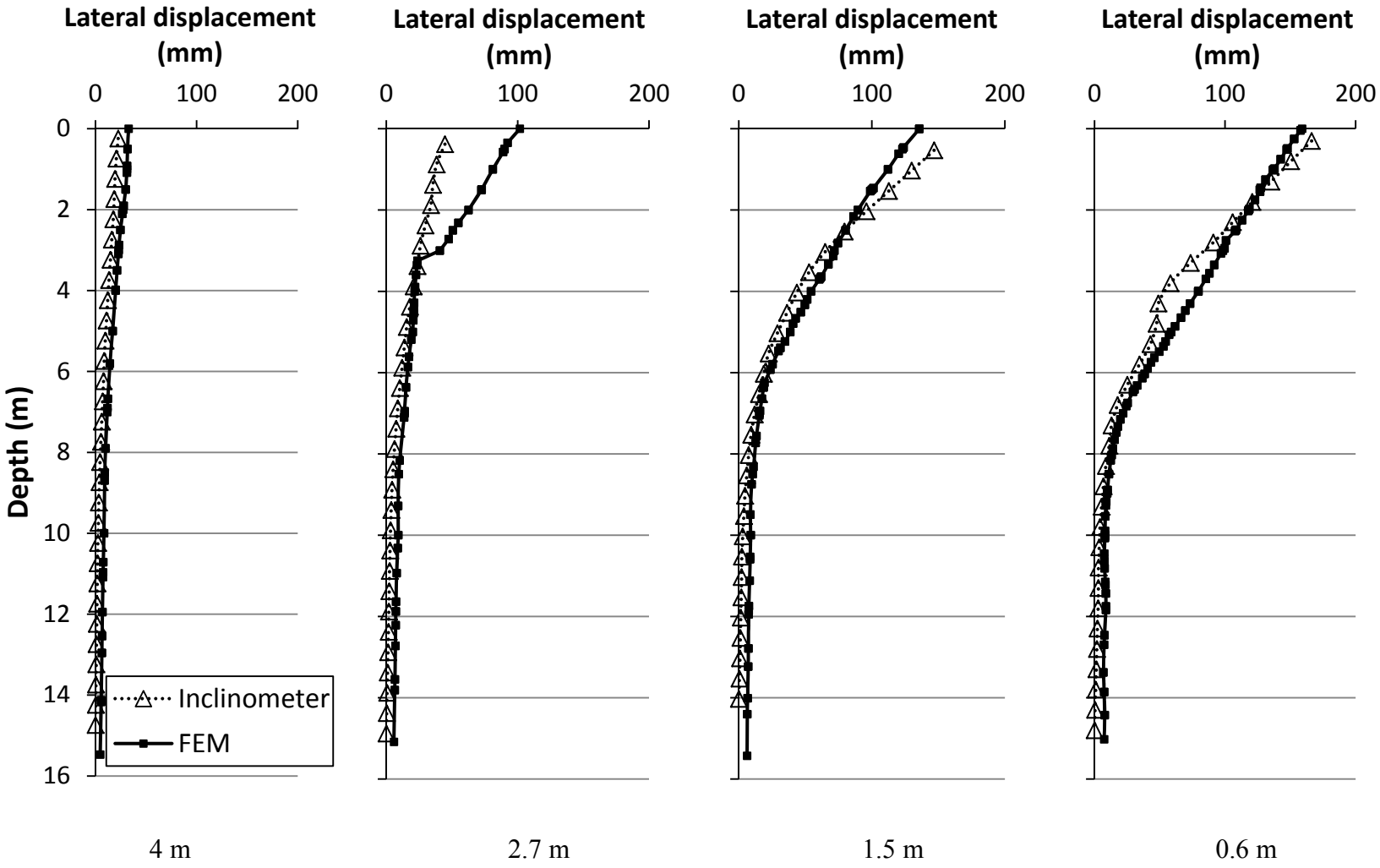

Figure 6-8 Comparisons between measured inclinometer data and numerical analysis results after 6.7 m excavation with suction profile change

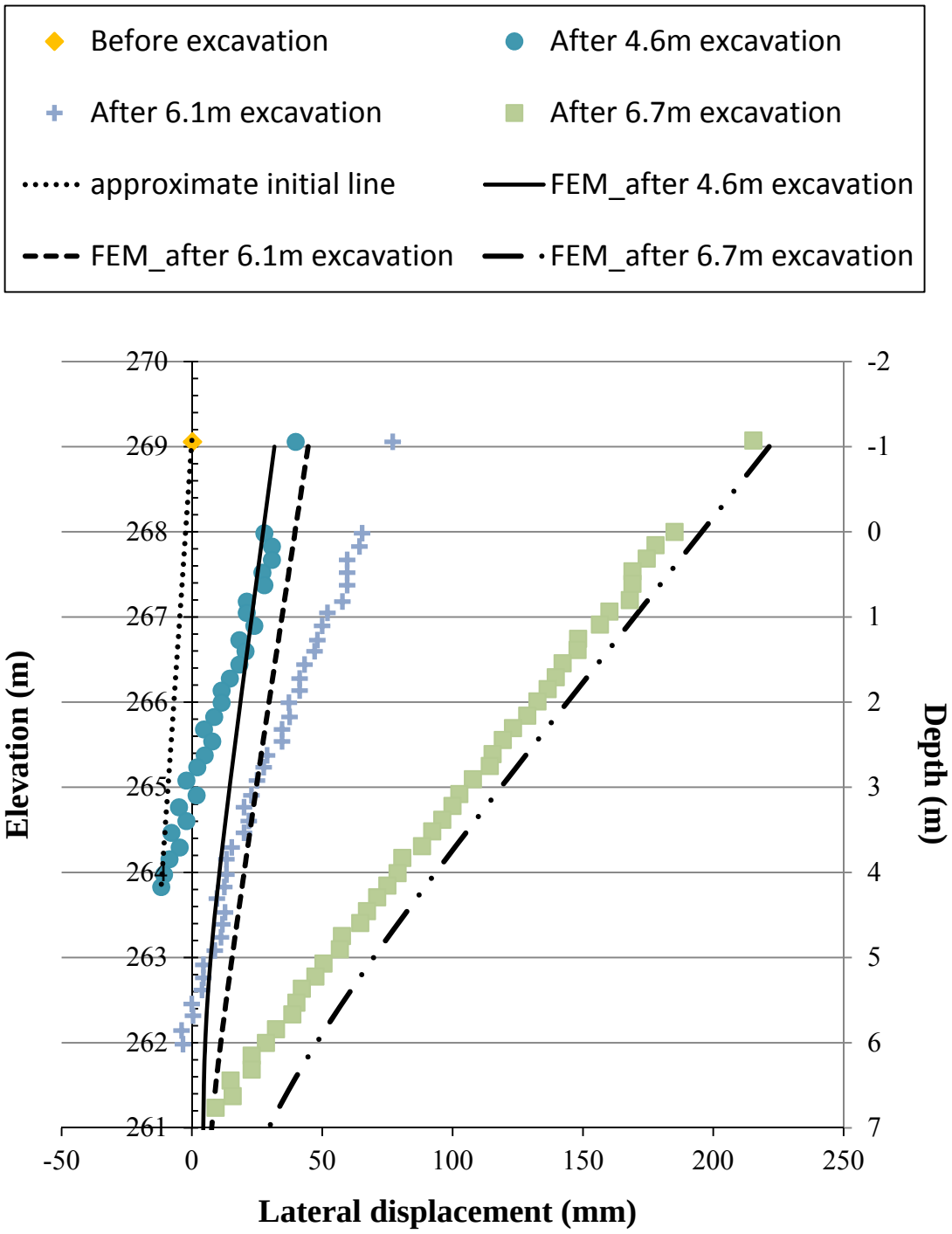

Figure 6-9 Comparison of measured deflections of sheet pile wall and numerical analysis results with infiltration

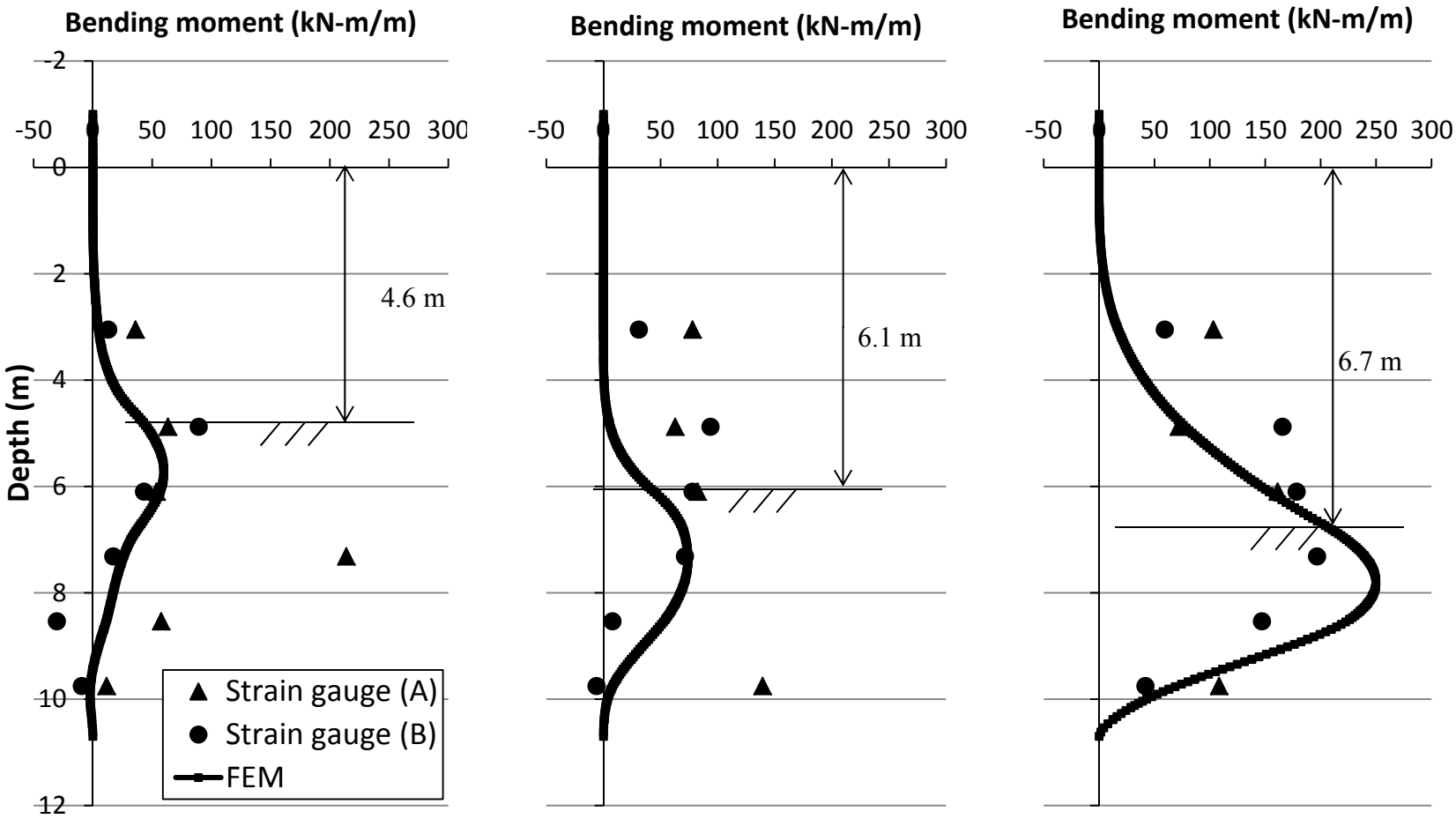

4.6 m excavation 6.1 m excavation 6.7 m excavation

Figure 6-10 Comparisons between measured bending moments and numerical analysis results with suction profile changes

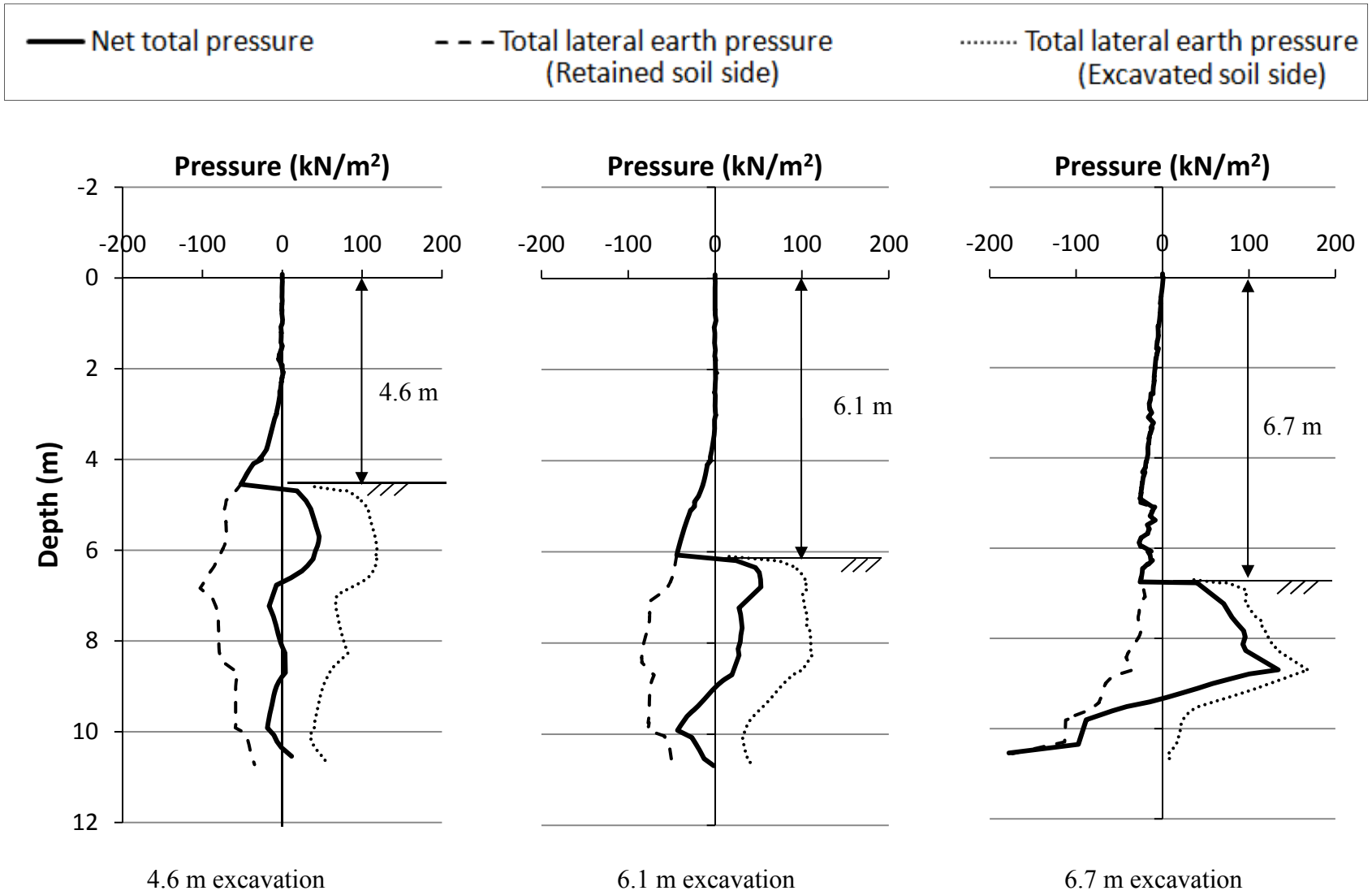

Figure 6-11 PLAXIS-predicted total and net lateral pressures on sheet pile wall with excavation depth

However, after excavation to a depth of 6.7 m, pressure was generated on the sheet pile wall. This response was due to the reduced suction that occurred over time from wetting, which caused increased shear deformation and resulted in the soil pushing against the sheeting.

As shown in **Figure 6-10**, the maximum bending moments in the sheeting increased and occurred at increasing depths below the excavated ground surface as the depth of the excavation increased. Based on the bending moments, the lateral earth pressure could be estimated using the differential equation of the deflection curve, as shown in Equation (6-1).

$$\text{Pressure on sheet pile wall} = \frac{d^2M}{dz^2} \tag{6-1}$$

where M is the bending moment, and z is the depth along the sheet pile wall.

Although the pressure diagram can be estimated using differentiation of the best fit curve to the strain -calculated bending moments, the number of data points was relatively sparse and a few gauges appeared to produce erratic results. Therefore, the field-measured data were used to validate the results of the numerical analyses. Once the bending moments and deflections of the sheet pile wall obtained from results of the numerical analysis agreed with those measured in the field, the bending moments from the numerical analysis were used to estimate the lateral pressure on the sheet pile wall.

Comparison between results of PLAXIS and Lu and Likos approach (2004) to predict lateral pressure on sheet pile wall

The goal of this task was to compare the pressure diagrams generated from PLAXIS and based on measurement data with the pressure diagrams generated using the approach proposed by Lu and Likos (2004). Lu and Likos (2004) proposed the active and passive pressure equations accounting for matric suction based on Bishop's effective stress concept with Rankine's theory as shown in Equations (6-2) and (6-3).

$$\text{Active earth pressure: } \sigma_h - u_a = (\sigma_v - u_a)K_a - 2c'\sqrt{K_a} - \chi(u_a - u_w)(1 - K_a) \tag{6-2}$$

Passive earth pressure: $\sigma_h - u_a = (\sigma_v - u_a)K_p + 2c'\sqrt{K_p} + \chi(u_a - u_w)(K_p - 1)$ (6-3)

Where, $K_a = \frac{1-\sin\phi'}{1+\sin\phi'}$, $K_p = \frac{1+\sin\phi'}{1-\sin\phi'}$, and $\chi = S_e$

However, since the PLAXIS analyses reported thus far have incorporated wall friction, a modification to the proposed equations was required. Therefore, for the purposes of this study, the Lu and Likos equations are used with the Coulomb values for Ka and Kp, with $\delta = 2/3\ \phi$ (thus, K_a = 0.279 and K_p = 5.75). For comparison purposes, the following analyses investigate two different conditions: the first assumes that the initial suction profile remains constant during the excavation process; and the second incorporates the time-dependent changes in suction due to surface-water infiltration previously described. **Figure 6-12** (a) compares the net pressure diagrams developed utilizing the initial suction profile from the results of the PLAXIS analysis to that from the Lu and Likos approach, after excavation to a depth of 9 m, where the FS is approximately equal to 1.

The results from PLAXIS show that the depth of embedded sheet pile, expressed as (D)/ Height of excavation (H), is 26 percent smaller than the D/H obtained from the Lu and Likos approach to obtain a FS=1. This means that excavation to a depth of 9 m requires the embedded depth of the sheet pile wall to be 1.7 m for a FS of 1 based on the PLAXIS analysis, while only 1.3 m is needed for a FS of 1 based on the Lu and Likos approach. Both pressure diagrams show that the pressure on the sheet pile wall down to a depth of 6 m is close to 0, due to the matric suction force that decreases the potential active pressure on the sheet pile wall. Conventional sheet pile wall analysis often calculates the value of *D* required for a FS=1 and then increases this value by 20-40% to provide the desired margin of safety.

Table 6-2 Summary of required D/H for FS=1 (including wall friction)

H (m)	Method	D/H	D (m)	Difference (%)
9 (Fig. 3.19 (a))	PLAXIS	0.19	1.7	26
	Lu & Likos	0.14	1.3	
7.6 w Infiltration (Fig. 3.19 (b))	PLAXIS	0.41	3.1	17
	Lu & Likos	0.34	2.6	

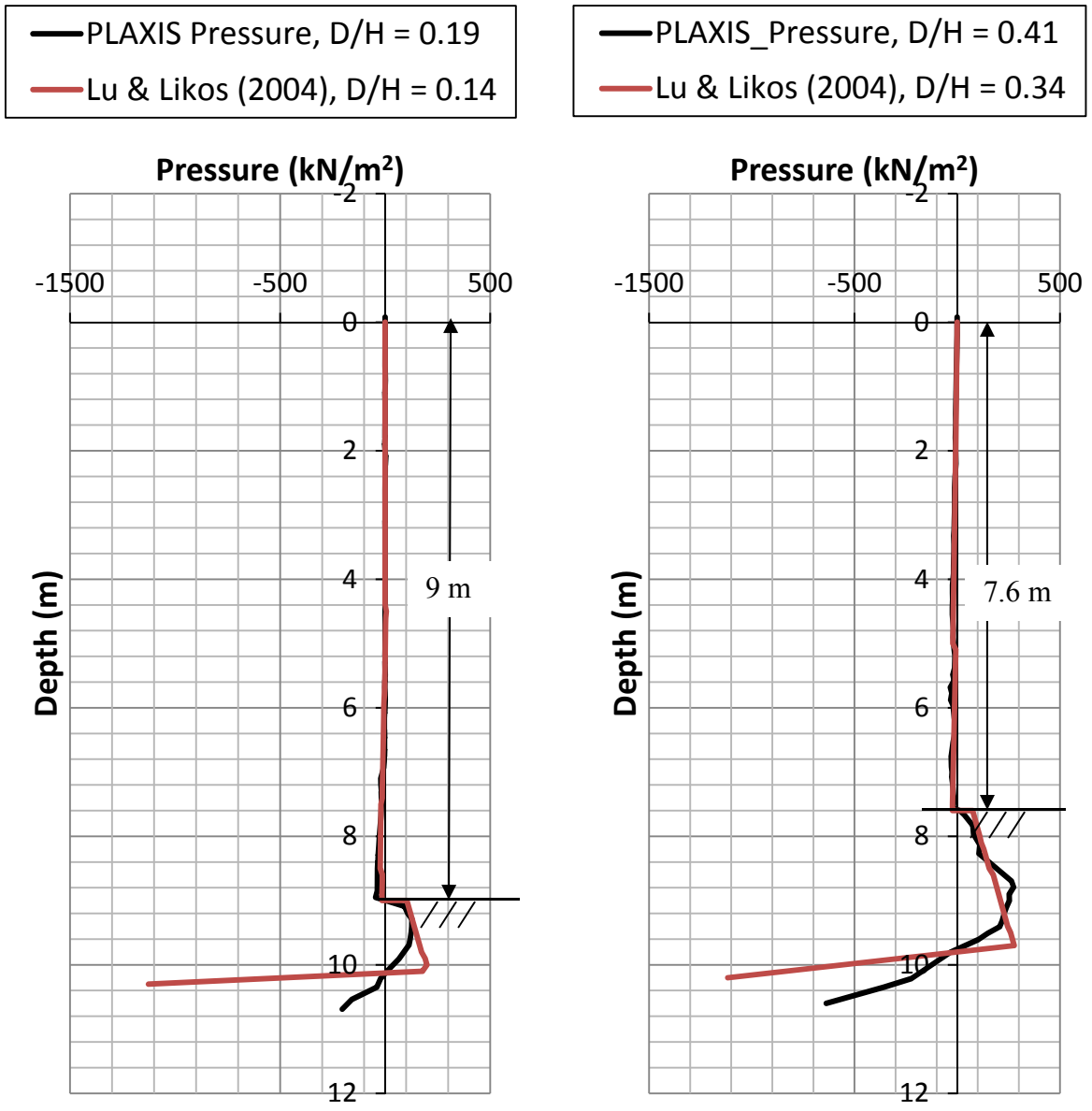

(a) (b)

Figure 6-12 (a) Excavation to 9 m to produce FS=1 with initial suction profile and (b) excavation to 7.6 m depth to produce FS=1 with suction profile at the end of field test (both (a) and (b) include wall friction)

When the detailed infiltration and evaporation analysis over time is performed, as previously described, the suction profile changed for each stage of excavation in the PLAXIS analysis. **Figure 6-13** (b) was developed using the estimated suction profiles existing at the respective times associated with each depth of excavation at the field test site. This figure shows

the pressure diagrams predicted to exist after 7.6 m excavation for the sheet pile wall with a total length of 10.7 m. In actuality, the excavation in the field was not made to this depth, as the calculated FS would have approached 1, and a likely failure condition. The active pressure on the sheet pile wall at a depth of 5 m from the ground surface was generated due to the loss of matric suction that was due to rainfall infiltration. The results of these analyses show that the PLAXIS-calculated required D/H (incorporating wall friction) for a FS=1 is 17 percent larger than the D/H obtained from the Lu and Likos approach.

As the Lu and Likos approach was proposed to develop the net pressure diagram based on Rankine theory, which assumes that the wall friction is zero, a comparison between this method and the PLAXIS results incorporating wall friction is presented. **Figure 6-13** (a) and (b) show the pressure diagrams without wall friction in the Lu and Likos analysis. As shown in Table 6-3, without considering wall friction, the resistance in the passive zone decreases significantly and the required embedded length of the sheet pile wall increases by 95 percent and 61 percent, respectively, for the 9 m and 7.6 m excavation analyses presented in **Figure 6-13** (a) and (b). These results indicate that, should one choose to use the simplified Lu and Likos approach without considering wall friction, the design of the sheet pile wall will be considerably more conservative than the actual field-measured performance of the monitored sheet pile wall would suggest is necessary.

Table 6-3 Summary of D/H without considering wall friction

H (m)	Method	D/H	D (m)	Difference (%)
9 (Fig. 3.20 (a))	PLAXIS	0.19	1.7	95
	Lu & Likos	0.37	3.3	
7.6 w Infiltration (Fig. 3.20 (b))	PLAXIS	0.41	3.1	61
	Lu & Likos	0.66	5.0	

Influence of suction profile change on pressure diagram

Recalling **Figure 6-5** and **Figure 6-6**, the suction in the near-surface soils is seen to decrease over time with surface water infiltration, eventually approaching a value of zero. One can also see in these figures that there is a rather sharp transition from the low suction values to the initial suction profile values, at the depth of the wetting front. In the PLAXIS analyses, these

variations over time were explicitly incorporated. Should one choose to use the Lu and Likos calculated lateral earth pressures and a conventional sheet pile design approach to determine the required depth of embedment, a way of incorporating infiltration-induced reductions in the suction stress is needed.

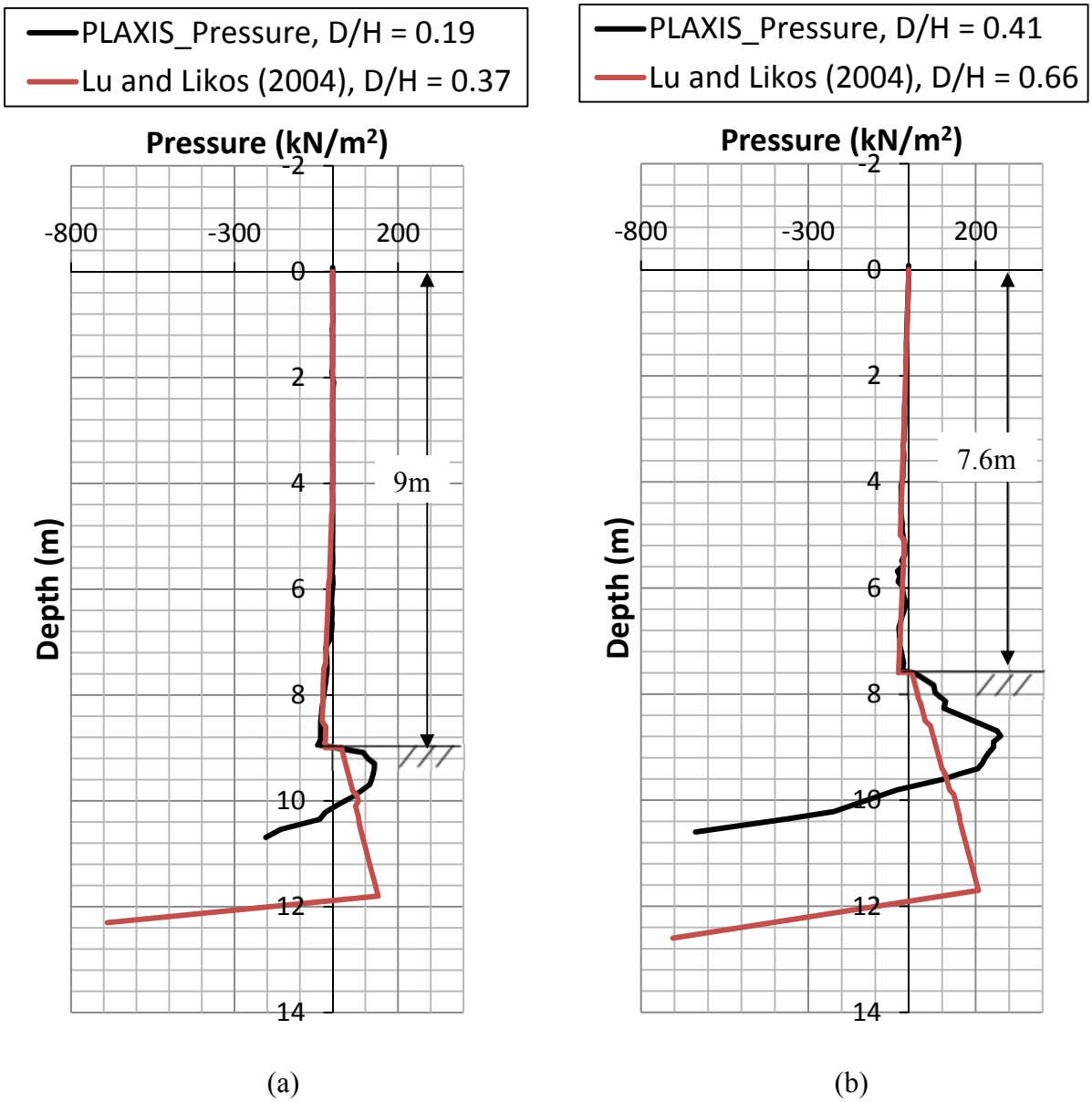

(a) (b)

Figure 6-13 (a) Excavation to 9 m to produce FS=1 with initial suction profile and (b) excavation to 7.6 m to produce FS=1 with suction profile at the end of field test (without considering wall friction in Lu and Likos approach)

In order to approximate the observed reductions in suction, a simplified approach is explored herein, where the initial suction profile is modified by setting all suction values above a certain depth equal to zero. This depth of infiltration, D_i , represents the depth to which the matric suction is zero, and is applied to the retained soil side. As the depth of the saturated zone increases, the required embedded depth of the sheet pile wall to produce a FS=1 increases, as shown in **Figure 6-14**.

However, if one compares the results presented in these analyses with those presented in **Figure 6-13** (b), a difference in the required D/H for a FS=1 is seen. The prior analyses suggested that D/H needed to be 0.41 to produce a FS=1, while the current analyses suggest 0.36. The reason for this difference is that in the prior analyses infiltration on the excavated soil surface was also taken into account, while in the current analyses the initial suction value of 65 kPa at the depth of 7.6m was maintained constant. This suggests that design decisions must also be made regarding appropriate suction losses to incorporate on the excavated soil side, not just the retained soil side.

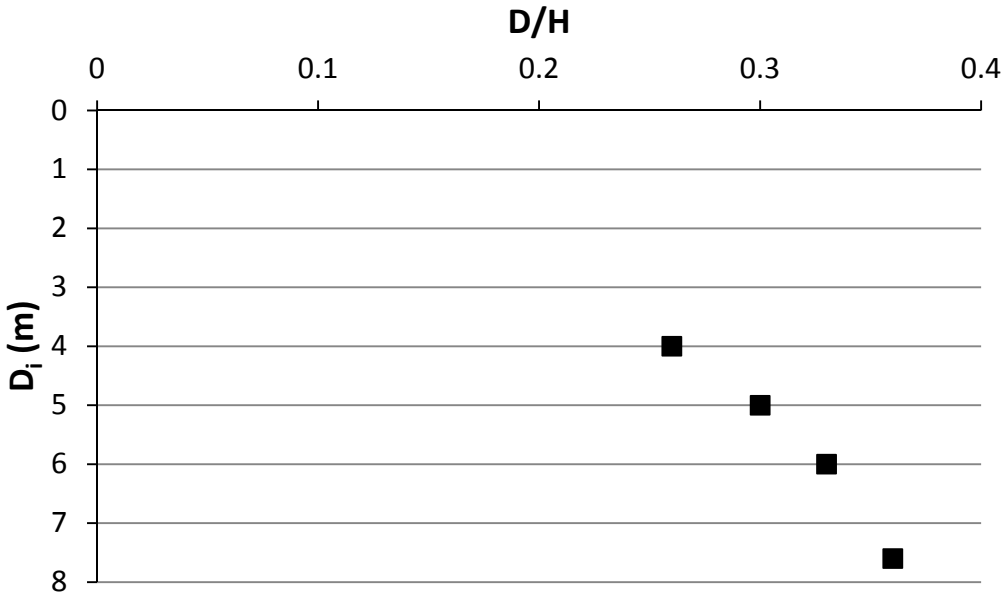

Figure 6-14 D/H required for a FS=1 as a function of infiltration depths (Di) for excavation to a depth of 7.6 m.

The integration of field measurements with the numerical analyses discussed in this Chapter and in Appendix G, produced the following observations:

1. Based on the optimization process for the unloading/reloading modulus ratio $E_{ur}^{ref} / E_{50}^{ref}$, used as input to PLAXIS, a reasonable value of the ratio was determined to be 6.0.
2. Based on regression analysis, the relationship between E_{50} from unsaturated triaxial tests and modulus values from PMTs, was found to be: $E_{50} = 0.76 \cdot E_{PMT}$. The at-rest lateral earth pressure coefficients (Ko_ψ) as a function of depth can be determined by considering the matric suction profile and the total lateral pressure obtained from the PMT. The Ko_ψ values for the Greensboro test site ranged from 0.4 to 2.1.
3. It was possible to develop a suction profile based on measured data and calculated net precipitation (from weather records) in conjunction with deformation analyses of the soil behind and in front of the sheet pile wall. The suction values in the A-4 soil area (BH2) decreased to zero over the depth from 0 m to 5 m after excavation to 6.7 m because rainfall infiltrated surface soil cracks and the gap between the sheet pile wall and soil.
4. The measured lateral displacement of the soil at 0.4 m behind the sheet pile wall was observed to be 170 mm, and the lateral deformation of the cantilever sheet pile wall at the ground surface was 200 mm after the 6.7 m excavation step. The numerical analyses accounting for the suction decrease in the A-4 soil produced both soil deflections and sheet pile wall deflections that were in reasonable agreement. This outcome indicates that the loss of matric suction over the upper 5 m of the profile caused reduced shear strengths and significant shear deformations and reduced the modulus values, which subsequently generated the larger displacements. The numerical modeling produced results that matched reasonably well the measured deflection data and strain gauge calculated bending moments of the sheet pile wall.
5. After verifying the numerical analyses with the soil and sheet pile wall measured deformations, a net lateral earth pressure diagram was produced. The predicted bending moments in the sheet pile wall also were validated by comparing them to the calculated bending moments determined from the measured strain-gauge data. The net pressure

accounted for the matric suction profile in the soil mass and the approach described can be used in the design of temporary excavation support systems.

6. The results of PLAXIS analyses predicted values of D/H required to reach a FS of 1 on the order of 26 and 17 percent smaller than the values obtained using the Lu and Likos approach, for an excavation depth of 9 m with initial suction profile and an excavation depth of 7.6 m with suction profile predicted to exist at the end of field test, respectively, when wall friction is incorporated in calculating Ka and Kp.
7. If one uses the Lu and Likos approach without incorporating wall friction, the resulting depths of embedment will be on the order of 95 and 61 percent greater than that determined from numerical analyses and confirmed by the performance of the field test wall for an excavation depth of 9 m with initial suction profile and an excavation depth of 7.6 m with suction profile predicted to exist at the end of the field test, respectively
8. Analyses showed that the suction profile on the excavated side of the sheet pile is important to the design of a temporary retained wall system, and appropriate reductions in suction due to anticipated surface water infiltration is required. These results also suggest that grading sites to divert water away from both the top of the retained soil side and the bottom of the excavated soil wall face will enhance the matric suction strengthening effect.

CHAPTER 7. Proposed Design Method for Cantilever Sheet Pile Walls

7.1. Factor of safety analysis of Greensboro test wall

In order to explore the reduction in FS that occurs with increasing depth of excavation, analyses were conducted for the monitored cantilever sheet pile wall system. The "safety calculation method" provided as an option in PLAXIS was used. This method computes the global safety factor using the "phi/c reduction approach", in which the strength parameters, $\tan\phi'$ and c', of the soil are successively reduced at the same ratio until failure of the structure occurs, or instability prevents numerical convergence. For the application of this approach in unsaturated soil conditions, the suction-strength term is also decreased by the same ratio, as the term contains the $\tan\phi'$ value, as shown in Equation (7-1).

$$F.S = \frac{c' + (\sigma_n - u_a)\tan\phi' + (u_a - u_w)S_e \tan\phi'}{c_{failure}' + (\sigma_n - u_a)\tan\phi_{failure}' + (u_a - u_w)S_e \tan\phi_{failure}'} \quad (7\text{-}1)$$

Based on the measured initial suction profile for April 10th, as shown in **Figure 7-1**, and the suction profile changes predicted due to rainfall infiltration, FS values were calculated as a function of excavation depth. The conditions for which these analyses were performed, including the time after initiation of excavation, and the resulting values of FS are tabulated in **Table 7-1** and plotted in **Figure 7-2**. The FS is seen to decrease nonlinearly with excavation depth.

The solid circles displayed in **Table 7-1** represent the first case, in which the initial suction profile is maintained constant over time. Excavation Stage 1 in **Table 7-1** indicates a FS of 5.25 after 3 m of excavation, for a sheet pile total length of 10.7 m (D/H=2.57). Excavation Stage 4 shows a FS of 1.93 after 6.7 m of excavation, which represents same height of excavation as the final field condition. After 9 m of excavation (D/H = 0.19), defined as excavation Stage 9, the FS is 1.13. The rate of decrease in FS is seen to change abruptly after the 7 m excavation depth because the 80 kPa suction layer in front of the sheet pile wall was excavated, and below the 7 m depth the suction value is approximately 40 kPa. It can be observed that the change in suction values on the excavated side, as well as the depth of the excavation, significantly influences the FS.

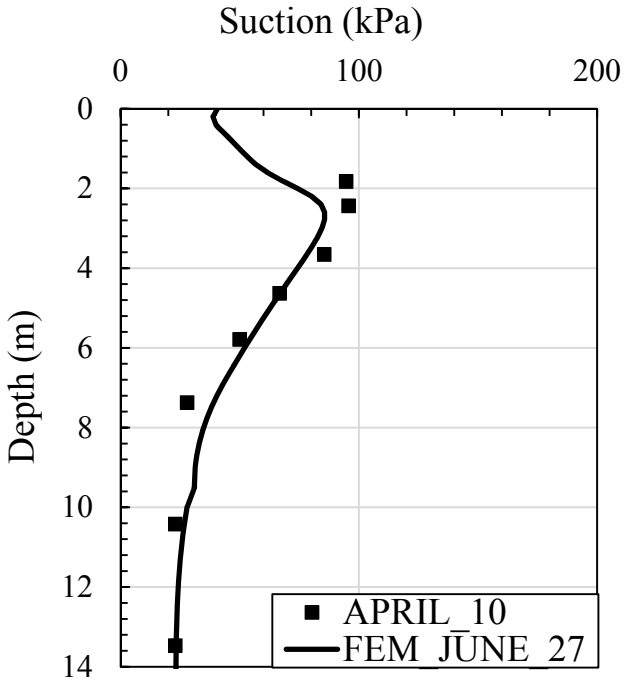

Figure 7-1 Initial suction profile for A-4 area (BH2)

The second case, which is represented by the open triangles and solid squares, explores the influence of surface water infiltration (the net of precipitation minus evaporation) and modifications to the matric suction profile on resulting values of FS. The open triangles describe the condition just after excavation to a given depth and take into account the suction profile changes just prior to excavation based on the infiltration analyses. The solid squares represent the resulting FS after the noted additional infiltration period is completed. Excavation Stage 4 in **Table 7-1** shows FS of 1.73 for the open triangle case, which represents 6.7 m excavation (D/H=0.6) with the suction profile corresponding to that existing at the moment after the excavation. The solid square represents a FS of 1.28 with the suction profile which was developed after three additional months of infiltration, which was the same condition experienced at the field test site previously described. During the three month simulation, the FS was calculated to have decreased from 1.73 to 1.28 due to the loss of suction caused by rainfall infiltration. The FS is generally seen to decrease after a period of infiltration, except for the one-month period after the 6.1 m excavation depth (Excavation Stage 3), because during that period the amount of rainfall was relatively small and evaporation was dominant, which caused essentially no change in the matric suction profile and therefore the resulting FS.

The final part of the infiltration simulation is represented by the open squares. In Stages 5 and 6, excavation proceeds to 7 m (D/H =0.53) and 7.6 m (D/H =0.41), respectively, while the suction profile from the end of Stage 4 is maintained unchanged. These analyses were performed to find the excavation depth at which the FS approached 1, while still maintaining convergence (a FS=1.05 was obtained) for D/H= 0.41.

Comparing the FS values obtained using the initial suction profile with those analyses incorporating infiltration, it is estimated that infiltration causes the FS to decrease more rapidly at greater excavation depths. This result is due to the infiltration-induced loss of suction and resultant decrease in shear strength of soil surrounding the sheet pile wall.

Table 7-1 Summary of FS analyses for excavation stages

Excavation Stage	Depth, H (m)	D/H	Symbol	Analysis	Time* (months)	F.S	Period of infiltration
1	3	2.57	●	1	0	5.25	None
2	4.6	1.33	●	1	0	3.21	None
			Δ	2	4	3.02	4 months
			■	3	6	2.91	2 additional months of infiltration @ 4.6 m depth
3	6.1	0.75	●	1	0	2.23	None
			Δ	2	6	2.03	6 months
			■	3	7	2.00	1 additional months of infiltration @ 6.1 m depth
4	6.7	0.60	●	1	0	1.93	None
			Δ	2	7	1.73	7 months
			■	3	10	1.28	3 additional months of infiltration @ 6.7 m depth
5	7	0.53	●	1	0	1.65	None
			□	2	10	1.20	No additional months of infiltration after 6.7 m depth
6	7.6	0.41	□	1	10	1.05	No additional months of infiltration after 6.7 m depth
7	8.5	0.26	●	1	0	1.29	None
8	8.8	0.22	●	1	0	1.21	None
9	9	0.19	●	1	0	1.13	None

*Time after establishment of initial suction profile.

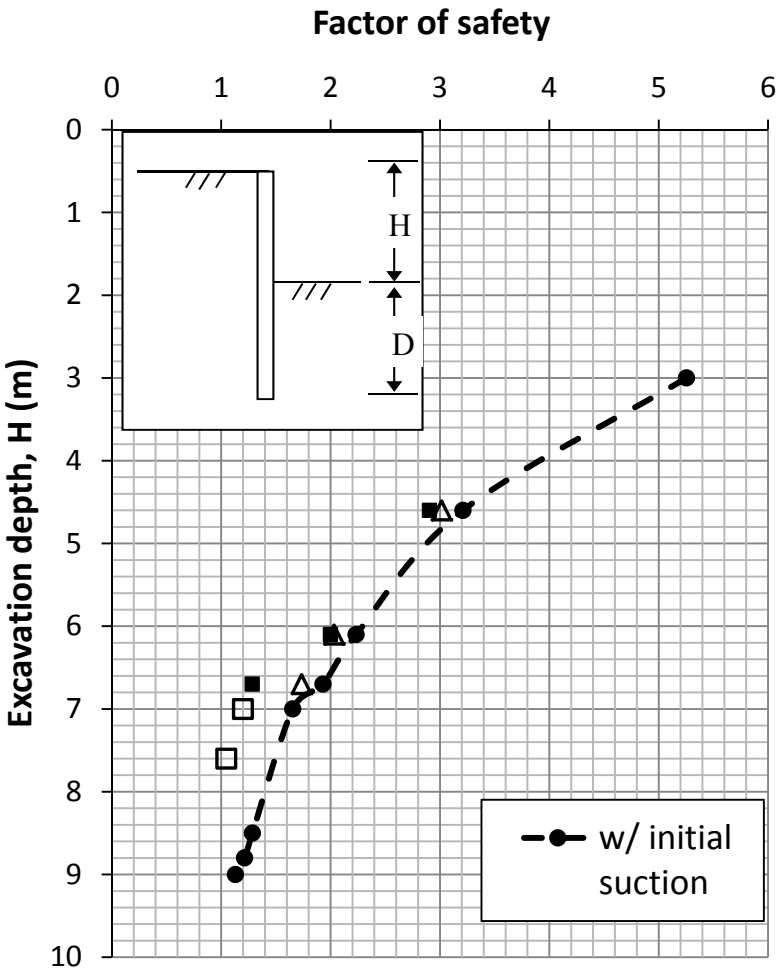

Figure 7-2 FS as a function of excavation depth

From the results of the deformation analyses incorporating the infiltration modified suction profile, the maximum lateral displacement of the sheet pile wall as a function of excavation depth and the FS as a function of D/H were plotted, as shown in Figures 7-3 (a) and 7-3 (b), respectively.

The lateral displacement of the sheet pile wall is predicted to gradually increase with excavation to a depth of 6 m, after which the rate of movement increases dramatically, resulting in a lateral displacement of 900 mm at an excavation depth of 7.6 m. As described previously, after the 6.7 m excavation depth the suction profile was not changed, as the excavation was assumed to rapidly proceed to the final depth of 7.6 m (D/H= 0.41), where the FS was calculated to be 1.05, as shown in Figure 7-3 (b).

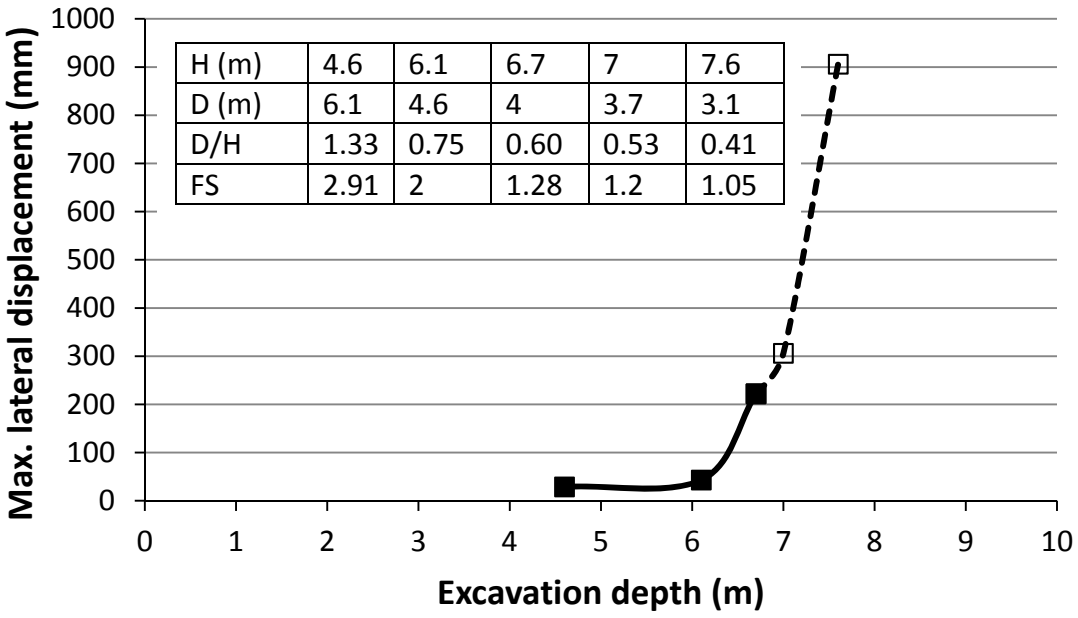

(a)

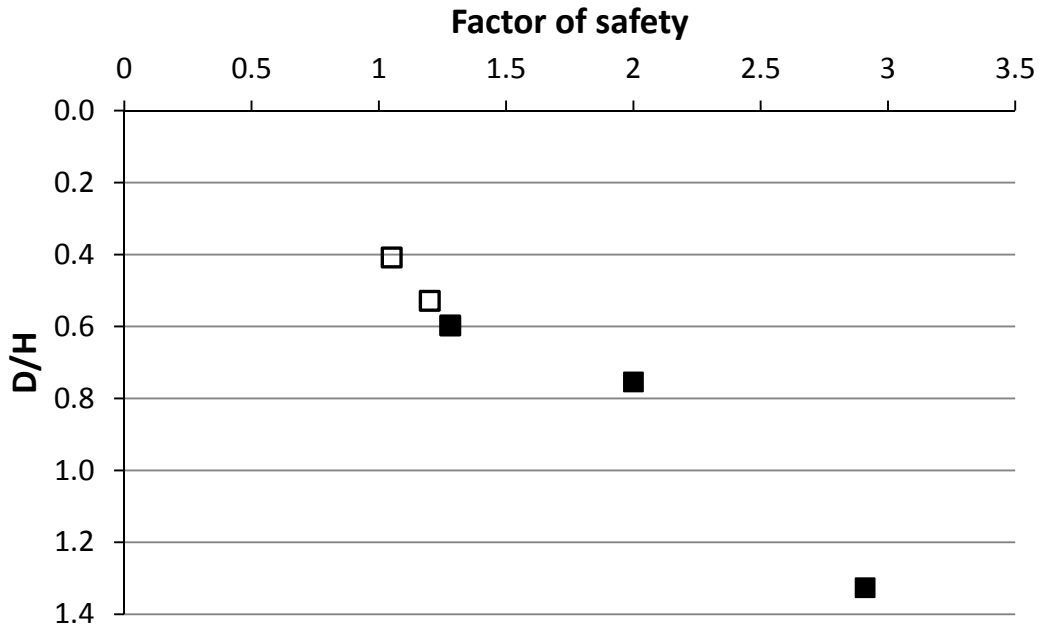

(b)

Figure 7-3 (a) Maximum lateral displacement of sheet pile vs. excavation depth and (b) FS corresponding to each stage of excavation with infiltration analysis

7.2. Development of a design chart for cantilever sheet pile walls

In order to develop a design approach for incorporating matric suction into cantilever sheet pile wall design in unsaturated soils, the idea of using an average matric suction value over the length of the proposed sheeting was explored. Suction values of 0 kPa, 30 kPa, and 50 kPa were assigned for each analysis for sheet piles having lengths of 4.6 m and 10.7 m (the length of the field-test piles). The analyses conducted for the two length sheet piles and three average matric suction profiles produced decreasing FS values with increasing excavation depth (or decreasing D/H values).

The concept of a Suction Stability Number (SSN) was introduced to account for the stabilizing influence of matric suction, in a similar manner to cohesion in the conventional stability number. Therefore, the SSN is defined as the absolute value of $\psi/(\gamma H)$, where the suction, ψ , is taken as the average matric suction over the length of the sheeting, γ is the average total unit weight and H is the depth of excavation. As would be expected, different suction conditions and D/H values produce different FS values. The results of stability analyses show that as D/H decreases, the FS of the sheet pile wall decreases linearly as a function of the SSN, as can be seen in **Figure 7-4**. Based on the simplified average suction profile assumption, the design chart for a cantilever sheet pile wall has been developed.

Using the observed linear relationships, and using linear regression on the data set for each average suction value, values of D/H can be predicted corresponding to FS values of 1.5, 1.7, and 2, and the SSN can be estimated for each condition, as shown in Table **7-2**. As would be expected, the data in Table **7-2** show increasing values of D/H for any desired FS as the average matric suction decreases from 50 kPa to 30 kPa to 0 kPa. These results clearly show that design in unsaturated soils will be more economical if the matric suction is included.

Table 7-2 Summarized case conditions for FS of 1.5, 1.7, and 2

			FS =1.5			FS =1.7			FS =2		
Symbol	L	ψ	H	D/H	ψ/(γH)	H	D/H	ψ/(γH)	H	D/H	ψ/(γH)
▪	10.7	50	7.28	0.47	0.46	6.57	0.63	0.51	5.81	0.84	0.57
Δ	4.6	50	4.31	0.07	0.77	3.94	0.17	0.85	3.49	0.32	0.95
●	10.7	30	6.67	0.60	0.30	6.09	0.76	0.33	5.38	0.99	0.37
◊	4.6	30	3.76	0.22	0.53	3.44	0.34	0.58	3.04	0.51	0.66
*	10.7	0	5.03	1.13	0.00	4.59	1.33	0.00	4.06	1.64	0.00
+	4.6	0	2.19	1.10	0.00	2.00	1.30	0.00	1.77	1.60	0.00

Utilizing the tabulated data presented in Table **7-2** and second order polynomial regression, contours for required D/H as a function of the SSN for values of FS values equal to 1.5, 1.7 and 2.0 were developed and plotted on **Figure 7-4**. This design chart can be used to estimate the required embedded sheet pile wall length for a desired FS for the case of a known excavation height (H) and average suction value for the soil surrounding the sheet pile wall. For using this chart, the height of excavation, average total unit weight of soil, and average suction value surrounding the sheet pile wall are needed to be known to estimate the SSN. Using the calculated SSN and the desired FS, the required the depth ratio (D/H) can be predicted. The required length of embedded sheet pile wall (D) can be determined by simply multiplying the intended excavation depth (H) by D/H.

In a similar manner, the sequential infiltration and excavation case was investigated. From **Figure 7-2**, and using the infiltration case (solid squares), the FEM analyses predict that a FS=1.5 existed at an excavation depth of approximately 6.5 m. Thus, to obtain a FS of 1.5 in this condition, a depth of embedment of 4.2 m was required. In order to produce a predicted embedment depth from the proposed design procedure for the excavation height of 6.5 m, an average matric suction value is needed. Using the FEM calculated matric suction profile for the excavation depth of 6.1 m shown in **Figure 6-6** (c), a calculated average matric suction value of 40 kPa was determined. The reason for selecting the suction profile corresponding to the 6.1 m excavation depth, rather than that for the 6.7 m depth was that the former occurred at a point in time closer to that at which the excavation to 6.5m was made.

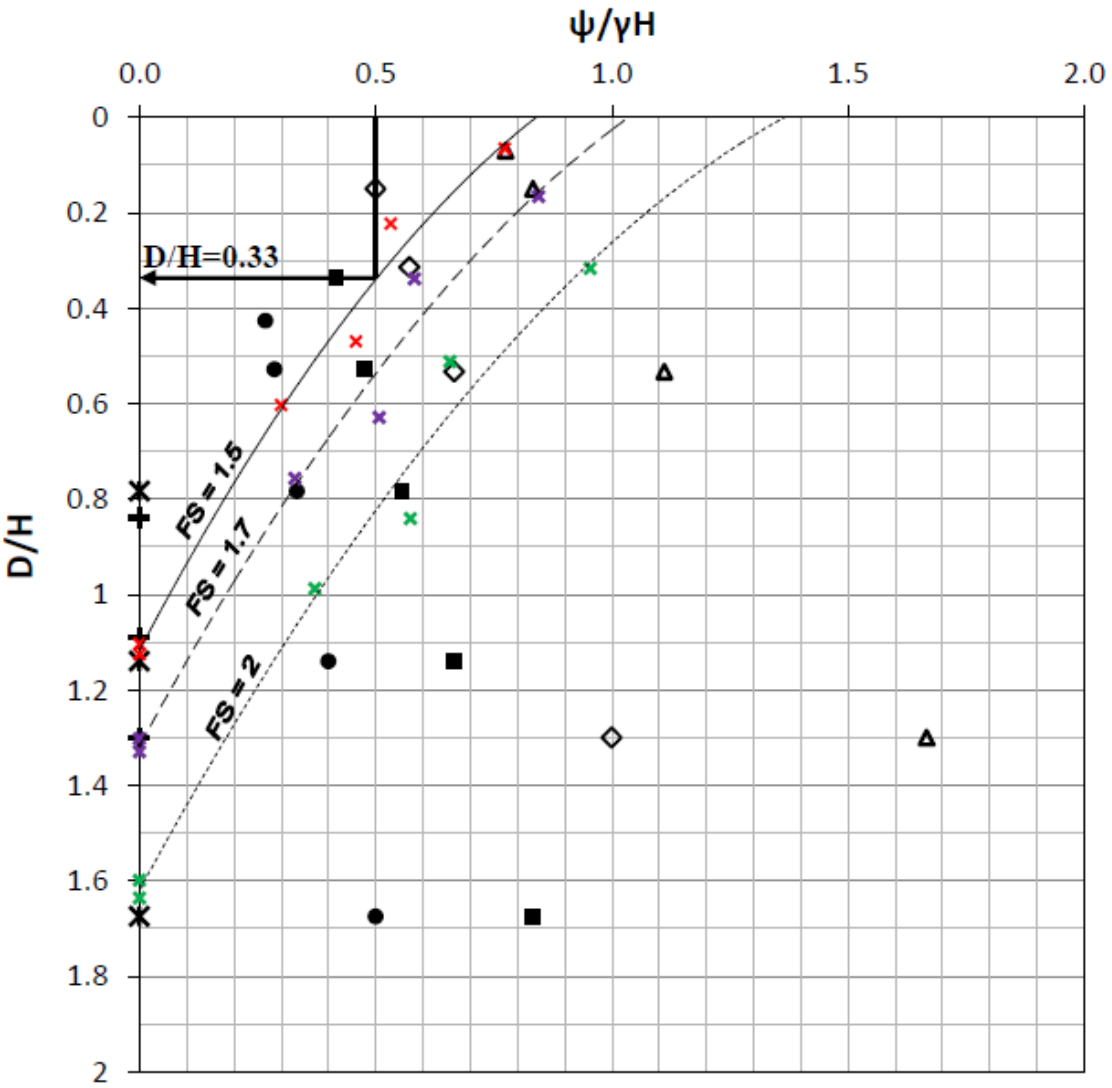

Figure 7-4 Design chart for cantilever sheet pile wall including matric suction

Using the values for H and average suction, a SSN of 0.38 is calculated. For this SSN and a FS=1.5, a D/H value of 0.5 is obtained from the design chart. As a result, a D of 3.25 m is suggested to be needed for a FS=1.5. This value is seen to be 23 percent shorter than that resulting from the FEM analyses and very close to the 22 percent under-prediction observed for the non-infiltration case. Accordingly, at the present time, it appears prudent to suggest that for a FS=1.5 the embedment depths predicted from the proposed method (Figure **7-4**) be increased by 22 to 23 percent, or approximately a factor of 1.25.

Because this simplified design approach using a calculated SSN and Figure **7-4** is presumed to be used in lieu of numerical analyses (detailed infiltration and FEM analyses), a correspondingly simple approach for producing a reduced average matric suction value accounting for the effects of infiltration was considered. On the basis of the measured field-suction values presented in Figure **7-1**, which shows the advance of the wetting front producing some depth of very low matric suction values, the simplified approach proposed herein assumes that the initial suction profile is modified by setting all suction values above a chosen depth equal to zero. This depth of infiltration, D_i, represents the depth where the matric suction is assumed to be zero on the retained soil side. As an example, let us consider a D_i of 5 m, which was the observed field condition due to rainfall infiltration through the gap between the sheet pile wall and soil, and surface cracks, at an excavation depth of 6.7 m. For this depth and calculated average suction value of 16 kPa, the SSN is computed to be 0.15. From this value, for a FS=1.5, D/H is determined to be 0.85, thus producing a required embedded depth of 5.7 m.

From Figure **7-2**, the infiltration analysis for excavation to a depth of 6.7 m (solid square), with a depth of embedment of 4 m, corresponded to a FS= 1.28. Therefore, the current analysis predicting a required depth of embedment of 5.7 m to produce a FS=1.5 appears reasonable. Nevertheless, it is still recommended that this value be multiplied by a factor of 1.25, if a FS=1.5 is desired.

The maximum lateral displacement and maximum induced bending moments for 4.6 m and 10.7 m length sheet pile walls have been predicted as a function of excavation depth with average suction values of 50 kPa, 30 kPa and zero suction, and are shown in **Figures 7-5** (a) and **7-5** (b) and **Figure 7-5** (a) and **7-6** (b), respectively. As the excavation depth increases, the maximum displacement of the sheet pile wall is seen to increase. The maximum lateral displacement takes place when the suction value is equal to 0 for both lengths of sheet pile, as shown in **Figure 7-5** (a) and (b). The maximum bending moment is seen to increase as a function of excavation depth for the 10.7 m length sheet pile. However, for the 4.6 m length sheet pile, the maximum bending moment decreases after 2.5 m of excavation, as shown in **Figure 7-6** (b). This behavior is as would be expected, due to a significant reduction in passive resistance on the excavated side and occurs along with a reduction in the curvature of sheet pile wall.

From the analyses and evaluations presented in this chapter, the following observations can be made:

1. The FS of a cantilever wall in unsaturated soil decreases nonlinearly with excavation depth. This behavior was observed for both the initial suction profile and one that was developed using an infiltration analysis based on net precipitation data, including both measured precipitation and predicted evaporation. Due to the loss of suction during rainfall infiltration, the FS is seen to decrease faster with excavation depth for the infiltration case than for the constant initial suction profile.
2. The developed design chart (Figure **7-4**), which incorporates the average suction profile thru the SSN, can be used to estimate the required embedded depth of sheet pile wall for a desired FS. However, the predicted depths for two cases were found to be approximately 23 percent shorter than results predicted from the FEM analyses of the field tests. Accordingly, at this time, it is considered prudent to apply a factor of 1.25 to the embedment depth obtained from the design chart to produce the desired FS.
3. The maximum lateral displacements and maximum bending moments of the sheet pile wall increase with decreasing values of suction. For the shorter, 4.6 m length, sheet pile wall, the maximum bending moment decreased after a 2.5 m excavation depth due to the reduction in passive resistance on the excavated side.

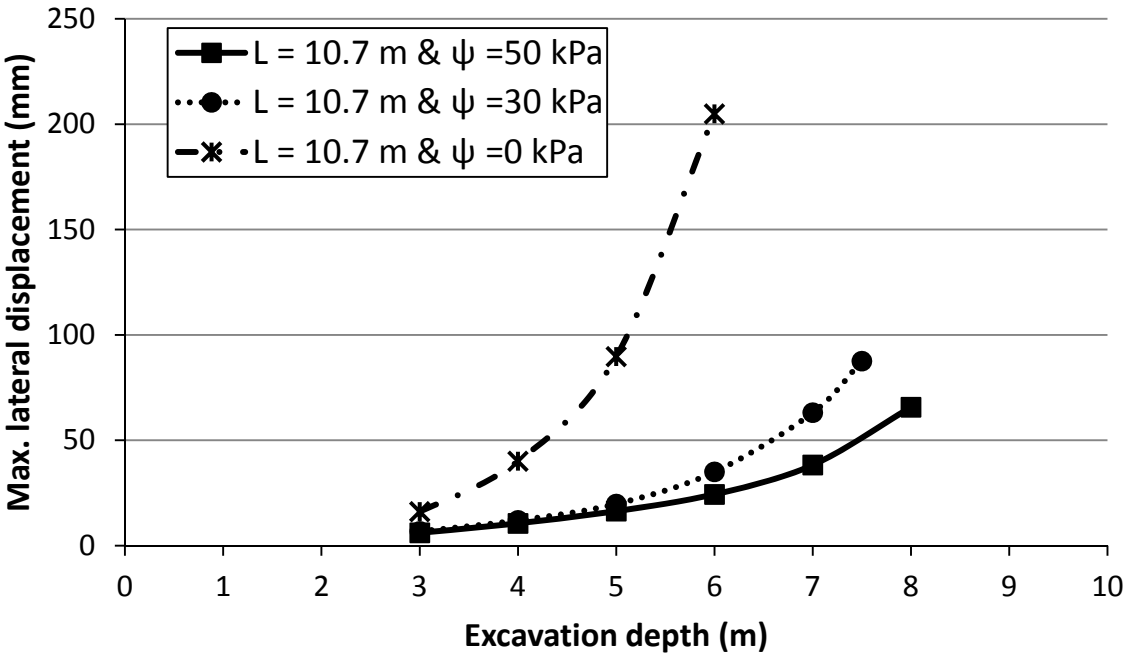

(a)

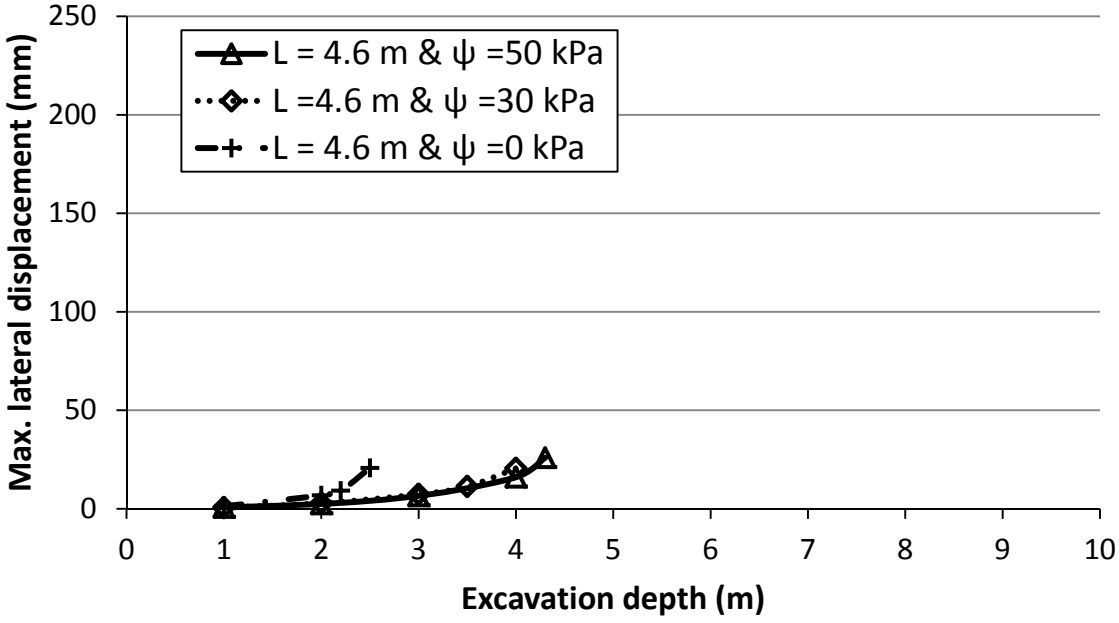

(b)

Figure 7-5 (a) Maximum lateral displacement of 10.7 m length of sheet pile wall and (b) 4.6 m length of sheet pile wall

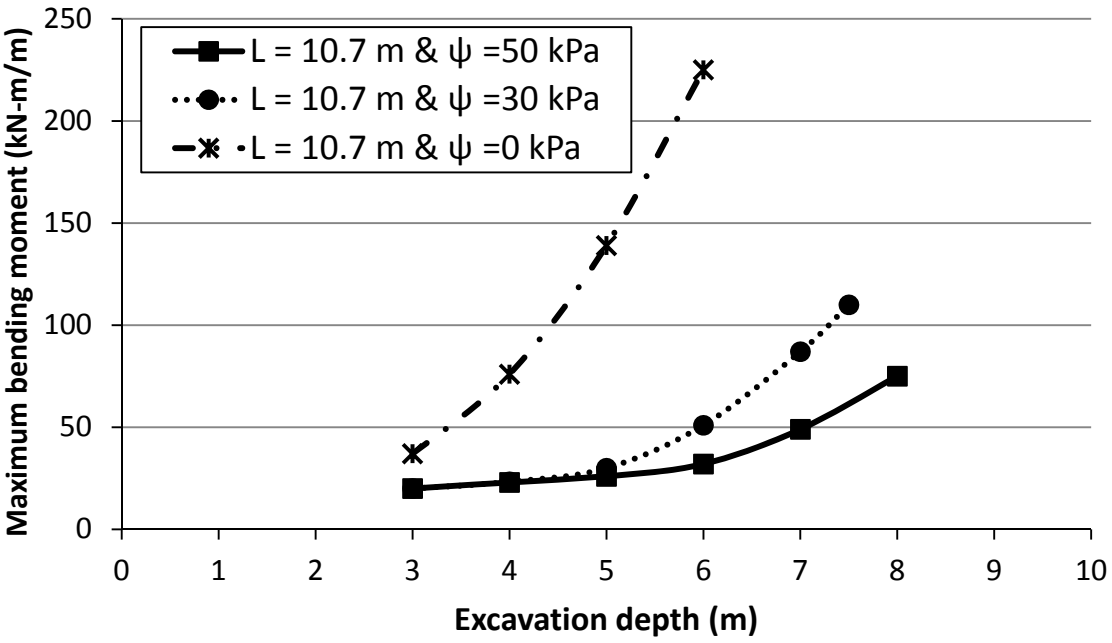

(a)

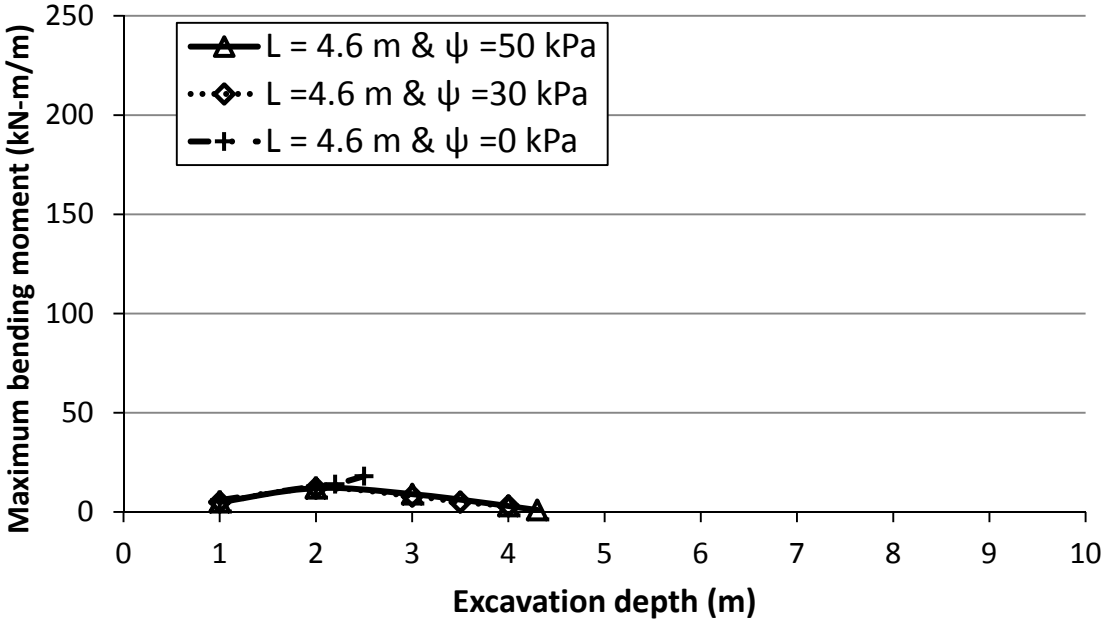

(b)

Figure 7-6 (a) Maximum bending moment of 10.7 m length of sheet pile wall and (b) 4.6 m length of sheet pile wall

CHAPTER 8. Findings and Conclusions

The research reported herein was undertaken to provide the data, analyses and measured field performance required to support the more economical design of temporary slopes and retaining structures (with an emphasis on sheet pile walls) in unsaturated residual soils. To accomplish this goal, an extensive program of field and laboratory tests were undertaken, the results of which are summarized in this report and accompanying Appendices. The specific areas of study included the measurement and prediction of matric suction, the measurement and prediction of unsaturated shear strength as a function of matric suction, the incorporation of matric suction into slope stability analyses, a comparison of PLAXIS numerical analyses with the measured performance of a cantilever sheet pile wall, and the evaluation of approaches for predicting lateral earth pressures to be used in the design of temporary retaining structures. As an aspect of the final task, a design chart was developed for the determination of the required embedment depth of cantilever sheeting in an unsaturated soil profile.

Based on the body of work completed in this research study, a number of findings and significant conclusions were reached. The following points are arranged according to the order of topics and chapters presented in this report.

Prediction models for matric suction

- Compared with the published suction prediction models of Zapata (R^2 = 51%) and SoilVision (R^2 = 48%), the proposed model from the current research is shown better able to represent the measured test data, with R^2 = 93%. The reasonableness of the model was verified using previously published data.
- It is proposed that SWCC curves representative of the field conditions, or "field curves," should be used in numerical analyses to more accurately predict existing matric suction. These field curves can be constructed by shifting the pressure-plate determined SWCC drying curve, if the actual suction is known at the existing field water content. Miniature potentiometers have been shown to be able to produce this data (in a field cut or tube sample) in less than 5 minutes.

Prediction models for unsaturated shear strength

An extensive database of unsaturated shear strength data was developed, with a total of 19 unsaturated triaxial tests, including 8 single stage tests and 11 multistage tests performed on the four groups of soils of the three types encountered at the test site, A-7-5, A-4 and A-2-6 (MH, ML and SC). Analysis of these data, as well as data reported in the literature on other residual soils, and evaluation of existing models for predicting unsaturated shear strength led to the following observations:

- Regression analyses on the Vanapalli et al. (1966) model-predicted values yielded a best-fit slope of 0.8, thus underestimating the measured values by approximately 20%. However, the values predicted are shown to be significantly influenced by the definition of the residual volumetric water content.
- Regression analysis on the Houston, et al. (2008) model yielded a prediction capability within +/- 15% of the measured data from the four groups of soil in this research. However, when additional SM and SM-SW data from the literature were evaluated, the "a" model parameter became a negative value; thus the model no longer yielded a hyperbolic equation and was therefore not able to provide reasonable shear strength predictions.
- In an effort to produce a model with better predictive capability for both the Greensboro test site soils and other residual soils reported in the literature, an improved empirical model for the κ parameter in the Fredlund (1996) strength equation was explored. Based on multivariate statistical analysis, a model including the soil parameters percent fines, Liquid Limit and Plasticity Index wa developed. Using the proposed equation for κ along with the Fredlund et al. (1996) model yielded the best estimation of apparent cohesion due to suction, with an average underestimation of 6 % and an average R^2 value of 0.9.
- The empirical equation developed in this research for κ was applied to Fredlund's independent variable concept, for estimating the increase of total cohesion as a function of matric suction. However, K_f lines on an MIT p'-q plot are presented to validate that the empirical equation can also be applied into a model that uses the effective stress concept.

Stability analysis of unsaturated soil slopes

The slope stability analyses were conducted using SEEP/W and SLOPW/W platforms (GEO-SLOPE International, Ltd.). The initial matric suction distribution within the modeled soil profiles and any subsequent variation induced by infiltration were simulated by SEEP/W. Then, using the generated pore water pressure contours and calculated unsaturated shear strength values, SLOPE/W was used to estimate the FS of the slope according to Bishop's Method of Slices. As discussed in Chapter 5, if an analyst chooses to perform stability analyses in a manner, or with a computer code, that does not accommodate the introduction of a soil-suction profile to use in an effective-stress analysis, then the total cohesion induced by the existing suction in any modeled soil layer can be determined and used as input with the effective friction angle to model the soil strength in the stability analysis.

- Compared to results with assuming no matric suction, the inclusion of a matric suction profile led to an increase in the stability FS. A matric suction that decreased from approximately 80 kPa near the ground surface to 25 kPa at the base of a 6.7 m cut in an A-7-5 soil profile caused the calculated FS of 0.25:1 and 0.5:1 slopes to increase from 0.8 to 1.55 and 1.02 to 1.75, respectively.
- The effect of continuous surface-water infiltration was shown to decrease both the matric suction and the resulting FS, with the 0.25:1 slope FS decreasing from 1.55 to 1.25 after 30 days and to 1.0 after 57 days, while the 0.5:1 slope FS decreased from 1.75 to 1.55 and 1.42 after 30 and 57 days of infiltration, respectively.

Modeling of a cantilever sheet pile wall

- A numerical model of the Greensboro test site cantilever sheet pile wall was constructed in PLAXIS. After demonstrating that the deformations within the retained soil and those of the sheet pile wall reasonably matched the field-measured data, net soil pressure diagrams were estimated. The bending moments in the sheet pile wall also were validated by comparing model-predicted values to those calculated from measured strain-gauge data. The results of the numerical analyses matched reasonably well the measured data to the maximum 6.7 m

excavation depth. It is shown that the net pressure diagram on the sheet pile wall over the excavation stages could be determined from the numerical analysis and then these values could be used for the design of a temporary retaining wall system.

- Apart from performing numerical analyses, similar to those performed using PLAXIS for this research, the approach proposed by Lu and Likos (2004) for calculating lateral earth pressures in unsaturated soils was evaluated. The results of PLAXIS analyses on the test site sheet pile wall show that the D/H required to reach a FS of 1 is on the order of 26% and 17% smaller than the D/H obtained from the Lu and Likos approach, for an excavation depth of 9 m with initial suction profile and an excavation depth of 7.6 m with suction profile representative of the end of field test condition, respectively, when wall friction is incorporated in calculating K_a and K_p. If one uses the Lu and Likos approach without incorporating wall friction, the resulting depths of embedment will be on the order of 95% and 61% greater than the values determined from numerical analysis and confirmed by the monitored field wall performance data.
- Analyses show that the suction profile on the excavated side of the sheet pile is important to the design of a temporary retained wall system, and appropriate reductions in suction due to anticipated surface water infiltration is required.

Development of a simplified design method for cantilever sheet pile walls in unsaturated soils

- The FS of a cantilever wall in unsaturated soil decreases nonlinearly with excavation depth. This behavior was observed for both the initial suction profile and one that was developed using an infiltration analysis based on net precipitation data, including both measured precipitation and predicted evaporation. Due to the loss of suction during rainfall infiltration, the FS is seen to decrease faster with excavation depth for the infiltration case than for the constant initial suction profile.
- The developed design chart, incorporating the average suction profile thru the concept of a Suction Stability Number (SSN) can be used to estimate the required embedded depth of sheet pile wall for a desired FS. However, the predicted depths for two cases were found to

be approximately 23 percent shorter than predicted from the FEM analyses of the field tests. Accordingly, at this time, it is considered prudent to apply a factor of 1.25 to the embedment depth obtained from the design chart to produce the desired FS.

- The maximum lateral displacements and maximum bending moments of the sheet pile wall increase with decreasing values of suction. For the shorter, 4.6 m length, sheet pile wall, the maximum bending moment decreased after the 2.5 m excavation depth due to the reduction in passive resistance on the excavated side.

CHAPTER 9. References

ASTM, D422; D854; D3080; D4318; D4767; D6838; D7181, *Annual Book of ASTM Standards, ASTM International*, West Conshohocken, PA

Anderson, M. G., and Richards, K. S. (1987). *Slope stability: geotechnical engineering and geomorphology.* John Wiley & Sons.

Arya, L. M., and Paris, J. F. (1981). "A physicoempirical model to predict the soil moisture characteristic from particle-size distribution and bulk density data." *Soil Sci.Soc.Am.J.,* 45(6), 1023-1030.

Au, S. (1998). "Rain-induced slope instability in Hong Kong." *Eng.Geol.,* 51(1), 1-36.

Bittelli, M., and Flury, M. (2009). "Errors in Water Retention Curves Determined with Pressure Plates." *Soil Science Society of America Journal,* 73(5), 1453-1460.

Bouma, J. (1989). "Using soil survey data for quantitative land evaluation." *Advances in soil science,* Springer, 177-213.

Chandler, R. J., and Gutierrez, C. I.,. (1986). "Filter-paper method of suction measurement." *Géotechnique,* 36(2), 265-268.

Chin, K., Leong, E., and Rahardjo, H. (2010). "A simplified method to estimate the soil-water characteristic curve." *Canadian Geotechnical Journal,* 47(12), 1382-1400.

Cornelis, W. M., Ronsyn, J., Van Meirvenne, M., and Hartmann, R. (2001). "Evaluation of pedotransfer functions for predicting the soil moisture retention curve." *Soil Sci.Soc.Am.J.,* 65(3), 638-648.

Cui, Y. J., Tang, A. M., Mantho, A. T., and De Laure, E. (2008). "Monitoring field soil suction using a miniature tensiometer." *Geotechnical Testing Journal,* 31(1), 95-100.

Diaz-Padilla, J., and Vanmarcke, E. H. (1974). *Settlement of Structures on Shallow Foundations: A Probabilistic Analysis.* Department of Civil Engineering, Massachusetts Institute of Technology.

Feng, M. (1999). "The effects of capillary hysteresis on the matric suction measurement using themral conductivity sensors". Maser of science. Department of Civil Engineering, University of Saskatchewan.

Feng, M., Fredlund, D. G., and Shuai, F. (2002). "A Laboratory Study of the Hysteresis of A Thermal Conductivity Soil Suction Sensor." *Geotechnical Testing Journal,* 25(3), 1-12.

Feng, M., and Fredlund, D. G. (2003). "Calibration of thermal conductivity sensors with consideration of hysteresis." *Canadian Geotechnical Journal,* 40(5), 1048-1055.

Fredlund, D. G., Rahardjo, H., and Fredlund, M. D. (2012). *Unsaturated Soil Mechanics in Engineering Practice.* Wiley, New Jersey.

Fredlund, D. G., and Morgenstern, N. R. (1977). "Stress state variables for unsaturated soils." *J.Geotech.Geoenviron.Eng.,* 103.

Fredlund, D. G., Rahardjo, H., and Fredlund, M. D. (2012). *Unsaturated soil mechanics in engineering practice.* Wiley.

Fredlund, D. G., Sheng, D., and Zhao, J. (2011). "Estimation of soil suction from the soil-water characteristic curve." *Canadian Geotechnical Journal,* 48(2), 186-198.

Fredlund, D. G., and Xing, A. (1994). "Equations for the soil-water characteristic curve." *Canadian Geotechnical Journal,* 31(4), 521-532.

Fredlund, D., Morgenstern, N., and Widger, R. (1978). "The shear strength of unsaturated soils." *Canadian Geotechnical Journal,* 15(3), 313-321.

Fredlund, M. D., Fredlund, D. G., and Wilson, G. (1997). "Prediction of the soil-water characteristic curve from grain-size distribution and volume-mass properties." *Proc., 3rd Brazilian Symp. on Unsaturated Soils,* Rio de Janeiro, 13-23.

Fredlund, M. D., Fredlund, D., and Wilson, G. W. (2000). "An equation to represent grain-size distribution." *Canadian Geotechnical Journal,* 37(4), 817-827.

Guan, Y., and Fredlund, D. (1997). "Use of the tensile strength of water for the direct measurement of high soil suction." *Canadian Geotechnical Journal,* 34(4), 604-614.

Gupta, S., and Larson, W. (1979). "Estimating soil water retention characteristics from particle size distribution, organic matter percent, and bulk density." *Water Resour.Res.,* 15(6), 1633-1635.

He, L., Leong, E. C., and Elgamal, A. (2006). "A miniature tensiometer for measurement of high matric suction." *Geotech Spec Publ,* 147(2), 1897.

Heartz, William. (1986). "Properties of a Piedmont residual soil". PhD. North Carolina State University, Raleigh, N.C.

Houston, S. L., Houston, W. N., and Wagner, A. M. (1994). "Laboratory Filter Paper Suction Measurements." *Geotechnical Testing Journal,* 17(2), 185-194.

Houston, W., Dye, H., Zapata, C., Perera, Y., and Harraz, A. (2006). "Determination of SWCC using one point suction measurement and standard curves." *Unsaturated Soils 2006,* ASCE, 1482-1493.

Iyer, K., Jayanth, S., Gurnani, S., and Singh, D. (2012). "Influence of initial water content and specimen thickness on the SWCC of fine-grained soils." *International Journal of Geomechanics,* 13(6), 894-899.

Johari, A., Habibagahi, G., and Ghahramani, A. (2006). "Prediction of soil–water characteristic curve using genetic programming." *J.Geotech.Geoenviron.Eng.,* 132(5), 661-665.

Leong, E. C., He, L., and Rahardjo, H. (2002). "Factors Affecting the Filter Paper Method for Total and Matric Suction Measurements." *Geotechnical Testing Journal,* 25(3), 322-333.

Leong, E. C., and Rahardjo, H. (1997). "Review of soil-water characteristic curve equations." *J.Geotech.Geoenviron.Eng.,* 123(12), 1106-1117.

Leong, E. C., Zhang, X. -., and Rahardjo, H. (2012). "Calibration of a thermal conductivity sensor for field measurement of matric suction." *Geotechnique,* 62(1), 81-85.

Likos, W. J., and Lu, N. (2002). "Filter paper technique for measuring total soil suction." *Transportation Research Record: Journal of the Transportation Research Board,* 1786(1), 120-128.

Lu, N., and Likos, W. J. (2004). *Unsaturated soil mechanics.* Wiley.

Mahler, C. F., and Mendes, C. A. R. (2005). "Measurement of Suction of Thick Textured Soil using Filter Paper Method and Equivalent Tensiometer - EQT." *Proceedings of the International Conference" From Experimental Evidence towards Numerical Modeling of Unsaturated Soils,",* Springer, Weimar, Germany, 183-192.

Marinho, F., and da Silva Gomes, J. E. (2012). "The Effect of Contact on the Filter Paper Method for Measuring Soil Suction." *Geotechnical Testing Journal,* 35(1), 1-10.

Meilani, I., Rahardjo, H., Leong, E., and Fredlund, D. G. (2002). "Mini suction probe for matric suction measurements." *Canadian Geotechnical Journal,* 39(6), 1427-1432.

Monroy, R., Zdravkovic, L., and Ridley, A. (2012). "Random Uncertainty in the Measurement of Matric Potential Using the Miniature Tensiometer." *ASTM Geotechnical Testing Journal,* 35(1), 41-49.

Mualem, Y. (1976). "A new model for predicting the hydraulic conductivity of unsaturated porous media." *Water Resour.Res.,* 12(3), 513-522.

Mundorff, M. J. (1948). *Geology and ground water in the Greensboro area, North Carolina.* North Carolina, Department of Conservation and Development.

Neter, J., Kutner, M. H., Nachtsheim, C. J., and Wasserman, W. (1996). "Applied linear regression models, 1996." *Irwin, Chicago, USA.p,* 1050.

Nichol, C., Smith, L., and Beckie, R. (2003). "Long-term measurement of matric suction using thermal conductivity sensors." *Canadian Geotechnical Journal,* 40(3), 587-597.

Noguchi, T., Mendes, J., and Toll, D. G. (2011). "Comparison of soil water retention curves obtained by filter paper, high capacity suction probe and pressure plate." *Unsaturated soils : theory and practice : proceedings of the 5th Asia-Pacific Conference on Unsaturated Soils,* Pattaya, Thailand, 409414.

Perera, Y., Zapata, C., Houston, W., and Houston, S. (2005). "Prediction of the soil–water characteristic curve based on grain-size-distribution and index properties." *Advances in Pavement Engineering (Ed.EM Rathje), Geotechnical Special Publication,* 130 49-60.

Perera, Y. Y., and Fredlund, D. G. (2004). "Measurement of Soil Suction In Situ Using the Fredlund Thermal Conductivity Sensor." *Presentation Material for Mining and Waste Management Short Course,* 1-17.

Pham, H. Q. (2002). "An engineering model of hysteresis fro the soil-water characteristic curve". Master. University of Saskatchewan, Saskatoon, SK.

Pham, H., Fredlund, D., and Barbour, S. (2003). "A practical hysteresis model for the soil-water characteristic curve for soils with negligible volume change." *Géotechnique,* 53(2), 293-298.

Power, K. C., Vanapalli, S. K., and Garga, V. K. (2008). "A Revised Contact Filter Paper Method." *Geotechncial Testing Journal,* 31(6), 461-469.

Rahardjo, H., Satyanaga, A., Leong, E. C., Ng, Y. S., and Tam, H. (2012). "Variability of residual soil properties." *Engineering Geology,* 141-142 124-140.

Rahardjo, H., Satyanaga, A., and Leong, E. C. (2011). "Unsaturated soil mechanics for slope stabilization." .

Randy Rainwater, N., Mcdowell, L. A., and Drumm, E. C. (2001). "Measurement of total soil suction using filter paper: investigation of common filter papers, alternative media, and corresponding confidence." *Geotechncial Testing Journal,* 35(2), 295-304.

Rawls, W., Brakensiek, D., and Saxton, K. (1982). "Estimation of soil water properties." *Trans.ASAE,* 25(5), 1316-1320.

Ridley, A., and Burland, J. (1996). "A pore water pressure probe for the in situ measurement of a wide range of soil suctions." *ADVANCES IN SITE INVESTIGATION PRACTICE. PROCEEDINGS OF THE INTERNATIONAL CONFERENCE HELD IN LONDON ON 30-31 MARCH 1995.* .

Ridley, A., and Burland, J. (1993). "A new instrument for the measurement of soil moisture suction." *Géotechnique,* 43(2).

Ryan, T. A., Joiner, B. L., and Ryan, B. F. (1982). *Minitab reference manual.* Pennsylvania State University, Statistics Department..

Sattler, P., and Fredlund, D. G. (1989). "Use of thermal conductivity sensors to measure matric suction in the laboratory." *Canadian Geotechnical Journal,* 26 491-498.

Saxton, K., Rawls, W., Romberger, J., and Papendick, R. (1986). "Estimating generalized soil-water characteristics from texture." *Soil Sci.Soc.Am.J.,* 50(4), 1031-1036.

Scheinost, A., Sinowski, W., and Auerswald, K. (1997). "Regionalization of soil water retention curves in a highly variable soilscape, I. Developing a new pedotransfer function." *Geoderma,* 78(3), 129-143.

Shuai, F., Clements, C., Ryland, L., and Fredlund, D. G. (2002). "Some factors that influence soil suction measurements using a thermal conductivity sensor." *UNSAT 2002, Proceedings of the 3rd international conference on unsaturated soils,* Recife, Brazil, 325-329.

Sillers, W. S., and Fredlund, D. G. (2001). "Statistical assessment of soil-water characteristic curve models for geotechnical engineering." *Canadian Geotechnical Journal,* 38(6), 1297-1313.

Sowers, G., and Richardson, T. (1983). "Residual Soils of Piedmont and Blue Ridge." *Transp.Res.Rec.,* (919),.

Sweeney, D. (1982). "Some in situ soil suction measurements in Hong Kong's residual soil slopes." *Proceedings of the 7th Southeast Asian Geot. conference, Hong Kong,* 91-106.

Take, W. A., and Bolton, M. D. (2003). "Tensiometer saturation and the reliable measurement of soil suction." *Géotechnique,* 53(2), 159-172.

Tan, E., Fredlund, D. G., and Marjerison, B. (2007). "Installation procedure for thermal conductivity matric suction sensors and analysis of their long-term readings." *Canadian Geotechnique Journal,* 44(2), 113-125.

Tarantino, A., and De Col, E. (2008). "Compaction behaviour of clay." *Géotechnique,* 58(3), 199-213.

Tarantino, A., Gallipoli, D., Augarde, C. E., De Gennaro, V., Gomez, R., Laloui, L., Mancuso, C., El Mountassir, G., Munoz, J. J., Pereira, J. -., Peron, H., Pisoni, G., Romero, E., Raveendiraraj, A., Rojas, J. C., Toll, D. G., Tombolato, S., and Wheeler, S. (2011). "Benchamark of experimental technique for measuring and controlling suction." *Geotechnique,* 61(4), 303-312.

Thakur, V. K., Sreedeep, S., and Singh, D. N. (2007). "Evaluation of various pedo-transfer functions for developing soil-water characteristic curve of a silty soil." *Geotech Test J,* 30(1), 25.

Tietje, O., and Tapkenhinrichs, M. (1993). "Evaluation of pedo-transfer functions." *Soil Sci.Soc.Am.J.,* 57(4), 1088-1095.

Townsend, F. C. (1985). "Geotechnical characteristics of residual soils." *J.Geotech.Eng.,* 111(1), 77-94.

Triola, M. F. (1998). *Elementary Statistics, School Version.* Addison-Wesley. .

Van Genuchten, M. T. (1980). "A closed-form equation for predicting the hydraulic conductivity of unsaturated soils." *Soil Sci.Soc.Am.J.,* 44(5), 892-898.

Vanapalli, S. K., Fredlund, D. G., and Pufahl, D. E. (1999). "The influence of soil structure and stress history on the soil-water characteristics of a compacted till." *Géotechnique,* 49(2), 143-159.

Vanapalli, S. K., Fredlund, D. G., Pufahl, D. E., and Clifton, A. W. (1996). "Model for the prediction of shear strength with respect to soil suction." *Canadian Geotechnical Journal,* 33(3), 379-392.

Vereecken, H., Maes, J., Feyen, J., and Darius, P. (1989). "Estimating the soil moisture retention characteristic from texture, bulk density, and carbon content." *Soil Sci.,* 148(6), 389-403.

Wang, C. E., and Borden, R. H.,. (1996). "Deformation characteristics of piedmont residual soils." *Journal of of Geotechnical Engineering,* 122(10), 822-830.

Wang, X., and Benson, C. (2004). "Leak-Free Pressure Plate Extractor for Measuring the Soil Water Characteristic Curve." *Geotechncial Tesing Journal,* 27(2), 1-10.

Yang, H., Rahardjo, H., Leong, E., and Fredlund, D. G. (2004). "Factors affecting drying and wetting soil-water characteristic curves of sandy soils." *Canadian Geotechnical Journal,* 41(5), 908-920.

Zapata, C. E., and Houston, W. N. (2008). *Calibration and validation of the enhanced integrated climatic model for pavement design.* Transportation Research Board..

Zapata, C. E., Houston, W. N., Houston, S. L., and Walsh, K. D. (2000). "Soil-water characteristic curve variability." *Geotech Spec Publ,* (99), 84-124.

Zhai, Q., and Rahardjo, H. (2012). "Determination of soil–water characteristic curve variables." *Comput.Geotech.,* 42 37-43.